VOLUME 13 (1959) No. 2

NUCLEAR PHYSICS

JOURNAL DEVOTED TO THE EXPERIMENTAL AND THEORETICAL STUDY OF THE FUNDAMENTAL CONSTITUENTS OF MATTER AND THEIR INTERACTIONS

EDITOR: L. ROSENFELD · COPENHAGEN

CHARLES K. BOCKELMAN, Slow neutron capture and the (d, p) reaction. . 205

E. J. SQUIRES, Brueckner theory and the shell model effective potential . 224

S. N. BISWAS and L. K. PANDIT, $K^- - K^0$ relative parity determination from nucleon-antinucleon annihilation 235

J. C. SEVERIENS and F. W. RICHTER, The measurement of short lifetimes by a refinement of the recoil technique. The lifetime of the first excited state of Ra^{224} 239

L. S. AZHGIREY, I. K. VZOROV, V. P. ZRELOV, M. G. MESCHERYAKOV, B. S. NEGANOV, R. M. RYNDIN and A. F. SHABUDIN, Nuclear interactions of 660 MeV protons and the momentum distribution of nucleons in nuclei 258

BEN R. MOTTELSON and SVEN GÖSTA NILSSON, The shape of the nuclear photoresonance in deformed nuclei. 281

L. B. AULL, G. C. REINHARDT and W. D. WHITEHEAD, Fast photoneutrons from tantalum and gold 292

LADISLAV ROB and ZDENĚK KORBEL, Protonic decay of a Σ^+ hyperon with an associated electron pair 300

I. GRATOT, M. LE PAPE, J. OLKOWSKY et G. RANC, Etude de quelques isotopes très déficients en neutrons du prométhéum et du samarium 302

S. L. ANDERSEN, T. HOLTEBEKK, O. LÖNSJÖ and R. TANGEN, Resonances for proton capture in magnesium 310

ERNEST M. HENLEY, Study of the direct (α, nucleon) reaction, including polarization. 317

NORTH-HOLLAND PUBLISHING COMPANY - AMSTERDAM

October (2) 1959

EDITORIAL BOARD

AUSTRALIA & NEW ZEALAND:	H. Messel (Sydney), M. L. Oliphant (Canberra)
AUSTRIA:	B. Karlik, (Vienna), H. Thirring (Vienna)
BELGIUM:	M. de Hemptinne (Louvain), J. Verhaeghe (Ghent)
CANADA:	G. Volkoff (Vancouver)
DENMARK:	C. Møller (Copenhagen), S. Rozental (Copenhagen)
FINLAND:	L. Simons (Helsinki)
FRANCE:	A. Berthelot (Saclay), S. Gorodetzky (Strasbourg)
GERMANY (DEM. REP.):	G. Hertz (Leipzig)
GERMANY (FED. REP.):	W. Gentner (Freiburg i. B.), J. H. D. Jensen (Heidelberg)
GREAT BRITAIN:	S. Devons (Manchester), T. H. R. Skyrme (Harwell)
HUNGARY:	L. Janossy (Budapest)
INDIA:	H. Bhabha (Bombay), R. Ramanna (Trombay)
IRISH REPUBLIC:	J. McConnell (Maynooth)
ISRAEL:	G. Racah (Jerusalem)
ITALY:	E. Amaldi (Rome)
JAPAN:	S. Kikuchi (Tokyo), S. Tomonaga (Tokyo)
MEXICO:	M. Moshinsky (Mexico)
NETHERLANDS:	H. Brinkman (Groningen), S. R. de Groot (Leiden)
NORWAY:	E. Hylleraas (Oslo), A. Lundby (Oslo), H. Wergeland (Trondheim)
POLAND:	L. Infeld (Warsaw)
PORTUGAL:	J. M. Araújo (Porto), J. R. de Almeida Santos (Coimbra)
SOUTH AMERICA:	G. Beck (Saõ Paulo), J. Leite Lopes (Rio de Janeiro)
SPAIN:	J. M. Otero (Madrid), C. Sanchez del Rio (Madrid)
SWEDEN:	O. Klein (Stockholm), K. Siegbahn (Uppsala), I. Waller (Uppsala)
SWITZERLAND:	P. Huber (Basel), P. Scherrer (Zürich)
U.A.R. & ARAB COUNTRIES:	F. El Bedewi (Alexandria), M. G. Nooh (Cairo)
U.S.A.	H. H. Barschall (Madison, Wisconsin), V. Weisskopf (Cambridge, Mass.)
U.S.S.R.:	M. A. Markov (Moscow), I. S. Shapiro (Moscow), D. V. Skobeltzyn (Moscow)
YUGOSLAVIA:	I. Supek (Zagreb)

CONTRIBUTIONS may be sent to the Editor, Professor L. Rosenfeld, NORDITA, Blegdamsvej 17, Copenhagen Ø, either directly, or preferably through the intermediary of one of the members of the Editorial Board of the country or region in which the author is working. They may be written in English, French or German.

NUCLEAR PHYSICS is published in fortnightly issues. The subscription price per volume of 700 pages is fl 57.00; 114s; $ 15.00. Post-free.

SUBSCRIPTIONS should be sent to the publishers, **NORTH-HOLLAND PUBLISHING COMPANY**, P.O.Box 103, Amsterdam or to any subscription-agent.

BOOKS FOR REVIEW should be sent to Professor Rosenfeld.

No part of this issue may be reproduced in any form, by print, photoprint, microfilm or any other means without written permission from the publisher. Reprints, photoprints or microfilms are obtainable at cost from the publisher.

Printed in the Netherlands

2.F *Nuclear Physics* **13** (1959) 205—223; © *North-Holland Publishing Co., Amsterdam*

Not to be reproduced by photoprint or microfilm without written permission from the publisher

SLOW NEUTRON CAPTURE AND THE (d, p) REACTION

CHARLES K. BOCKELMAN

Institute for Theoretical Physics, University of Copenhagen, Denmark †

Received 1 July 1959

Abstract: The suggestion of Lane and Wilkinson that the similarity between (d, p) and (n, γ) spectra may be understood in terms of the target as a unique parent state is applied in detail. An examination of all the available data shows six nuclei for which the assumption appears to be satisfied, and four ambiguous situations. Clear disagreement is found for three nuclei. In order to inquire further into the circumstances responsible for the cases of agreement, the cross section for direct neutron capture with the emission of an electric dipole γ-ray is evaluated with the help of the optical model. Comparison with experiment shows that one of the six cases of agreement can be attributed to direct capture. However (d, p) data do not exist in the region where the optical model predicts the largest direct cross sections. These maxima occur at the same A for which the s-wave strength function is greatest. Measured (n, γ) cross sections for E1 transitions are in many cases compatible with the direct process.

1. Introduction

The correspondence between the intensity of proton groups in a (d, p) reaction and the intensity of neutron capture gamma rays proceeding to the same levels has been noticed long ago [1]). The observed angular distributions of strong proton groups usually indicate direct interaction, and the more intense initial capture γ-rays commonly terminate on the same levels. In surveying the data for the present investigation, only four reasonably well-established exceptions were found to the general statement that all initial neutron capture gamma rays proceed to levels characterized by stripping-type proton angular distributions ††. This circumstance suggests that direct interaction also occurs in the capture process. Groshev *et al.* [2]) have compared the reduced widths of a final level deduced from the (d, p) experiment with the observed gamma ray intensity to that level, divided by the cube of the gamma ray energy. The correspondence is particularly good for the target nuclei Mg^{24}, Si^{28}, S^{32} and Ca^{40}; but it is rather poor in certain other cases. The purpose of the present note is to examine precisely what correspondence may be expected, to obtain from all the evidence available the degree of correspondence, and to offer an explanation for the results.

Two distinct methods of comparison are outlined. The first, and more

† Permanent address: Yale University, New Haven, Connecticut, U.S.A.

†† The four final levels which are exceptions are: N^{15} (5.31 MeV), Al^{28} (1.37 MeV), Si^{29} (2.43 MeV), and S^{33} (1.97 MeV).

general, approach was proposed by Lane and Wilkinson [3]). It is based on the assumption that each of the reactions can be represented in terms of very simple shell model wave functions; no specification of the details of the interaction is made. Evidence is found that such situations do occur, but the treatment cannot define a specific picture of the process. The second method is a comparison in detail; it is an estimate of the matrix element for direct emission of electric dipole radiation. The capture cross section is found to be proportional to the reduced width governing the (d, p) cross section.

2. Shell Model Comparison

2.1. THEORY

A precise basis on which proton intensities in a (d, p) reaction may be related to γ-ray intensities in an (n, γ) reaction has been pointed out by Lane and Wilkinson [3]). These authors show (eq. (3) of ref. [3])) that for any single-particle operator the matrix element can be written

$$\gamma = n\chi \sum_i c_i \omega_i, \tag{1}$$

where n is the number of particles needed to specify the initial and final states,

χ is the reduced single-particle matrix element,

c_i is the product of the coefficients of fractional parentage of the initial and final states for the parent state i,

and ω_i is a weighting coefficient which may depend on all the angular momenta as well as the nature of the interaction.

This expression simplifies if either the initial state or the final state is well characterized by a product of wave functions, one representing the target nucleus, the other the neutron moving about it. In this case, the sum in eq. (1) has only one term. Such a situation is described by calling the target nucleus a unique parent of the state concerned; the assumption that such a situation obtains will be called hereafter the unique-parent postulate. Lane and Wilkinson remark that a correspondence in intensities in the (d, p) and (n, γ) reactions is expected if one assumes that the target nucleus is a unique parent for the initial states of both reactions. However, the conclusion is equally true if the unique-parent assumption holds for the final state †; for in either case the conclusion follows from the fact that eq. (1) consists of a single term. With this postulate, eq. (1) shows that the ratio of the reduced width for neutron capture, $\gamma^2_{n\gamma}$, to the reduced width for the (d, p) reaction, γ^2_{dp}, to the same final state is

† The author is indebted to Prof. A. Bohr for pointing this out.

$$\gamma^2_{n\gamma}/\gamma^2_{dp} = K(\omega^2_{n\gamma}/\omega^2_{dp})(\chi^2_{n\gamma}/\chi^2_{dp}). \quad (2)$$

Here, K is the ratio of the squares of the parentage coefficients for the initial states in the two reactions. As a consequence of the unique-parent assumption, and the restriction to a common final state, the third factor should depend only on the orbital angular momentum transfer l_n.

A practical test of eq. (2) against experiment is to make a relative comparison of such ratios for two different final states a and b. The weighting coefficients have the form of a factor depending on the nature of the interaction (e.g., whether it is electromagnetic) multiplied by a coupling factor. For reasons outlined in the next section, the comparison will be restricted to final states for which the angular momentum transfer is the same. Then, for the two final states a and b, eq. (2) leads to

$$\frac{(\gamma^2_{n\gamma}/\gamma^2_{dp})_a}{(\gamma^2_{n\gamma}/\gamma^2_{dp})_b} = \frac{(\omega^2_{n\gamma}/\omega^2_{dp})_a}{(\omega^2_{n\gamma}/\omega^2_{dp})_b} = \frac{r_a^{\,2}}{r_b^{\,2}}. \quad (3)$$

In general, r_a and r_b are ratios of products of Racah coefficients which are functions of all the angular momenta involved and the manner in which they are coupled.

Eq. (3) shows that appropriate ratios of reduced widths for the two reactions are expressible in terms of ratios of angular momentum quantum numbers if the unique-parent assumption is satisfied. There remains the problem of obtaining numerical values for r. Explicit expressions for the cases in hand are available. The electromagnetic matrix elements are given by Lane and Radicati [4]), and the (d, p) matrix elements by Lane [5]). The ratio of these expressions for a common final state can be formed to evaluate r. For the capture of s-wave neutrons with the emission of electric radiation, the assumption of jj-coupling leads to a particularly simple expression

$$r_a^{\,2} = \frac{2J_a+1}{(2J+1)(2l_n+1)}. \quad (4)$$

Here, J_a is the total angular momentum of the final state a, and J is the total angular momentum of the initial state in the (n, γ) reaction.

When l_n, as well as the spin of the target nucleus, is fixed, eq. (4) limits the allowed variation in r. If I is the target spin, then $J = I \pm \frac{1}{2}$, while J_a is limited by $|I-l_n-\frac{1}{2}| \leqq J_a \leqq |I+l_n+\frac{1}{2}|$. For $l_n = 1$, table 1 shows that the variation in $r_a^{\,2}/r_b^{\,2}$ ranges between a factor 2 for target spin 0 to a factor 15 for target spin $\frac{1}{2}$. Eq. (4) may therefore limit the variation allowed the ratios of reduced widths to factors considerably smaller than would be expected for random choices of reduced widths. Unfortunately, ignorance of nuclear coupling schemes means that eq. (4) cannot be rigorously applied to all the available data. The expression which corresponds to eq. (4) in the case of LS-coupling is cumbersome, but can be evaluated if the spin of the final state

is known. It is possible that the expression for intermediate coupling would lie outside the limits obtained from the extreme couplings. However, calculation of a few specific cases in LS-coupling suggests that the variations permitted by eq. (4) are typical of both extremes. We shall assume that eq.

TABLE 1

Values of r^2 from eq. (4) for $l_n = 1$

Spin of target nucleus	r^2_{max}	r^2_{min}	r^2_{max}/r^2_{min}
0	$\frac{2}{3}$	$\frac{1}{3}$	2
$\frac{1}{2}$	$\frac{5}{3}$	$\frac{1}{9}$	15
1	1	$\frac{1}{6}$	6
$\frac{3}{2}$	$\frac{7}{9}$	$\frac{1}{15}$	$\frac{35}{3}$
2	$\frac{2}{3}$	$\frac{1}{9}$	6
$\frac{5}{2}$	$\frac{3}{5}$	$\frac{1}{7}$	$\frac{21}{5}$
3	$\frac{5}{9}$	$\frac{1}{6}$	$\frac{10}{3}$

(4) may be used to obtain a reasonable standard of comparison for the data.

There are two cases in which lack of knowledge of the coupling scheme does not qualify the application of eq. (4). For zero spin target nuclei, the coupling does not enter, and eq. (4) becomes

$$r_a^2 = \frac{2j+1}{2(2l_n+1)}, \tag{4'}$$

where j is the total angular momentum of the captured neutron in the final state. In the special case of M1 transitions for zero spin targets, the expressions given in ref. [4]) and [5]) show that r_a is expected to be independent of a.

2.2. COMPARISON WITH DATA

Reliable (d, p) data exists for many (but not all) of the easily available target nuclei below $A = 60$. However, as is well known, the extraction of reduced widths from the data is open to question, particularly with regard to absolute values. This difficulty is lessened by comparing only reduced widths associated with a given value of l_n. One may hope that such experimentally obtained ratios will represent the ratios of the reduced widths. Another ambiguity exists with regard to the statistical factor, since often the spins of the final states are not known. Therefore the quantity Ω_{dp} is listed, defined as the relative reduced width times $2J_a+1$. These quantities are taken directly from the papers cited.

Measurements of the spectra of gamma rays emitted after thermal neutron capture have been summarized recently by the two groups most active in the field [6, 7]). Again, problems occur in the extraction of the matrix elements from the data. Since few coincidence data are available, certain ambiguities in the decay schemes exist. These decay schemes used in the present analysis are essentially the same as those tabulated by Groshev *et al.* [6]).

A second difficulty is presented by the possibility of mixed multipole order of the γ-rays, in which case the reduced widths cannot be extracted from the extant data. The parity of the ray is fixed by the (d, p) results as $(-)^{l_n}$, but multipole order is not uniquely determined. However, for l_n odd, magnetic radiation must compete with electric radiation of lower order. Therefore, an E1 assignment is made to those γ-rays which terminate in an $l_n = 1$ level. For the special case of $l_n = 0$ proton groups produced from even target nuclei, only M1 radiation is allowed. The present survey is limited to these two unambiguous cases. When the target nucleus has a spin, conserva-

TABLE 2

Even target nuclei

Final nucleus	$\sum_i I_{\gamma i}$	l_n	E_{ex} (MeV)	Ω_{dp}	$\Omega_{n\gamma}$	$\Omega_{n\gamma}/\Omega_{dp}$	Experimental $\left(\frac{r_a}{r_b}\right)^2_{max}$	Theoretical $\left(\frac{r_a}{r_b}\right)^2_{max}$	(d, p) reference
C^{13}	1	1	0	100	100	1	46	2	[10])
			3.68	57	2600	46			
Mg^{25}	0.97	0	0.58	100	100	1	2.9	1	
			2.56	48	140	2.9			
			5.27	18	<7900				[11])
			5.49	250	<21000				
		1	3.41	100	100	1	2.5	2	
			4.27	28	69	2.5			
			5.79	<16	<250				
Si^{29}	0.72	1	4.93	100	100	1	5.0	2	[12])
			6.38	34	170	5.0			
S^{33}	0.81	1	3.22	100	100	1			
			4.21	12	25	2.1	2.6	2	[13])
			4.91 / 4.94	6.2	<3.5				
			5.71	69	180	2.6			
Ca^{41}	0.60	0	2.68	100	100	1	1.8	1	
			3.41	118	196	1.8			[13]), [14])
		1	1.95	100	100	1	6.5	2	
			2.47	34	22	0.65			
			2.97	2.2	<6.4				
			3.62	6.4	<24				
			3.74	4.0	<26				
			3.95	40	170	4.2			

TABLE 3

Target nuclei not even

Final nucleus	$\sum_i I_{\gamma i}$	l_n	E_{ex} (MeV)	Ω_{dp}	$\Omega_{n\gamma}$	$\Omega_{n\gamma}/\Omega_{dp}$	Experimental $\left(\frac{r_a}{r_b}\right)^2_{max}$	Theoretical $\left(\frac{r_a}{r_b}\right)^2_{max}$	(d, p) reference
Li^7	?	1	0	100	100	1	1.5	6	[10]
			0.48	67	100	1.5			
Be^{10}	1	1	0	100	100	1	2	11.6	
			3.37	71	36	0.51			[10]
B^{11}	?	1	0	100	100	1	300	3.3	
			2.14	18	<190				
			4.46	32	9700	300			[10]
			5.03	10	<1700				
			6.76, 6.81	118	>1700 but <57000	>15 but <500			
N^{15}	0.91	1	0	100	100	1	57	6	[10]
			6.33	36	2020	57			
F^{20}	0.86	1	5.04, 5.19	100	100	1			
			5.27	110	710(?)	6.5(?)	6.5	15	[10]
			5.87, 5.95	820	≈1250	1.5			
Al^{28}	0.72	1	3.46	100	100	1			
			3.59	130	50	0.41			
			3.88	38	130	3.4	7.8	4.2	[15]
			4.69	200	230	1.1			
			4.76	160	390	1.9			
			4.90	100	≈110	1.1			
			5.13	110	350	3.3			
P^{32}	0.65	1	3.26, 3.32	100	100	1			
			4.03	110	240	2.1			
			4.43	13	<180		7.9	15	[16]
			4.90	62	96	1.6			
			5.37	87	210	2.4			
			5.53	25	200	7.9			
			5.82	100	<1400				
			6.09	38	<250				
			6.34	13	<730				

TABLE 3
(continued)

Final nucleus	$\sum_i I_{\gamma i}$	l_n	E_{ex} (MeV)	Ω_{dp}	$\Omega_{n\gamma}$	$\Omega_{n\gamma}/\Omega_{dp}$	Experimental $\left(\frac{r_a}{r_b}\right)^2_{max}$	Theoretical $\left(\frac{r_a}{r_b}\right)^2_{max}$	(d, p) reference
K^{40}	0.49	1	1.64	0.47	2.2				
			2.04	100	100	1			
			2.06						
			2.10	32	29	0.91			
			2.19	0.61	?				
			2.29	0.55	21	38			
			2.42	2.3	<71				
			2.62	18	30	1.7			[17] †
			2.66	2.8	<13				
			2.74	8	62	7.7			
			2.80						
			3.02	1.6	26	16			
			3.14	24(?)	16	0.67	42	11.6	
			3.23	1.4	?				
			3.27	5	?				
			3.37	0.27	<40				
			3.48	7.7	<43				
			3.56	1.6	<45				
			3.60	42	72	1.7			
			3.77	3.1	<53				
			3.87	25	140	5.6			
			3.92	1.6(?)	<60				
			4.10	21	140	6.7			
			4.25	52	78	1.5			
			4.40	29	180	6.4			
			4.46	30	<71				
			4.54	16(?)	<76				
			4.66	8(?)	<85				
			4.80	12	<130				
			4.90	9	<180				

† Recent data [34]) seem to be in fair agreement.

tion of angular momentum and parity may allow two values of l_n to a final state. Though eq. (3) is valid for each l_n separately, the reduced γ-ray intensities for each l_n separately cannot be simply obtained. Such cases (e.g., Co^{59}) are not discussed.

As in the case of the proton groups, the determination of the statistical factor requires knowing the spin of the final state. Therefore the quantity $\Omega_{n\gamma}$, proportional to the product of the matrix element by $2J_a+1$, is obtained merely by dividing the observed γ-ray intensity by the cube of the γ-ray energy for levels characterized by $l_n = 0$ or 1.

The comparison, using all the relevant data known to the author, is shown

in two tables. In table 2 are listed the final nuclei produced from even targets. All the levels are included for which an $l_n = 0$ or 1 (d, p) reduced width is available, unless only one such level of a given l_n is known. Table 3, for target nuclei not even, lists all levels for which $l_n = 1$ comparisons can be made. For each radiating nucleus is listed the relative Ω_{dp} and $\Omega_{n\gamma}$ for the levels shown. For each l_n, these Ω's are arbitrarily normalized to the lowest energy state compared. An indication of the accuracy of the γ-ray decay scheme is given by the sum, denoted $\sum_i I_{\gamma i}$, of the absolute intensities in photons per neutron captured for *all* the initial radiations, whether or not these transitions are listed in the tables. The departure of this sum from unity signifies either that significant features of the decay scheme are not understood, or that an appreciable amount of the initial radiation lies in the continuum underlying the resolved peaks. The resolution is generally better in the (d, p) reactions; for many levels only weak proton groups are observed, and no γ-rays. In these cases, an upper limit has been placed on the γ-ray intensity from cursory inspection of the published data.

The seventh column of the tables gives the ratio $\Omega_{n\gamma}/\Omega_{dp}$. The ratio of the experimentally obtained reduced widths, $\gamma^2_{n\gamma}/\gamma^2_{dp}$, is given by

$$\gamma^2_{n\gamma}/\gamma^2_{dp} = g(\Omega_{n\gamma}/\Omega_{dp}), \tag{5}$$

where g is constant. The factor g is independent of the spin of the final state J_a since each Ω is proportional to $2J_a+1$. The numerical value of g is not important since it drops out when two final levels are compared.

In the 8th column of the tables is listed the experimental $(r_a/r_b)^2_{max}$, which is obtained by dividing the largest $\Omega_{n\gamma}/\Omega_{dp}$ in the previous column by the smallest. The 9th column lists the limit to $(r_a/r_b)^2$ obtained from eq. (4).

The adequacy of the unique-parent description is obtained by comparing the range of $\Omega_{n\gamma}/\Omega_{dp}$ given in columns 8 to the leeway permitted by eq. (4), as given in columns 9. The accuracy of the experimental $\Omega_{n\gamma}/\Omega_{dp}$ is difficult to ascertain. In view of uncertainties in stripping theory, a 30 % estimate of error in relative Ω_{dp} may be optimistic when the energy difference in the final levels is large. The error in $\Omega_{n\gamma}$ is the error in relative γ-ray intensities. Judging from the comparisons available in refs.[6]) and [7]), from which the (n, γ) data are taken, this uncertainty is also of the order of 30 %. Thus, the error in the values in columns 7 may be as large as 50 %, although smaller in favourable cases. In making the comparisons with columns 9, it must be recalled that eq. (3) applies to table 3 only in the limit of extreme jj-coupling; nevertheless, it is felt to be a reasonable test to ascertain whether the assumptions of the theory are fulfilled.

The comparison can be sharpened in the cases in which the spins of the levels have been measured. The comparison involves the use of configurations suggested [8]) for specific levels in both extreme couplings. For Li^7 levels

$(r_{\text{excited}}/r_{\text{ground}})^2$ must lie between $\frac{1}{8}$ and $\frac{3}{2}$; for the Be^{10} levels the range is 3 to $\frac{25}{3}$. For C^{13} and N^{15}, *LS*-coupling yields 2 and 1, respectively, while 0 is obtained in *jj*-coupling since the configuration of the excited states does not have the target nucleus as parent.

2.3. INTERPRETATION

It must be admitted that, for target spins $\frac{1}{2}$ and $\frac{3}{2}$, the range allowed $(r_a/r_b)^2$ by eq. (4) is so large that agreement is practically forced by the limited range of intensities measurable. Therefore the criterion is of no great significance for F^{20}, P^{32} and K^{40} in table 3. Considering the known spins of the Be^{10} states, the consequences of the simple theoretical assumptions fail satisfaction by a factor of at least three. For C^{13} in table 2, and B^{11} and N^{15} in table 3, the criterion is violated by a large factor, indicating that neither initial nor final states are simple. It is interesting to note that just for the last three nuclei has resonance capture been suggested on independent grounds. In these cases, it appears necessary to attack the neutron capture with the full armory of dispersion theory, as has been done for C^{13} by R. G. Thomas [9]).

For Mg^{25}, Si^{29}, S^{33} and Ca^{41} in table 2, and Li^7 and Al^{28} in table 3, when one considers the 70 % errors in the numbers in columns 8, eq. (4) is approximately satisfied. We shall consider that these states satisfy the unique-parent assumption. This means that either the initial or the final states are reasonably well represented as a neutron moving about the target nucleus as a core. Indeed, it is conceivable that both initial and final states may be of this type. Such a situation would correspond to a direct process, wherein the capture radiation is emitted as the neutron transits from initial to final state in the presence of the target nucleus. To inquire further into this possibility we turn to consideration of the cross sections expected for direct capture.

3. Cross Section for Direct E1 Capture

3.1. THEORETICAL

The term "direct capture" will signify here that the radiation is emitted in a neutron transition from an initial $s_{\frac{1}{2}}$ state to a final p_j state by an interaction with a potential well which represents the target nucleus. The cross section for such a process has been given by Breit and Yost [18]), and may be written

$$\sigma = \frac{2(2j+1)}{9\hbar v}\left(\frac{E_\gamma}{\hbar c}\right)^3\left(\frac{eZ}{A+1}\right)^2 |\gamma_{n\gamma}|^2; \quad \gamma_{n\gamma} = \int_0^\infty \varphi_f^* r \varphi_i r^2 \mathrm{d}r. \tag{6}$$

In this equation, v is the relative velocity, E_γ is the energy of the capture γ-ray, and Z and A refer to the target nucleus. The symbols φ_i and φ_f

represent the radial parts of the initial and final wave functions, respectively. As suggested by Shut'ko and Zaretskii [19]), the radial integral can be estimated by the device of Courant [20]): the electric dipole operator r is replaced by $-\omega^{-2}\ddot{r}$, and $\ddot{r}$ is equal to the negative of the potential gradient divided by the reduced mass μ. For a square well, the potential gradient is a delta function, so that the integral is replaced by the value of the wave function at the nuclear surface. If a square well potential of depth V_0, radius R is assumed,

$$\gamma_{n\gamma} = \frac{\hbar^2}{\mu}\frac{V_0 R^2}{E_\gamma{}^2}\varphi_1(R)\varphi_f{}^*(R). \tag{7}$$

The last factor, $\varphi_f{}^*(R)$, is intimately related to the reduced width of the final state, which is just the matrix element in the (d, p) reaction, γ_{dp}^2. Following R. G. Thomas [21]),

$$|\varphi_f(R)|^2 = \frac{N^2}{R^3};\ N^2 = \frac{\gamma_{dp}^2(2\mu R/\hbar^2)}{1+\varepsilon\gamma_{dp}^2(2\mu R/\hbar^2)};\ \varepsilon = \frac{\rho+2}{2(\rho+1)^2};\ \rho = \left(\frac{2\mu E_\gamma}{\hbar^2}\right)^{\frac{1}{2}} R. \tag{8}$$

If the (d, p) cross section has been measured, we shall evaluate $|\varphi_f(R)|^2$ from the experimental (d, p) reduced widths. If not, a reasonable upper limit can be obtained by putting N^2 equal to unity, approximately equivalent to assuming the final state to be a pure single particle state (width equal to $\hbar^2/2\mu R$). The factor ε contributes a correction less than 10 % for the instances of measured γ_{dp}^2.

For the initial state, one can follow the prescription [22])

$$\varphi_1(r) = \frac{i\sqrt{\pi}}{kr}\{\exp(-ikr) - \eta_0 \exp(ikr)\},\quad r \geqq R, \tag{9}$$

where only the s-wave part of the general relation is written, since only low energy neutrons are considered. (A factor $(4\pi)^{-\frac{1}{2}}$ has been absorbed in obtaining the statistical factor of eq. (6).) We note that, in contrast to higher momentum partial waves, eq. (9) is not restricted to the asymptotic region. Exploiting the connection between the complex reflection coefficient η_0 and the logarithmic derivative at the nuclear surface, $f_0 = f_1 + if_2$, one may write

$$|\varphi_1(R)|^2 = \frac{4\pi}{f_1{}^2 + (f_2 - x)^2};\quad x = kR = \frac{\mu v}{\hbar}R. \tag{10}$$

In the spirit of a direct capture process as defined above, the quantities f_1 and f_2 have been evaluated by using the optical model [23]). This model has given a good representation of the neutron cross section data averaged over resonances in the region from $A = 20$ to $A = 80$ when the target nucleus is represented as a complex square well potential with depth $V_0 = 42$ MeV, $R = 1.45\,A^{\frac{1}{3}} \times 10^{-13}$ cm, and absorption coefficient $\zeta = 0.03$. A graph of

eq. (10) in the limit $x = 0$ with these parameters is shown in fig. 1. The maxima of eq. (10) coincide with maxima of the s-wave strength function.

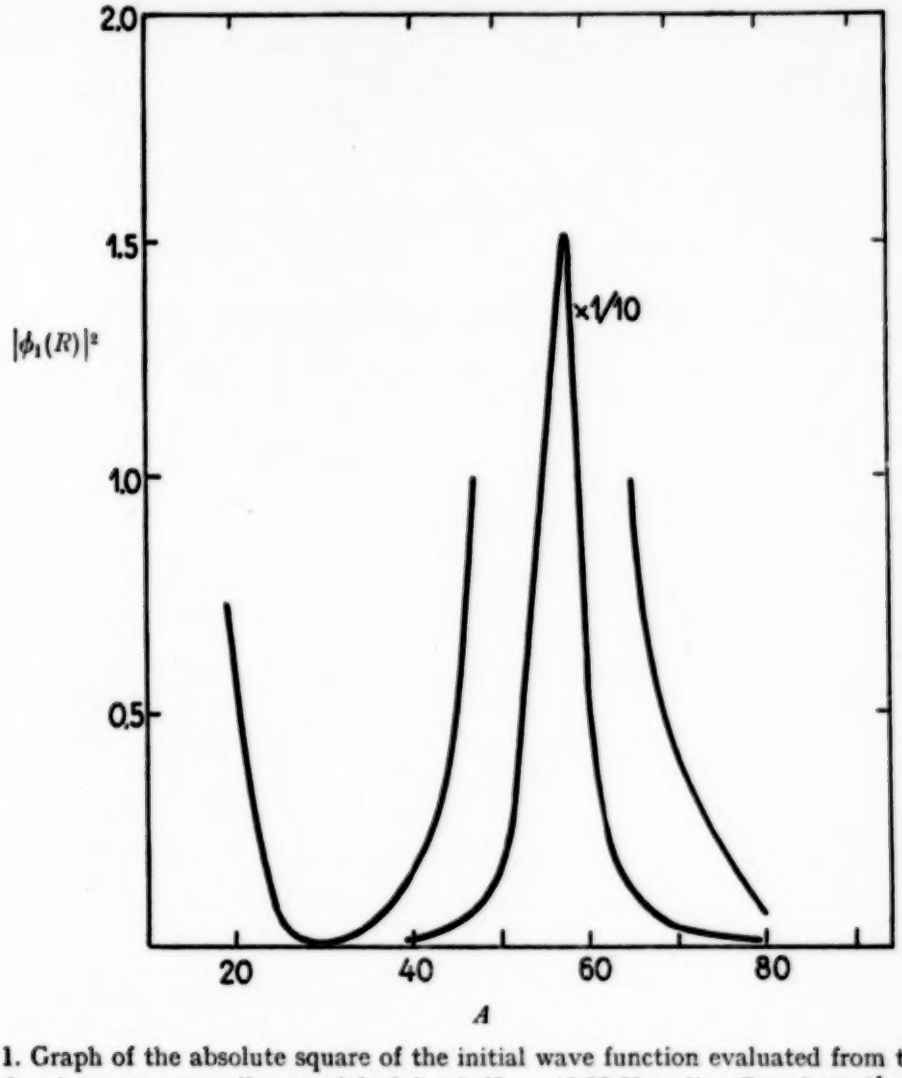

Fig. 1. Graph of the absolute square of the initial wave function evaluated from the optical model, using a square well potential of depth $V_0 = 42$ MeV, radius $R = 1.45\, A^{\frac{1}{3}} \times 10^{-13}$ cm, and absorption coefficient $\zeta = 0.03$.

3.2. COMPARISON WITH EXPERIMENT

The comparison with experiment is given in tables 4 and 5. The insertion of eqs. (7) and (8) into (6) yields the numerical expression

$$\sigma = 1.11 \left(\frac{Z^2}{A(A+1)}\right) \frac{R}{E_\gamma} |\varphi_1(R)|^2 N^2 (2j+1) \times 10^{-24}\ \text{cm}^2, \qquad (11)$$

where R is in units of 10^{-13} cm and E_γ in MeV, and $|\varphi_1(R)|^2$ may be read from fig. 1. Table 4 lists those E1 gamma rays for which (d, p) reduced widths are available. These reduced widths have been extracted from the

TABLE 4

Predicted direct cross sections for states with known reduced widths

Final nucleus	E_{ex} (MeV)	$\gamma^2_{dp}/(\hbar^2/2\mu R)$	theoretical σ (mb)	Experimental σ (mb)
Li^7	0	0.18	7.4	16
	0.48	0.27	5.9	12
Be^{10}	0	0.21	90	7.4
	3.37	0.03	27	2.5
C^{13}	0	0.21	840	2.5
	3.68	0.06	1970	0.8
N^{15}	0	0.14	950	9
	6.33	0.009	950	13
F^{20}	5.27	0.011	22	3.6
Mg^{25}	3.41	0.084	7.8	22
	4.27	0.048	2.9	5
Al^{28}	3.46	0.004	0.064	13
Si^{29}	4.93	0.093	0.71	36
	6.38	0.084	0.54	13
Ca^{41}	1.95	0.059	7.9	120

data cited earlier without correction for Coulomb effects and may be underestimated by factors as large as 5 [24]). Table 5 lists the gamma rays identified as E1 by an $l_n = 1$(d, p) angular distribution [6]), but for which no reduced widths are available. Also included are transitions between initial and final states, which satisfy the E1 selection rules. The limit listed in column 3 is obtained by setting $N^2 = 1$ in eq. (11).

3.3. DISCUSSION

From derivation it is clear that eq. (11) is of limited applicability. The representation of the light nuclei in terms of a potential well is suspect. Use of the Courant device restricts eq. (11) to cases when the potential changes rapidly at the nuclear surface. In addition, the optical model with the parameters used does not seem to apply accurately for $A < 20$. The very large theoretical cross sections in the region of $A = 13$ arise from a maximum in $|\varphi_1(R)|^2$ not plotted in fig. 1. In the face of these objections, it is best to ignore the predictions of eq. (11) for $A < 20$.

It is believed that, for $A > 20$, eq. (11) will give a reasonable estimate for final states bound by at least several MeV. We note that the two levels in Mg^{25}, which satisfied eq. (4), are also in reasonable agreement with the direct capture process when we remember that the (d, p) reduced widths should probably be increased. However, for Al^{28}, Si^{29}, S^{33} and Ca^{41}, which also satisfied eq. (4), the direct cross sections are too small to be accounted for by inaccuracy in the reduced widths. Thomas [21]) has noted that neutron capture by Li^7 can be explained entirely by the extra-nuclear contribution to the

TABLE 5

Theoretical limit to direct cross sections

Final nucleus	E_{ex} (MeV)	Theoretical max. $\sigma/(2i+1)$ (b)	Experimental σ (b)
Li^{8}	0	0.087	0.033
B^{11}	0	0.16	?
	4.45	0.33	
	6.76	0.39	
P^{32}	3.22+3.26	0.0015	0.019
S^{33}	3.22	0.0030	0.29
K^{40}	2.04	0.029	0.21
Ti^{49}	1.38	0.20	3.2
	1.72	0.20	2.4
V^{52}	0	0.49	0.26
	0.78	0.55	0.54
	1.55	0.63	0.33
Cr^{53}	0	0.79	0.37
	0.56	0.85	0.10
	2.31	1.1	0.073
	2.66	1.2	0.029
Cr^{54}	0	0.86	2.3
	0.84	0.95	6.5
	2.67	1.2	1.1
Mn^{56}	0	1.9	1.63
Fe^{55}	0	1.3	1.2
	0.41	1.4	0.13
Fe^{57}	0	2.3	0.90
	1.24	2.7	0.018
Fe^{58}	0	1.6	0.12
Co^{60}	0	1.7	1.0
Ni^{59}	0	2.1	1.80
	0.46	2.2	0.77
	1.75	2.6	0.042
	2.15	2.8	0.68
Ni^{61}	0	0.89	1.00
	0.28	0.91	0.85
	1.19	1.0	0.43
Cu^{64}	0	0.34	1.12
	0.277	0.35	0.56
Cu^{66}	0	0.17	0.32
Zn^{67}	0.092	0.16	0.10
	0.388	0.17	0.02
Zn^{68}	1.08	0.093	0.1
Zn^{69}	0	0.11	0.055

matrix element, a statement consistent with the entry in table 5, but possibly in accidental agreement.

The largest cross sections for direct E1 capture will occur when a maximum in $|\varphi_1(R)|^2$ is accompanied by low lying p-states. Examination of fig. 1 shows that the most likely region lies between $A = 45$ and $A = 65$. Un-

fortunately, no (d, p) reduced widths are known for these nuclei, and eq. (11) can therefore be used only to obtain an upper limit, as given in table 5. We note that if $j = \frac{3}{2}$, an experimental cross section which does not exceed $\frac{1}{2}$ of the entry in column 3, table 5, can be considered as direct without requiring a large reduced width for the final state. It is clear that many of the states cited from V to Zn are excellent candidates for direct capture. This is just the region in which Lynn and Lane [25]) have suggested that direct capture might dominate compound nucleus capture.

One other observation may be taken as fairly clear evidence for resonance capture. Single-particle $s_{\frac{1}{2}} \rightarrow s_{\frac{1}{2}}$ transitions are strictly forbidden in a well arising from central velocity-independent forces [26]), and introduction of the usual $\mathbf{l} \cdot \boldsymbol{\sigma}$ velocity dependence will not help. Therefore, for zero spin targets, the observation of reasonably strong capture gammas proceeding to levels formed by $l_n = 0$ neutrons in the (d, p) reaction suggests that a resonance is involved. Several such cases are listed in table 2. While direct E1 capture would occur even in the absence of resonance, there would seem to be no compelling reason that a resonance would not also contribute to the E1 radiation. This comment is not applicable to Mg^{25}, since the target nucleus is not spherical.

3.4. HEAVIER NUCLEI

As a preliminary to the application of eq. (11) to heavier nuclei, we recall that the reflection coefficient η_0 can be written in terms of cross sections. A scattering length R' may be defined in terms of the scattering cross section σ_{sc} as

$$R' \equiv \lim_{k \to 0} (\sigma_{sc}/4\pi)^{\frac{1}{2}}, \tag{12}$$

where k is the wave number of the incident neutron. We can also define an absorption length δ by

$$\delta \equiv \lim_{k \to 0} (k\sigma_{abs}/4\pi). \tag{13}$$

Using the well-known relations between η_0 and these cross sections, eq. (10) can be written

$$|\varphi_1(R)|^2 \xrightarrow[k \to 0]{} 4\pi\{1+(R'/R)^2-2[(R'/R)^2-(\delta/R)^2]^{\frac{1}{2}}\}. \tag{14}$$

We note that, if $\delta \ll R'$, this reduces to the well-known form

$$|\varphi_1(R)|^2 \xrightarrow[k \to 0]{} 4\pi\{1-R'/R\}^2. \tag{15}$$

Shut'ko and Zaretskii [19]) have used the Courant device, eq. (7), to obtain an estimate of the direct capture cross section for formation of the ground state of Pb^{208}. Their estimate of $|\varphi_1(R)|^2$ is just eq. (8) with $N^2 = 1$, while, with the insertion of the experimental value of R', eq. (15) was used for the initial state. Using $R = 1.35A^{\frac{1}{3}} \times 10^{-13}$ cm, $R' = 9.6 \times 10^{-13}$ cm, and $V_0 =$

42 MeV, eq. (11) gives a cross section of 0.24 b for $j = \frac{1}{2}$. This is a factor of two smaller than the published estimate because of a difference in the statistical factor. We prefer to utilize the complete eq. (14), employing the optical model for the calculation of R' and δ. From its definition,

$$\delta = (\pi/2k_0)(\overline{\Gamma_n^0/D}). \tag{16}$$

Here, $\overline{\Gamma_n^0/D}$ is the s-wave strength function normalized to 1 eV neutron energy, and k_0 is the wave number of a 1 eV neutron, 2.14×10^9 cm^{-1}. With $V_0 = 42$ MeV, $R = 1.35\times A^{\frac{1}{3}}\times 10^{-13}$ cm, and $\zeta = 0.03$, one obtains $R' = 9.3\times 10^{-13}$ cm, $\delta = 0.58\times 10^{-13}$ cm, and a cross section of 0.17 b. It is clear that direct capture may give a significant contribution to the experimentally measured cross section of 0.70 b.

The probability for direct capture being largest at maxima of the s-wave strength function, the rare-earth region is most likely to supply examples. For application to deformed nuclei, the estimate must be reconsidered, since the wave functions used above are not appropriate. In a spheroidal well, the wave functions can be written as linear combinations of several values of l. Further, Magolis and Troubetzkoy [27]) have shown that even for low energy neutrons the waves of $l > 0$ (restricted to even l by parity conservation) participate. The electric dipole operator can have non-zero matrix elements connecting the $l > 0$ components in the initial wave function to the final state. The partial waves at the nuclear surface have values of the order of $\varepsilon^{\frac{1}{2}l}$, ε being the nuclear eccentricity. For nuclear eccentricities as large as 0.2, the contribution of matrix elements associated with $l > 0$ may not be negligible. Nevertheless, to obtain the rough estimate envisioned, matrix elements from partial waves with $l > 0$ will be neglected.

The most important effect of the $l > 0$ waves is to modify strongly the value of η_0 in the initial wave function. Employing eq. (14), we can use the calculations of Chase, Wilets and Edmonds [28]) to account for the modification in η_0 and obtain $|\varphi_1(R)|^2$. These authors calculate R' and $\overline{\Gamma_n^0/D}$, using a deformed tapered well with mean radius equal to $1.35\,A^{\frac{1}{3}}\times 10^{-13}$ cm and a surface thickness of 2.2×10^{-13} cm. Application of the Courant device in this connection requires the additional assumption that $\varphi_1\varphi_l r^2$ averaged over the surface layer is equal to the value of that same function at the midpoint of the interval. Fig. 2 is a plot of $|\varphi_1(R)|^2$ as obtained from eqs. (14) and (16), using the values of $\overline{\Gamma_n^0/D}$ and R' taken from figs. 14 and 15 in ref. [28]).

Since no information is available on the reduced widths of the final states, only an upper limit to the direct capture cross section can be obtained, by setting $N^2 = 1$. In the following, the statistical factor $2j+1$ has been equated to three. While no extensive comparison with the data is given here, a few points of interest may be mentioned:

(1) The maxima in the limiting cross sections occur at $A = 147$ and

$A = 182$. In Nd^{147} the limit for production of a 5 MeV E1 gamma ray would be 1.90 b. Unfortunately the gamma ray spectrum for this nucleus has not been measured. For the ground state of W^{184} the limit is 0.57 b. The observed cross section is 0.55 b.

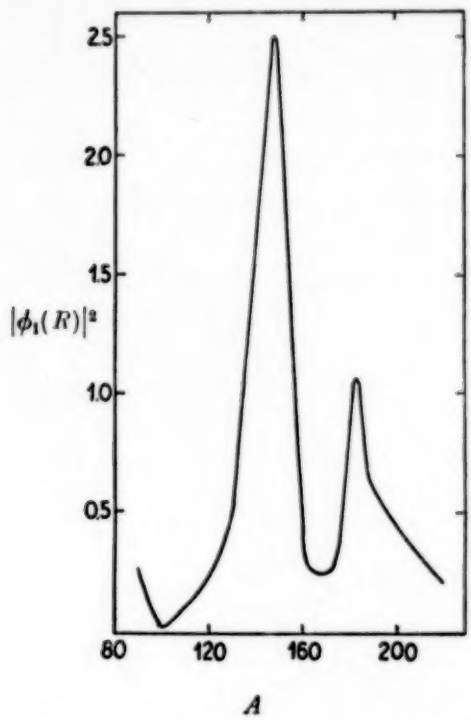

Fig. 2. Graph of the absolute square of the initial wave function evaluated from the optical model, using the results of Chase, Wilets and Edmonds [28]). The calculations employed a diffuse, deformed well of mean radius $1.35\,A^{\frac{1}{3}} \times 10^{-13}$ cm, surface thickness of 2.2×10^{-13} cm, depth 44 MeV, absorption coefficient 0.05, with deformations consistent with the observed quadrupole moments.

(2) For many other heavy nuclei, not necessarily in the immediate neighbourhood of the maxima, the direct capture limits are of the same order of magnitude as the observed cross sections. Examples are:

La^{140} ground state, $\sigma_{exp} = 1.0$ b, $\sigma_{11m} = 1.3$ b;
Ta^{182} ground state, $\sigma_{exp} = 0.2$ b, $\sigma_{11m} = 0.7$ b;
Pt^{196} ground state, $\sigma_{exp} = 0.11$ b, $\sigma_{11m} = 0.26$ b.

(The observed cross sections quoted assume that the resolved structure at the high energy end of these gamma-ray spectra are indeed single gamma rays.)

(3) Gamma radiation produced by direct capture can be a valuable tool for the identification of the final states, particularly in the case of nuclei for which K is a good quantum number. Since direct capture implies that the target nucleus is parent to the final state, direct E1 capture cannot produce states in the final nucleus unless $|K_1 - K_f| \leqq \frac{3}{2}$ and the vibrational quantum

number does not change. For example, direct E1 capture by $H^{177}(I = K = \frac{7}{2}^-)$ cannot form a state in the ground state rotational band of $Hf^{178}(K = 0^+)$. Unfortunately, the data are in disagreement here. Ignoring the selection rule, the limiting cross section for the production of the 4^+ level at 0.31 MeV is 0.31 b. Groshev *et al.*[29]) report an upper limit of 0.06 b, but Campion and Bartholomew [30]) give a cross section of 0.34 b for the production of a 7.33 MeV gamma ray. When the direct process dominates, it is possible to predict relative intensities of gamma rays terminating in levels of a given rotational band. This calculation has been done [31]) for Mg^{25} levels produced in the (d, p) reaction and applies in detail to the (n, γ)-process as well. The observed reduced intensities cited in table 2 are in qualitative agreement with the prediction.

4. Summary

The intensities of thermal neutron capture γ-rays are closely related to those of proton groups from a (d, p) reaction [eqs. (3) and (4)] if either the initial or the final state in each reaction can be written as a simple product of wave functions representing the target and the incident neutron separately. Clear violation of the predicted relation is found for residual nuclei B^{11}, C^{13} and N^{15}. For these nuclei, stripping theories adequately describe the measured angular distributions; on the other hand, the variation of the capture cross section with neutron energy suggests resonant capture, i.e., a complicated initial state wave function. Presumably, violation of eq. (4) occurs because neither the wave function of the radiating system nor the final wave function contains the target nucleus as a simple factor.

For residual nuclei Li^7, Mg^{25}, Al^{28}, Si^{29}, S^{33} and Ca^{41}, eq. (4) is satisfied. While simplicity in the final state wave function is sufficient explanation, it would be possible, if only this evidence were considered, that the intial state is also a simple product. Factorizability of both states corresponds to direct capture of the neutron without the intervention of a complex intermediate state. This hypothesis is tested by comparing the measured cross section to a theoretical expression [eq. (11)] evaluated with the help of the optical model. With the exception of Li^7 and Mg^{25}, the experimental cross sections for the last-mentioned nuclei are considerably larger than the theoretical. The optical model is not applicable to Li^7.

Further tests in the region most favourable for direct capture (A = 45—65) await the measurement of (d, p) cross sections for relatively pure $l_n = 1$ proton groups. Recent work similar to that of Bowcock [32]) permits the hope that reliable absolute reduced widths may be extracted from such data. Lacking knowledge of these reduced widths, no definite assignments of direct capture can be made. However, it is pointed out that the measured

cross sections in the region $A = 45$—65, and also for heavier elements, are compatible with direct E1 capture in that they do not imply anomalously large reduced widths for the final states.

The present paper presents only a phenomenological estimate of direct capture cross sections. A complete study must be built on the framework of dispersion theory, for only in this way can one hope to understand the relationship between resonant and direct capture [33]). The purpose here is to point out that there may be many instances in which the direct process plays a dominant role in thermal neutron capture. It is important to recognize these cases, not only for the understanding of capture cross sections, but also because the mechanism provides a simple means whereby the study of γ-rays following slow neutron capture can make important contributions to the spectroscopy of bound levels not accessible by radioactive decay.

The author would like to thank Professor Niels Bohr for the opportunity to share the stimulating atmosphere of this Institute. Several discussions with Professor A. Bohr, A. M. Lane, and B. Elbek were extremely helpful; the application of the optical model resulted from one of them. R. Sorensen, L. Kisslinger, and L. C. Biedenharn contributed illuminating remarks. Careful reading of the manuscript by T. Ericson and R. E. Bell helped its author to clarify the presentation.

References

1) Kinsey, Bartholomew and Walker, Phys. Rev. **83** (1951) 519
2) Groshev, Demidov, Lutsenko and Pelekhov, paper 15/P/2029, Geneva Conference (1958)
3) A. M. Lane and D. H. Wilkinson, Phys. Rev. **97** (1955) 1199
4) A. M. Lane and L. A. Radicati, Proc. Phys. Soc. A **67** (1954) 167
5) A. M. Lane, Proc. Phys. Soc. A **66** (1953) 977
6) Groshev, Demidov, Lutsenko and Byelekov, Atlas of Gamma Ray Spectra from the Capture of Thermal Neutrons (Moscow, 1958)
7) G. A. Bartholomew and L. A. Higgs, A.E.C.L. 669, Chalk River, Ontario (1958)
8) D. R. Inglis, Revs. Mod. Phys. **25** (1953) 390
9) R. G. Thomas, Phys. Rev. **88** (1952) 1109
10) F. Ajzenberg-Selove and T. Lauritsen, Energy Levels of Light Nuclei VI, Nuclear Physics **11** (1959) 1
11) Hinds, Middleton and Parry, Proc. Phys. Soc. A **71** (1958) 49
12) J. R. Holt and T. N. Marsham, Proc. Phys. Soc. A **66** (1953) 467
13) J. R. Holt and T. N. Marsham, Proc. Phys. Soc. A **66** (1953) 565
14) C. K. Bockelman and W. W. Buechner, Phys. Rev. **107** (1957) 1366
15) H. Enge, L. N. S. Progress Report, Mass. Inst. of Tech. (Nov. 30, 1956)
16) Dalton, Hinds and Parry, Proc. Phys. Soc. A **70** (1957) 586
17) Enge, Irwin and Weaner, L. N. S. Progress Report, Mass. Inst. of Tech. (May 1958)
18) G. Breit and F. L. Yost, Phys. Rev. **48** (1935) 203
19) A. V. Shut'ko and D. F. Zaretskii, JETP **29** (1955) 866; English translation, Soviet Physics JETP **2** (1956) 769
20) E. D. Courant, Phys. Rev. **82** (1951) 703
21) R. G. Thomas, Phys. Rev. **84** (1951) 1061

22) J. Blatt and V. Weisskopf, Theoretical Nuclear Physics (Wiley, New York, 1952) p. 320
23) Feshbach, Porter and Weisskopf, Phys. Rev. **96** (1954) 448
24) Fujimoto, Kikuchi and Yoshida, Prog. Theo. Phys. **11** (1954) 264
25) A. M. Lane and J. E. Lynn, Proceedings of the International Conference on the Neutron Interactions with the Nucleus, T.I.D. 7547, Oak Ridge (1957)
26) S. A. Mozkowski, Beta- and Gamma-Ray Spectroscopy, edited by K. Siegbahn (North-Holland Publishing Co., Amsterdam, 1955) p. 373
27) B. Margolis and E. S. Troubetzkoy, Phys. Rev. **106** (1957) 105
28) Chase, Wilets and Edmonds, Phys. Rev. **110** (1958) 1080
29) Groshev, Demidov, Lutsenko and Pelekhov, Atomnaya Energiya **4** (1958) 5
30) P. J. Campion and G. A. Bartholomew, Can. J. Phys. **35** (1957) 1361
31) Litherland, McManus, Paul, Bromley and Gove Can. J. Phys. **36** (1958) 378
32) J. E. Bowcock, Proc. Phys. Soc. A **68** (1955) 512
33) A. M. Lane, Nuclear Physics **11** (1959) 625
34) Dalton, Parry and Scott, Proc. Phys. Soc. A **73** (1959) 677

1.C *Nuclear Physics* **13** (1959) 224—234; © *North-Holland Publishing Co., Amsterdam*
Not to be reproduced by photoprint or microfilm without written permission from the publisher

BRUECKNER THEORY AND THE SHELL MODEL EFFECTIVE POTENTIAL

E. J. SQUIRES
U.K.A.E.A. *Research Group*, A.E.R.E. *Harwell, Didcot, Berks.*

Received 1 May 1959

Abstract: A discussion is given of the properties of the shell model effective potential obtained from Brueckner theory. Correction terms to the simple picture, in which the effective potential is just the Brueckner t matrix, are indicated explicitly for certain cases and their origin discussed. Analogy with known properties of the t matrix for infinite nuclear matter suggests that some of these corrections are of importance. It is suggested that while there may be some meaning to the concept of a simple effective potential in certain situations, the idea is not of general applicability.

1. Introduction

Brueckner theory [1]) has been applied to the problems of infinite nuclear matter [2]) and finite closed shell nuclei [3]) in their ground states with reasonable success. It is the purpose of this note to indicate some of the predictions of the theory for non-closed shell nuclei (or excited states of closed shell nuclei), in order to see whether the theory provides any justification for the procedures used in shell model calculations, and also to obtain expressions for the shell model effective potential in terms of an assumed nucleon-nucleon potential.

It is well known [1]) that, in lowest order, Brueckner theory does lead to the normal shell model procedures, with the t matrix as the effective potential. The latter, being non-local and velocity dependent, is not so simple as the effective potentials usually used in shell model calculations, but it is possible that these could represent suitable averages over more complicated forms. We shall see, however, that there are corrections to this simple description which are likely to be important. One of the consequences of these corrections is that it is probably not realistic to use the same effective potential in binding energy and single particle energy calculations as in the interactions among several particles outside a closed shell.

2. Corrections to the Simple Picture

Brueckner theory starts from a rearrangement and partial summation of the perturbation expansion of, say, the energy. The perturbation is here the

two-body nucleon-nucleon potential minus the one-body "self consistent" potential. For details we refer to the many papers on the subject [1]). Instead of the original series in the interaction v, a series is obtained in a quantity, denoted by t, which describes the complete iterated interaction of two particles in the nucleus. The equation describing this interaction of two particles in the nucleus, known as the Bethe-Goldstone equation, differs from the free space Schrödinger equation in two ways. First, that part of v which scatters into single particle states which are occupied in the unperturbed ground state is removed. This is an effect of the exclusion principle. Secondly, the two particles move in a single particle potential, which is defined in terms of t in a similar way to the definition of the self consistent potential in the Hartree-Fock method. It is these two differences which give rise to the corrections to the simple picture discussed in the introduction.

The formal definition of the t matrix is

$$\langle l_1 l_2|t|m_1 m_2\rangle = \langle l_1 l_2|v|m_1 m_2\rangle_{\mathrm{A}} + \tfrac{1}{2}\sum_{k_1, k_2} \frac{\langle l_1 l_2|v|k_1 k_2\rangle_{\mathrm{A}}\langle k_1 k_2|t|m_1 m_2\rangle}{E_{m_1}+E_{m_2}-E_{k_1}-E_{k_2}} \qquad (1)$$

where $|l\rangle$, $|k\rangle$ and $|m\rangle$ represent single particle states in the self consistent field and E_l etc. are the energies of these states. The suffix A on the v matrices means that these are antisymmetrised. We use the notation of Hugenholtz [4]), that $m(k)$ refer to states which are occupied (unoccupied) in the unperturbed ground state, and l to either. The self consistent potential is defined to remove all second order contributions to the energy. This requires [1])

$$\langle l'|V|l\rangle = \sum_m \langle l' m|t|lm\rangle, \quad \text{for} \quad l \neq l'. \qquad (2)$$

The condition of removing second order contributions to the energy does not in fact define the diagonal part of V, which is usually fixed by requiring that certain "self consistency" third order terms cancel. This leads to a rather complicated set of equations (ref. [5])) for the diagonal part of V. For the finite nucleus, however, it is not possible to do the complete self consistent calculations and it is usual to assume that some simple choice of V gives a sufficiently good approximation.

Only the first order term in t is usually retained and we have for the ground state "potential energy"

$$E = \tfrac{1}{2}\sum_{m_1, m_2} \langle m_1 m_2|t|m_1 m_2\rangle = \tfrac{1}{2}\sum_m \langle m|V|m\rangle. \qquad (3)$$

We shall throughout omit to write dovn the kinetic energy term which is just the expectation value of the kinetic energy operator in the given states.

The choice of the self consistent potential and the use of the exclusion principle ensures that there are no second order terms in the complete series in t. No very reliable estimates have yet been made of the third order terms

but crude estimates [1]) indicate that they are small. Also, the method gives reasonable results for nuclear matter [2]), which suggests that the neglected terms may be unimportant.

It is important to notice that some of the third order terms have already been included in the expression for the energy. These arise from the self consistent potential parts of the energy denominators in eq. (1). That such third order terms are important for nuclear matter is shown by the work of Brueckner and Gammel [2]). Their inclusion alters the mean binding energy by about 15 MeV. The reason why these particular third order terms are more important than other third order terms is that they use just the diagonal part of t in the intermediate interaction.

Now let us consider a single particle, outside a closed shell, in a state k. In lowest order the energy of this single particle would be just its interaction with all the closed shell nucleons, i.e. we would have

$$E_k = \sum_m \langle km|t|km\rangle = \langle k|V|k\rangle. \tag{4}$$

There are, however, important modifications to this, which can be considered in either of two ways. One way, which will be used in the next section, is to keep the same t matrix for the interaction of the closed shell nucleons, in which case additional terms will occur in the series for the energy. Alternatively, we can regard the additional particle as changing the "medium" in which the interactions take place, and therefore changing the t matrix. We shall use the latter method in this section since it gives the better physical picture.

The change in the "medium" caused by the additional particle has two effects; first, in order to satisfy the exclusion principle, one more state must be excluded as an intermediate state in the interaction of v to form t, and, secondly, the interaction with the extra particle must be included in V. The latter effect leads to a change in the wave-functions, as well as a change in t due to the effect on the energy denominators. This change in wave-functions with fixed t, however, has no first order effect on the energy, since the self consistency condition (eq. (2)) means that the energy is stationary with respect to variations in the wave-functions with t constant. Thus we have to consider only the change in the t matrix. The exclusion principle and self consistent potential effects in the t matrix give rise to corrections to the single particle energy which are of second and third order respectively in t. These corrections are known as the rearrangement energy.

To find an expression for the rearrangement energy we have †

$$E_k = \langle k|V|k\rangle + \tfrac{1}{2} \sum_{m_1, m_2} \langle m_1 m_2|t_{(k)} - t|m_1 m_2\rangle \tag{5}$$

† Discussions similar to this have been given for infinite nuclear matter by Squires [6]) and Thouless [6]).

where $t_{(k)}$ is the t matrix in presence of the extra nucleon in the state k. Since the change introduced in t by the extra particle is small we can write, symbolically,

$$t_{(k)}-t = \Delta_{(k)}t = t\Delta_{(k)}\left(\frac{Q}{e}\right)t \tag{6}$$

where e is the energy denominator and Q an operator which excludes occupied states. Now

$$\Delta_{(k)}\left(\frac{Q}{e}\right) = \frac{\Delta_{(k)}Q}{e} - \frac{Q\Delta_{(k)}e}{e^2} \tag{7}$$

and we have, therefore, for the rearrangement energy,

$$\begin{aligned} R(k) &= \tfrac{1}{2}\sum_{m_1 m_2}\langle m_1 m_2|t_{(k)}-t|m_1 m_2\rangle \\ &= -\tfrac{1}{2}\sum_{m_1,m_2}\sum_{k}\frac{|\langle m_1 m_2|t|kk'\rangle|^2}{E_{m_1}+E_{m_2}-E_k-E_{k'}} \\ &\quad +\tfrac{1}{2}\sum_{m_1,m_2}\sum_{k_1 k_2}\frac{|\langle m_1 m_2|t|k_1 k_2\rangle|^2\langle k|\{\langle k_1|t|k_1\rangle-\langle m_1|t|m_1\rangle\}|k\rangle}{(E_{m_1}+E_{m_2}-E_{k_1}-E_{k_2})^2}. \end{aligned} \tag{8}$$

We must now ask how important these terms are. We note first that, to be consistent with what is done for the closed shell nuclei, they should be included. For nuclear matter, the rearrangement energy is known [6]) from the work of Brueckner and Gammel to be about 15 MeV, which is certainly an appreciable effect. There does not appear to be any reason why it should be significantly smaller for finite nuclei.

Attempts to calculate the rearrangement energy terms explicitly for nuclear matter have been made by Thouless [6]) and Brueckner [7]). These calculations suggest that both the second order (exclusion principle) and third order (self consistent potential) terms contribute appreciably to the effect. We also remark that Brueckner's calculation of the second order contribution, with t replaced by a Yukawa potential, gives only 1.4 MeV, which suggests that the hard core plays a significant role in the rearrangement energy.

The fact that the rearrangement energy is large shows that the effective potential (t) which gives the binding energy correctly does not give correct single particle energies when used in eq. (4). Skyrme [7]) and Squires [6]) have shown how this difficulty can be removed by including a three-body term in the effective potential.

For non-closed shell nuclei the unperturbed states are degenerate and the perturbed states are found by solving a secular equation in the familiar shell model manner. In the simple picture the effective potential is just the t matrix but again corrections to this, having similar origin to the rearrangement energy terms, arise. For example, if we consider two nucleons in

states k_1, k_2 outside a closed shell, corrections to the use of t as the effective potential arise in the following way.

I. Second order (exclusion principle):

(i) The presence of $k_1(k_2)$ alters the exclusion principle operator in interaction of $k_2(k_1)$ with the core nucleons.

(ii) The effect of the exclusion of k_1 and k_2 as intermediate states in the interaction of any two core nucleons has been counted twice: in the rearrangement energies of the single particle levels of k_1 and k_2.

II. Third order (self consistency):

(i) $k_1(k_2)$ affects the self consistent field in the interactions of $k_2(k_1)$ with the core nucleons.

(ii) $k_1(k_2)$ affects the self consistent field in the rearrangement energy part of the single particle level of $k_2(k_1)$.

As these corrections are of similar origin to the rearrangement energy terms they are likely to be important. Without detailed calculation it is not possible to say whether any of them are more important than the others or even whether it is really adequate only to include third order terms. Also, the correction terms are such that they may be expected to affect the splitting of the levels, and not just to give an overall shift.

Explicit expressions for these correction terms could be obtained in the same manner as used to obtain the expression for $R(k)$. However, we shall obtain the results by the more mechanical methods of the next section, and postpone writing them till then.

It is important to notice that the corrections to the effective potential in the case of two particles outside a closed shell bear no simple relation to those which arise in the rearrangement energy. It seems therefore unrealistic to use the effective potential obtained from the binding energies of closed shell nuclei and from single particle energies in the secular equations for degenerate states. This throws doubt on the procedure for finding the effective potential used by Skyrme [7]).

When there are more than two particles outside a closed shell, the effective potential contains the same two-body interaction, together with three, four etc. body interactions between the extra nucleons. Provided the number of particles outside the closed shell is small compared to A, these are likely to give only small effects since their contribution will be $O(1/A)$ or less compared to the contribution of the two body terms. Thus, the two-body interaction obtained for two particles outside a closed shell may have a reasonably wide range of applicability.

3. Diagrammatic Analysis of Correction Terms

Diagrams for the many-body problem were first introduced by Goldstone[8]). We shall use the type of diagram used by Hugenholtz [4]), in which a line to

the left represents a "particle" and line to the right represents a "hole". For the vacuum state we take the nearest closed shell nucleus in its ground state and the exclusion principle operator will always be with respect to this vacuum. A t interaction will be represented by a dot at the vertex [9]). By proper choice of the self consistent field energy denominators, diagrams which are "reducible" in the sense of Hugenholtz [4]) need not be included. Diagrams in which two successive vertices are connected by two particle lines are not to be drawn since these have already been included in the t matrix.

Thus the ground state energy is given by

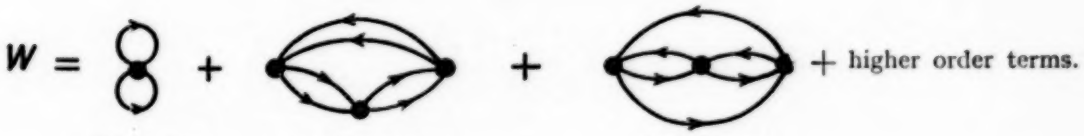

(1st order) (3rd order). (3rd order)

The first order term is just that given in eq. (3).

For single particle energies we have

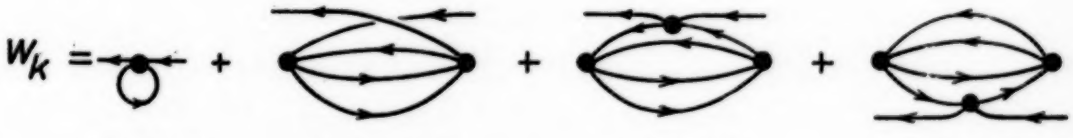

(1st order) (2nd order) (3rd order) (3rd order)

+other third order terms+higher order terms.

The terms drawn are those which are given in eq. (8).

For the case of degenerate nuclei we shall give a few more details since the work is less familiar. The formal treatment of perturbation theory for this case has been given by Bloch and Horowitz [10]) and we shall use their result. We consider a closed shell (c) together with a number p of nucleons in an unfilled shell. The unperturbed ground states of the degenerate nucleus we denote by $|\alpha_0\rangle$ and its excited states by $|\alpha\rangle$. The unperturbed energies of these states are ε_{α_0} (independent of the particular α_0) and ε_α, and the perturbed values are E_{α_0} and E_α respectively. As before the "perturbation" is the difference between the two-body interactions and the self consistent potential.

The energy shift due to the interaction can be separated into two parts, one being the energy of the core alone, which is given by the usual expression for non-degenerate nuclei, and the other, say $\Delta E^{(p)}_{\alpha_0}$, being given by the solution of the secular equation

$$[\Delta E^{(p)}_{\alpha_0} - W(\varepsilon_{\alpha_0} + \Delta E^{(p)}_{\alpha_0})]|\chi_{\alpha_0}\rangle_0 = 0 \tag{9}$$

where $|\chi\rangle_0$ means the projection of $|\chi\rangle$ on the space of the $|\alpha_0\rangle$, and where W is an operator in the space of the $|\alpha_0\rangle$ given by

$${}_0\langle\chi'|W(\varepsilon)|\chi\rangle_0 = {}_0\langle\chi'|V \sum_0^\infty (-1)^s [Q_0(H_0-\varepsilon)^{-1}V]^s|\chi\rangle_{0L}. \tag{10}$$

In eq. (10) the operator Q_0 projects out of the space occupied by the α, L means that only connected diagrams without vacuum parts [9]) are to be included in the sum, and H_0 and V are the unperturbed Hamiltonian and the perturbing interaction respectively.

It is convenient to fix the self consistent potential as being that due to the closed shells alone and to include the effect of the other particles as explicit diagrams. We further separate $\Delta E^{(p)}_{\alpha_0}$ into two parts, $\Delta E^{(s)}_{\alpha_0}$ and e_{α_0}, where $\Delta E^{(s)}_{\alpha_0}$ is the sum of the single particle energy shifts and is therefore independent † of the particular α_0. The interaction term W is also split into a single particle part ($W^{(s)}$) containing those diagrams of eq. (10) in which only one of the p particles interact, and a remainder. Since we require the single particle to be independent of the particular α_0 we write

$$W^{(s)}(\varepsilon_{\alpha_0} + \Delta E^{(p)}_{\alpha_0}) = W^{(s)}(\varepsilon_{\alpha_0} + \Delta E^{(s)}_{\alpha_0}) + e_{\alpha_0}\left[\frac{\partial W^{(s)}(\varepsilon)}{\partial \varepsilon}\right]_{\varepsilon=\varepsilon_{\alpha_0}+\Delta E^{(s)}_{\alpha_0}} \tag{11}$$

and

$$W(\varepsilon_{\alpha_0} + \Delta E^{(p)}_{\alpha_0}) = W^{(s)}(\varepsilon_{\alpha_0} + \Delta E^{(s)}_{\alpha_0}) + w. \tag{12}$$

We then obtain for $\Delta E^{(s)}_{\alpha_0}$ just the sum of single particle energies previously considered. The secular equation (9) becomes

$$(e_{\alpha_0} - w)|X_{\alpha_0}\rangle_0 = 0. \tag{13}$$

The effective potential w contains all the diagrams of eq. (10) in which at least two of the extra p nucleons interact, and it also contains the last term of eq. (11) (which is a third order self consistency term).

We now specialise to the case of two particles outside a closed shell. In this case the diagrams contributing to w are the following:

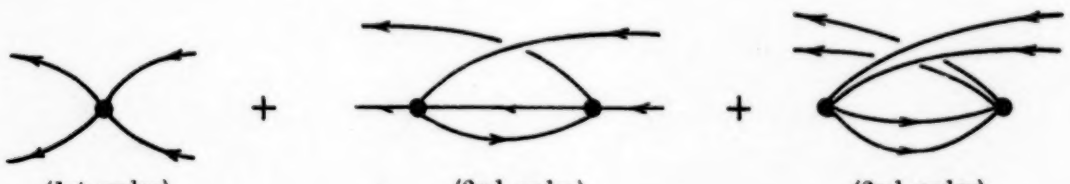

(1st order) (2nd order) (2nd order)

† We are considering the case where the single particle leads are strictly degenerate. Cases of near degeneracy as in 2s and 1d levels require a slight modification of the treatment given.

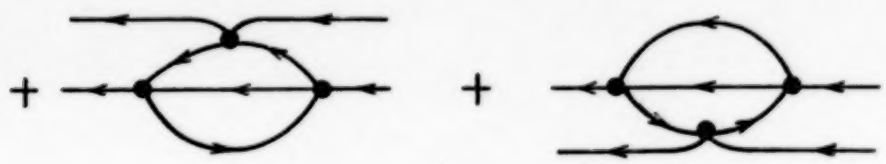

(3rd order)

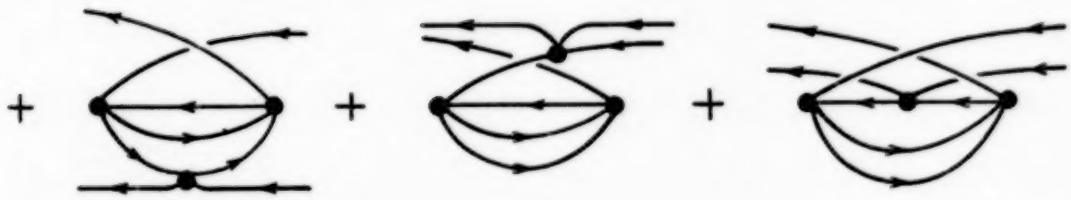

Physically, the corrections correspond, in the order drawn, to those listed in section 2. The contribution to w arising from the last term of eq. (11) combines naturally with the self consistency diagrams. The diagonal matrix element of w corresponding to the above diagrams is given by

$$\begin{aligned}
\langle k_1k_2|w|k_1k_2\rangle &= \langle k_1k_2|t|k_1k_2\rangle \\
&- \sum_{k,m}\left[\frac{\langle k_1m|t|kk_1\rangle\langle k_2k|t|mk_2\rangle}{(E_k-E_m)} + (1\to 2) - \frac{\langle k_2m|t|kk_1\rangle\langle k_1k|t|mk_2\rangle}{(E_k-E_m)} + (1\to 2)\right] \\
&- \tfrac{1}{2}\sum_{m_1,m_2}\frac{|\langle k_1k_2|t|m_1m_2\rangle|^2}{(E_{k_1}+E_{k_2}-E_{m_1}-E_{m_2})} \\
&+ \tfrac{1}{2}\sum_{m,k_3,k_4}\frac{|\langle k_1m|t|k_3k_4\rangle|^2\langle k_2|\{\langle k_3|t|k_3\rangle+\langle k_4|t|k_4\rangle-\langle m|t|m\rangle-\langle k_1|t|k_1\rangle\}|k_2\rangle}{(E_{k_3}+E_{k_4}-E_m-E_{k_1})^2} + (1\to 2) \\
&+ \tfrac{1}{2}\sum_{k_2,m_1,m_2}\frac{|\langle m_1m_2|t|k_3k_1\rangle|^2\langle k_2|\{\langle k_3|t|k_3\rangle+\langle k_1|t|k_1\rangle-\langle m_1|t|m_1\rangle-\langle m_2|t|m_2\rangle\}|k_2\rangle}{(E_{k_3}+E_{k_1}-E_{m_1}-E_{m_2})^2} + (1\to 2).
\end{aligned} \tag{14}$$

In this equation $(1 \to 2)$ means the same as the previous term with k_1 and k_2 interchanged.

In general the state α_0 will contain a sum of different single particle pairs, so that off diagonal elements will also be required. These can be obtained in an analogous way to the above. We shall not write down all the terms but as an example shall give just the first of the second order and first of the third order terms (in the order of eq. (14)), for the matrix element $\langle k'_ok'_2|W|k_1k_2\rangle$. These are

$$\sum_{k,m}\frac{\langle k'_1m|t|kk_1\rangle\langle k'_2k|t|mk_2\rangle}{(E_k-E_m)}$$

and

$$\tfrac{1}{2}\sum_{m,k_3,k_4,k'_3,k'_4}\frac{\langle k_1m|t|k_3k_4\rangle\langle k'_3k'_4|t|k'_1m\rangle\langle k'_2|\{\langle k'_3|t|k_3\rangle+\langle k'_4|t|k_4\rangle-\langle m|t|m\rangle-\langle k'_1|t|k_1\rangle\}|k_2\rangle}{(E_{k_3}+E_{k_4}-E_m-E_{k_1})(E_{k'_3}+E_{k'_4}-E_m-E_{k'_1})},$$

respectively. We emphasise that of the third order terms we are only including a selection of terms, i.e. those which are analogous to the "self consistency" terms included in the closed shell case.

Finally, we consider the situation where there are three particles outside a closed shell. The diagrams in which only two particles take part are the same, so the two-body effective potential is unaltered. In addition there are diagrams in which the three extra particles take part and these give rise to an effective three-body potential. In second order there are two such diagrams:

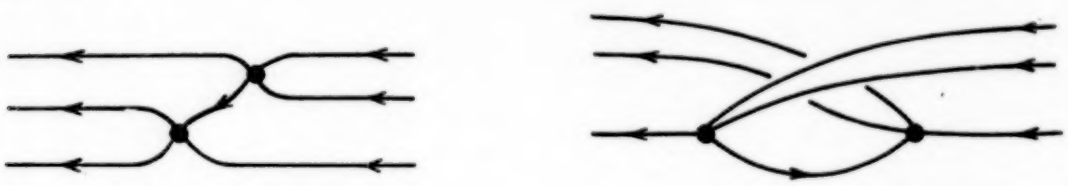

In the first of these, which does not involve the closed shells, the intermediate state must be out of the space of the $|\alpha_0\rangle$. The second term gives a contribution to the three-body interaction $\langle k_1 k_2 k_3|w^{(3)}\ |k_1 k_2 k_3\rangle$ given by

$$-\sum_m \left[\frac{|\langle k_2 k_3|v|mk_1\rangle|^2}{(E_{k_1}-E_m)}+(1\to 2)+(1\to 3)\right].$$

There are also of course third order contributions.

4. Discussion

We have seen that there exist corrections, which are likely to be important, to the use of the t matrix as the effective potential in shell model calculations. Some confirmation of the importance of these terms for finite nuclei is available from the work of Eden and Emery [11]) who have shown that the rearrangement energy in O^{16} is of the order of 10 MeV. These correction terms will depend, in general, on the state being considered, and a simple effective potential will therefore not apply to all situations. For example, the effective potential chosen to fit binding energies and single particle energies will not be appropriate for fitting the separation of levels away from closed shells.

Within a given shell the use of an effective potential, chosen so as to include the correction terms, may be expected to give good results provided the total number of particles in the shell being filled is small compared to the number in the filled shells. Thus, the likely importance of some of the correction terms considered here is not contradicted by the success of the shell model in fitting the spectra of neighbouring nuclei, e.g. the work of Goldstein and Talmi [12]) on Cl^{38} and K^{40}. Three and four etc. body potentials

will occur but, provided the number of extra particles is small compared to A, the effect of these is likely to be rather small. The three-body potentials found by Pandya and French [13]) could probaly be explained in this way.

Apart from these, purely phenomenological, considerations it would be interesting to endeavour to calculate the correction terms. For nuclear matter this would be a practical proposition but the results would perhaps not be very useful for application to finite nuclei. The difficulty in doing the calculations for finite nuclei is that one needs, in general, to know the matrix elements of t between all states and not just between occupied states. This is not true for the third diagram drawn for the effective potential w, and it would be reasonable to calculate the contribution of this particular diagram. An alternative way of obtaining the exclusion principle correction for small nuclei would be to use the method of section 2 and calculate directly the t matrix with the modified exclusion principle operator. This, however, would require greater care in the evaluation of the t matrix than has usually been used, since it would not be possible to make the angular average of the exclusion principle operator which is necessary in order to be able to solve the t matrix equation in relative coordinates only.

Some discussion of corrections to the simple model has been given previously by Brueckner, Eden and Francis [14]). However, these authors ignore the exclusion principle effect, and, in considering the case of two particles outside a closed shell, wrongly assert that the self consistent potential effect only gives rise to fourth order terms. Calculations of Sawicki and Folk [15]) of the spin orbit splitting in O^{17} include some corrections to the simple model by using Dąbrowski wave functions rather than shell model wave functions in the spin orbit part of eq. (4). The precise relationship of the Dąbrowski treatment to the Brueckner treatment is not too clear, but it seems likely that this method includes the third order corrections approximately but ignores the second order corrections (due essentially to antisymmetrising).

Discussions with Drs. J. S. Bell and R. J. Eden are acknowledged.

References

1) R. J. Eden, Nuclear Reactions, Vol. 1 (North Holland Publishing Co., Amsterdam 1958)
2) K. A. Brueckner and J. L. Gammel, Phys. Rev. **109** (1958) 1023
3) R. J. Eden and V. J. Emery, (to be published)
4) N. M. Hugenholtz, Physica **23** (1957) 533
5) E. J. Squires, A.E.R.E. report (1958)
6) E. J. Squires, Nuclear Physics **8** (1958) 41;
D. J. Thouless, Phys. Rev. **112** (1958) 906
7) T. H. R. Skyrme, Nuclear Physics **9** (1958/59) 615

8) J. Goldstone, Proc. Roy. Soc. A **239** (1957) 267
9) N. M. Hugenholtz and L. Van Hove, Physica **24** (1958) 363
10) C. Bloch and J. Horowitz, Nuclear Physics **8** (1958) 91
11) Private communication, see also ref. [3])
12) S. Goldstein and I. Talmi, Phys. Rev. **102** (1956) 589
13) S. P. Pandya and J. P. French, Annals of Physics **2** (1957) 166
14) K. A. Brueckner, R. J. Eden and N. C. Francis, Phys. Rev. **99** (1955) 76
15) J. Sawicki and R. Folk, Nuclear Physics **11** (1959) 368

8.B *Nuclear Physics* **13** (1959) 235—238; © *North-Holland Publishing Co., Amsterdam*
Not to be reproduced by photoprint or microfilm without written permission from the publisher

K^-—K^0 RELATIVE PARITY DETERMINATION FROM NUCLEON-ANTINUCLEON ANNIHILATION

S. N. BISWAS and L. K. PANDIT
Tata Institute of Fundamental Research, Bombay

Received 22 July 1959

Abstract: It is suggested that the S_1-violating production process $\bar{p}+n \rightarrow K^-+K^0$ may lead to a definite conclusion whether or not the relative $(K^- - K^0)$ parity is odd.

1. Introduction

Recently Pais [1]) has suggested a scheme of strong and moderately strong meson-baryon interactions, in an attempt to simplify the interaction scheme obtained on the basis of charge independence alone. The basis of his scheme is that within the framework of meson-baryon interactions the $\Lambda-\Sigma$ mass difference may be neglected. Then the isobaric singlet Λ^0 and the triplet Σ can be replaced by two isobaric doublets called N_2 and N_3. In this so-called doublet approximation, all the baryons appear as isobaric doublets, the π-mesons as isobaric triplets and the various K-mesons are isobaric singlets. Pais finds that the symmetries of the interaction lead to the separate conservation of two new quantum numbers S_1 and S_2, the sum of these two numbers being the Gell-Mann–Nishijima strangeness number S. The S_1-conservation of Pais is really the conservation of the third component of the total isobaric spin T_3 (in the new "doublet" assignment).

In Pais' scheme certain observed processes are not allowed on account of S_1-conservation. To save the situation Pais observes that since K^+ and K^0 are now no longer members of the same isobaric multiplet, they may very well have opposite intrinsic parities. Thus he is led to the possibility of introducing a (comparatively weak) T_3-violating and parity-conserving direct $\bar{K}^+K^0\pi^+$ interaction. This new interaction, then, (since it does not conserve T_3 or S_1) allows the forbidden processes mentioned above. Consider, as an example, the processes (nucleon anti-nucleon annihilation):

$$p+\bar{n} \rightarrow K^+ + \bar{K}^0,$$
$$\bar{p}+n \rightarrow K^- + K^0.$$

These processes are certainly allowed according to S-conservation; but they are forbidden by Pais' T_3 selection rule and can only take place if the $KK\pi$ interaction is invoked.

The purpose of this note is to study these reactions according to the old as well as to the new schemes as a possible means of deciding whether the $(K^- - K^0)$ relative parity is even or odd †. We might add that nucleon-antinucleon annihilation as a method has been suggested by Barshay [2]) for obtaining the $(\Sigma\Lambda)$-parity also.

Results of the lowest order calculations in the covariant perturbation theory are presented here. We find that already in this order very distinctive features for the different cases of parity are obtained. The results are reliable as the effective coupling constants involved are much smaller than the pion-nucleon coupling constant.

2. Results

Fig. 1 shows the lowest order Feynman diagram for the process in Pais' scheme with $KK\pi$ interaction. In fig. 2 the same process is shown according to the usual Gell-mann-Nishijima scheme.

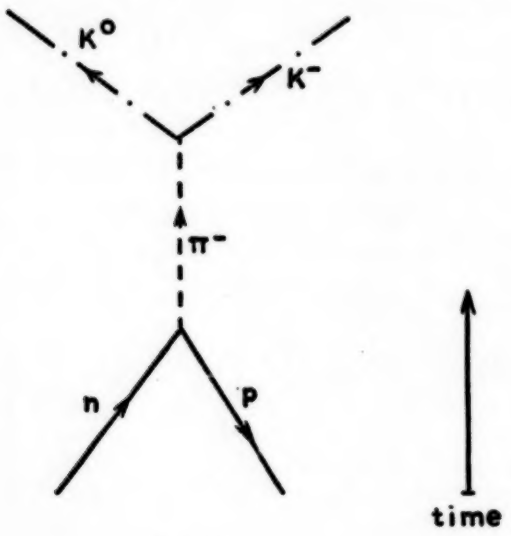

Fig. 1.

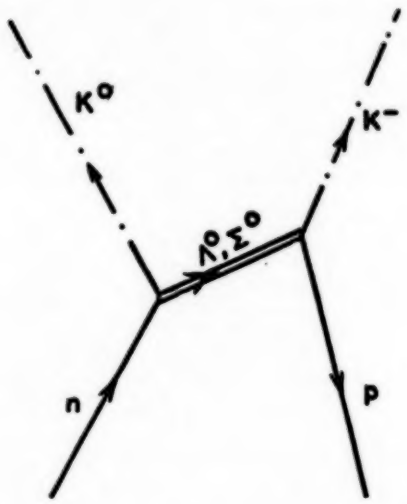

Fig. 2.

The usual straightforward calculations lead to the following results. In calculating the process †† shown in fig. 2, we take relative (Λ, Σ) parity even (spins $\frac{1}{2}$ for Λ, Σ; and spin 0 for K). *Both* possibilities of relative (K—Y) parity have been considered. The symbol p(K, Y) will be used to denote relative (K—Y) parity.

The angular distribution for K^- in the centre of mass system, $R(\theta)$, is shown in table 1 for a laboratory kinetic energy $E=375$ MeV.

† Experimentally, perhaps, the process considered is difficult to study. It is easier to observe the process $\pi^- + p \to p + K^- + K^0$. Calculations for this process on similar lines are being carried out by Dr. V. Gupta (Bombay).

†† The $\Sigma - \Lambda$ mass difference has been neglected here also.

TABLE 1

Angular distribution of K⁻ meson for $E=375$ MeV

Interaction scheme	$R(\pi)$	$R(\frac{1}{2}\pi)$	$R(0)$
p(K⁻, K⁰) *odd* (fig. 1)	1	1	1
p(K⁻, K⁰) *even* p(K, Y) *even* (fig. 2)	0.01	6.00	6.30
p(K⁻, K⁰) *even* p(K, Y) *odd* (fig. 2)	6.0	2.7	1.0

In table 2 we give the total cross-section σ at different incident kinetic energies E of the $\bar{p}$ in the laboratory system.

TABLE 2

Total cross section at various energies

E (MeV)	167	375	668	1503
σ in units of $\frac{G^2}{4\pi}\times\frac{f^2}{4\pi}\times 10^{-27}$ cm² p(K⁻, K⁰) *odd*	0.39	0.27	0.17	0.08
σ in units of $\left(\frac{G_\Lambda^2}{4\pi}-\frac{G_\Sigma^2}{4\pi}\right)^2\times 10^{-27}$ cm² p(K⁻, K⁰) *even*, p(K, Y) *even*	0.74	0.61	0.54	0.42
σ in units of $\left(\frac{G_\Lambda^2}{4\pi}-\frac{G_\Sigma^2}{4\pi}\right)^2\times 10^{-27}$ cm² p(K⁻, K⁰) *even*, p(K, Y) *odd*	0.59	0.42	0.34	0.24

3. Discussion

With pion-nucleon coupling constant $G^2/4\pi \approx 15$ and KKπ-interaction constant $f^2/4\pi \approx 0.01$, the total cross-section for *odd* p(K⁻, K⁰) at $E=167$ MeV turns out to be ≈ 0.06 mb. On the other hand, if we take $G_\Lambda = \sqrt{3}G_\Sigma$, $G_\Sigma^2/4\pi = 0.5$ and p(K, Y) *even*, as required by K⁺–p scattering [3]), the cross-section at the same energy is ≈ 0.74 mb. It is interesting to note that both these values will be of the same order of magnitude if we take f^2 slightly larger or G_Σ^2 slightly smaller.

From table 2 we notice that the energy dependence of the total cross-section for all three relative parity assignments is more or less similar, starting with a high value at low energies and slowly decreasing at high energies. Thus, from the energy dependence alone it will not be possible to make any definite conclusions about the parity assignments. We must, therefore, turn to angular distribution, which we notice (see table 1) to be sharply different in the cases considered.

We find that with $p(K^-, K^0)$ *odd* the KKπ-interaction leads to a completely isotropic angular distribution. There is, on the other hand, complete anisotropy with $p(K^-, K^0)$ *even*, in which case we find forward peaking for $p(K,Y)$ *even* and backward peaking for $p(K, Y)$ *odd*. This marked difference in the angular distributions should thus make it possible to ascertain whether or not the relative parity of charged to neutral K-mesons is *odd*. If the latter turns out to be *even*, it is again possible to decide whether (K—Y) relative parity is even or odd.

We should like to thank Mr. B. M. Udgaonkar, Dr. Yash Pal and Dr. M. S. Swamy for valuable comments.

References

1) A. Pais, Phys. Rev. **110** (1958) 574; **112** (1958) 624
2) S. Barshay, Phys. Rev. **113** (1959) 349
3) L. K. Pandit and S. N. Biswas, Nuclear Physics **12** (1959) 521

3.B *Nuclear Physics* **13** (1959) 239—257; © *North-Holland Publishing Co., Amsterdam*
Not to be reproduced by photoprint or microfilm without written permission from the publisher

THE MEASUREMENT OF SHORT LIFETIMES BY A REFINEMENT OF THE RECOIL TECHNIQUE. THE LIFETIME OF THE FIRST EXCITED STATE OF Ra^{224}

J. C. SEVERIENS and F. W. RICHTER †
Institute for Theoretical Physics, University of Copenhagen

Received 18 July 1959

Abstract: It is shown that, by using a simple electron microscope lens to magnify the distance a nuclear recoil travels in the excited state, it is feasible to measure the time down to 2.0×10^{-11} sec in strongly converted transitions from states populated in alpha disintegration. The de-exciting conversion electrons are counted only if they are coming from recoils having a velocity selected by using a delayed coincidence technique. Further developments are discussed which may bring the limits down into the 10^{-12} sec range. The method has been tested on the first excited state of Ra^{224} populated in the Th^{228} alpha decay. The lifetime found was $(6.0 \pm 1.6) \times 10^{-10}$ sec, in agreement with other reported measurements.

1. Introduction

The recoil motion imparted to a nucleus in a nuclear reaction or disintegration has been used successfully in the past to measure nuclear lifetimes in ranges that are difficult or impossible to cover with the delayed coincidence technique. As has been pointed out by others [1]), the various techniques fall roughly into two categories: (1) a direct measurement of the mean distance the excited nucleus travels before radiating, (2) a measurement of the Doppler shift in the de-exciting radiation produced by the recoil motion. The direct method has been used to measure down to about 10^{-11} sec. The Doppler method has extended the range down to about 10^{-15} sec.

In this paper, we describe a refinement of the method for measuring the mean distance travelled by a group of exicted nuclei before radiating. The technique has been developed to give a greater accuracy of the distance measurement and, at the same time, to eliminate the uncertainties in the evaluation of the recoil velocity. It makes use of an electron microscope lens to enlarge the small distances the recoil travels in the excited state. The recoil velocity is actually measured by recording the time interval between the de-exciting conversion electrons coming from the recoiling nuclei and the arrival of the de-excited nuclei at a recoil counter placed several cm away from the source.

† Present address: Physikalisches Institut der Universität, Marburg a. d. Lahn, Germany.

The method has been used to measure the lifetime of the 84.4 keV first excited state in Ra^{224}, and has been shown to have a sensitivity down to about 2×10^{-11} sec in its present form. Further possible developments are discussed to bring this limit further down.

2. Description of the Method

The present method is designed to study the states in heavy nuclei populated in alpha decay where the de-exciting radiation will be mostly conversion electrons. The nuclei receive a recoil velocity from the preceding alpha disintegration and, if the source is sufficiently thin, some of them will travel out of the source into the vacuum, while still in the excited state. For example, a 5 MeV alpha disintegration will produce a maximum recoil velocity of about 3×10^{7} cm/sec. This means that, for a state having a lifetime of 2×10^{-11} sec, the recoils will travel a mean distance of 6 microns before de-exciting. In order to enlarge this distance and still have a reasonable solid angle we have constructed an electron microscope lens that focusses the de-exciting conversion electrons on an analyzing slit far away. This lens is mounted perpendicular to the recoil direction (defined through a coincidence requirement, see below) so that it produces an enlarged image of the exponential decay of the number of nuclei in the excited state. In the present set up, we have chosen the object and image distances so as to give a linear magnification of about 25. The lens action was achieved through the use of magnetic fields, and the lens type itself was the analogue of an optical cylindrical lens bent in a circle with its ends joined together. This is shown schematically in fig. 1, where the optical case is illustrated. This type of lens was chosen in order to line-focus the electrons and yet have a reasonable solid angle. After passing through the analyzing slit, the electrons enter a simple beta spectrometer and are collected and counted in a thin plastic scintillator.

The second new feature of the technique is that the electron coming from the radiating nucleus is counted only if it is in delayed coincidence with the arrival of the de-excited nucleus at a suitable counter. This is done by placing a recoil counter (a secondary emission multiplier) about 4 cm away from the source. The counter detects recoils that have left the source surface in a roughly perpendicular direction. The pulses from the electron counter are delayed by an amount of time equal to that which it takes the recoil to travel from the source to the recoil counter, and are then coincided with the recoil pulses. This setup thus allows one to

(1) count only those conversion electrons actually coming from a fairly narrow beam of radiating nuclei travelling outwards from the source;

(2) pick out only those recoils that have a velocity uniquely determined

by the source-to-counter distance and the amount of delay in the coincidence circuit.

Burde and Cohen [2]) in Israel, and Siekman and de Waard [3, 4]) in Holland, have also measured lifetimes via the recoil effect following alpha-decay. Their experiments differ from the present one in that they measured in a beta spectrometer the Doppler shift of a conversion line due to the recoil motion. The lifetime data is obtained by controlling the stopping distance of the recoils through insertion of thin foils near the source. Their experiments have four difficulties, viz., (1) source effects, in that the source cannot be treated as being uniformly thin, (2) folding effects due to the different emission angles of the recoils with respect to the source, which are, however, partially overcome by requiring a coincidence with the backward-going alphas, (3) short recoil distances which must be controlled accurately by the thin recoil stopping foils, (4) electron energy losses in the recoil stopping foils.

Our setup is insensitive to source thickness effects in that recoils of a definite velocity can be selected. The angular definition is better because a beam of directed recoils is being used. The sensitivity of the distance measurement is increased by the use of a magnifying lens. The absolute value of electron energy has no direct influence on the measured decay distance.

There are of course drawbacks in our technique as well. A major one seems to be the source diameter size, because it has bearing on the resolution of the lens and slit system.

In the following, we give a more detailed description of the apparatus and its advantages and limitations. Later on, we shall show how it was used to measure the lifetime of the first excited state of Ra^{224}.

3. The Main Apparatus

Fig. 1 shows a schematic drawing of the apparatus. The source is mounted on the end of a rod which is attached in turn to a calibrated screw so that the source can be moved up and down very accurately ($< 3\mu$) over small distances. By means of the recoil detector placed underneath the source — and the subsequent delayed coincidence between the electron pulse and the recoil pulse — it is possible to study only those recoils which move downwards and have a selected velocity. The distance between the source and the recoil counter was 4.1 cm and, hence, a recoil travelling at 2.8×10^7 cm/sec will produce a pulse delayed approximately 145 ns with respect to the electron pulse.

The electrons are emitted very close to the source and are collected and focussed by the cylindrical electron microscope lens. This lens is indicated

schematically by its optical analogue in the diagram. The electrons are focussed on an analyzing slit either 1 or 2 mm wide, about 26 cm away from the source. Thereupon they enter a beta spectrometer which bends their paths as indicated and collects the electrons on a thin, plastic scintillator. The pulses from this counter are then delayed and coincided with those from the recoil counter.

The measurement of the decay distance is made by moving the source up and down with the calibrated screw, and counting the electron intensity in the slit in coincidence with the recoil pulses. For mechanical reasons, it was easier and more accurate to sweep the source image across the slit by moving the source than by moving the whole slit.

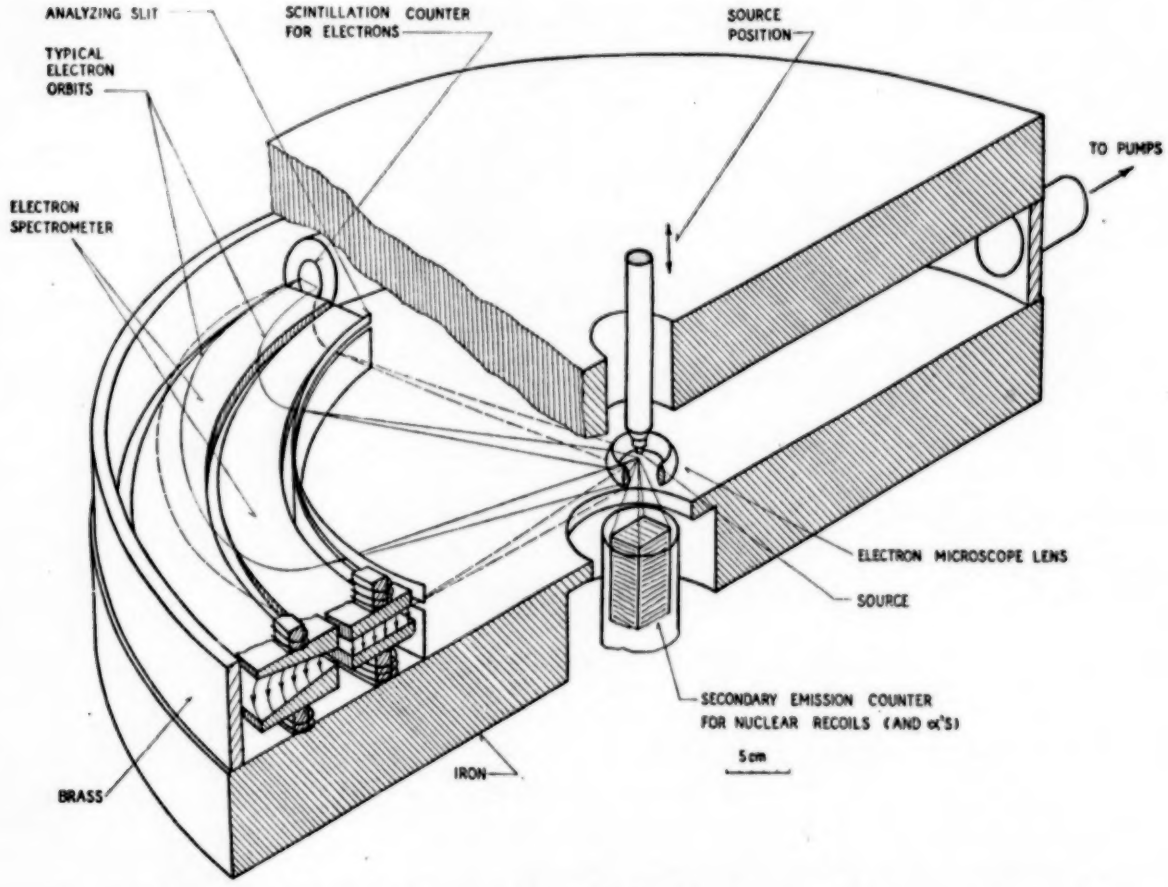

Fig. 1. Schematic drawing of the apparatus. The cylindrical magnetic electron microscope lens is drawn as its optical analogue.

The figure indicates that only a sector of about 90 degrees of a possible 360 degree geometry is used. This is done to simplify the line-up requirements and the mechanical design. There is no fundamental reason why a full circular symmetry cannot be used, other than that the design of the beta spectrometer becomes more critical. The solid angle for the conversion electrons is about 0.6 % with the 90 degree arrangement as shown. This is

influenced by the amount of lens opening used and the source distance. The solid angle for the recoil counter was about 2.5 %.

4. The Source Mounting System and the Electron Microscope Lens

Fig. 2 shows a cross section of the whole apparatus. The electron microscope, calibrated screw, and source mounting system were placed in the centre of the iron flange system as indicated. A detailed diagram of the electron microscope, shown hatched-in in fig. 2, is given in fig. 3.

The sources were deposited on small holders and attached to the end of a long rod as shown in fig. 3. This rod was firmly held to a shaft by means of

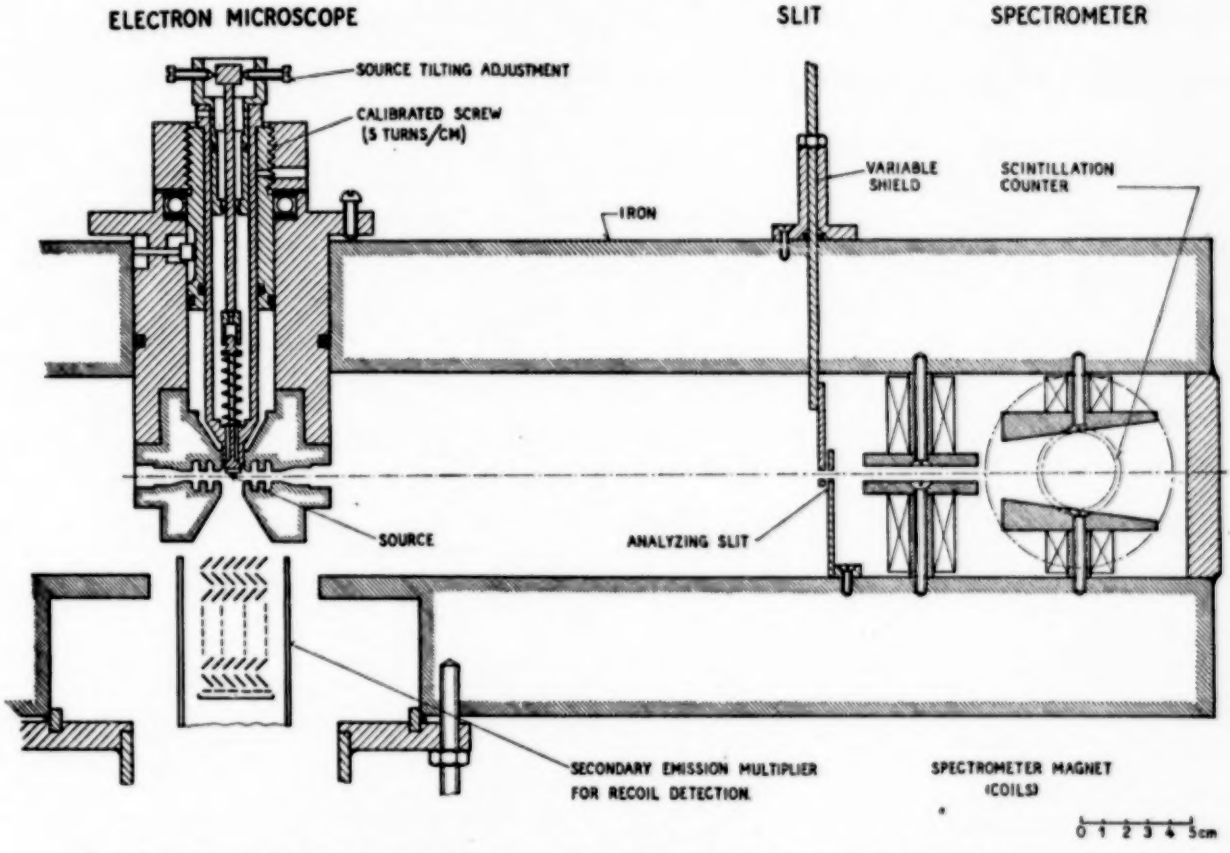

Fig. 2. Cross section (not completely to scale) of the apparatus. The electron microscope lens is shown, drawn schematically in the hatched region around the source. The opening of the analyzing slit was usually 1.0 or 2.0 mm. The scintillation counter for the electrons and its housing is shown dashed in.

the spring shown in fig. 2. The shaft was prevented from rotating by means of some spacers in a slot. The shaft can, however, move up and down. This motion is controlled by the rotation of a calibrated nut which rotated on a ball-bearing. Back-lash is kept to a minimum due to the constant air pressure on the screw. In fact, no back-lash was observed and had therefore to be less than a few μ.

For these measurements it is of course important that the sources be mounted such that their surfaces are perpendicular to the central (up-and-down) axis on the lens system. To do this, a device was constructed to allow a tilting adjustment of the source. This is shown in fig. 2. The bottom of the rod (this detail is seen more clearly in fig. 3) is enlarged and rounded so that it can rotate against the bottom of the shaft. The actual tilting is then done through a couple and lever-system pivotted by an O-ring joint and brought out of the vacuum system. Screws at the top hold the lever system in the desired position. The necessary adjustments were made by optically observing through a telescope (not shown) the location of the source with respect to the lens and slit system.

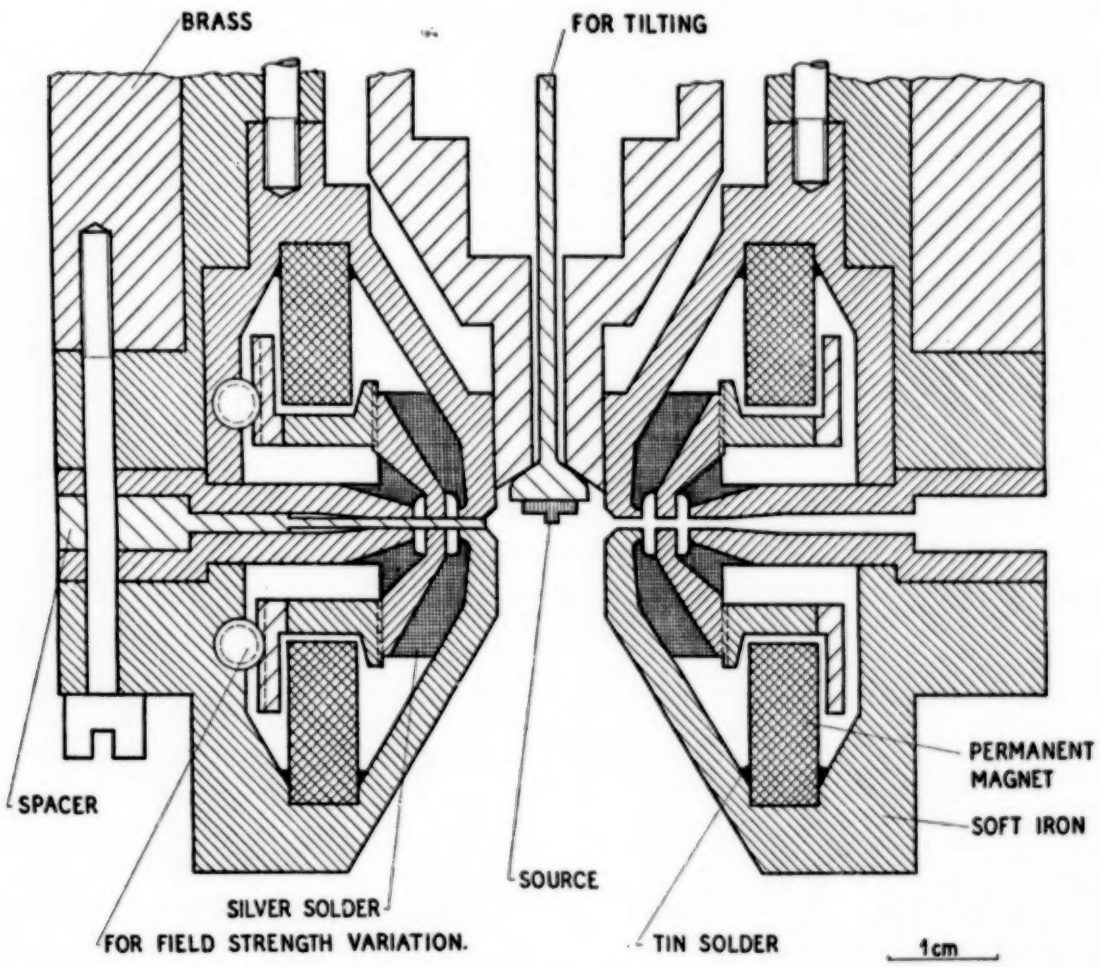

Fig. 3. Cross sectional drawing of the double-magnetic lens system used for the electron microscope. The field is generated by a permanent magnet and can be varied by an adjustable yoke through a wormgear.

A cross section of the electron microscope is shown in fig. 3. The focal length for a single, thin, cylindrical magnetic lens can be calculated to first order and is given by

$$1/f = (e/pc)^2 \int_{-\infty}^{\infty} H_0(x)^2 \mathrm{d}x,$$

where f = focal length, p = momentum of the electrons going through the lens, and $H_0(x)$ is the field strength in the magnetic central plane of the lens. The integration axis is taken to lie in the magnetic centre plane of the lens (see fig. 4). To make this calculation, the lens has been assumed to stretch out infinitely along the y-axis. This is of course not so with the actual lens used, which is bent in a circular form and has its ends joined so that it closes upon itself. However, it is a close approximation to the real case and allows one to solve the field equations.

Unfortunately, a single lens of this type cannot be used alone if the electrons entering it have an initial velocity component perpendicular to the

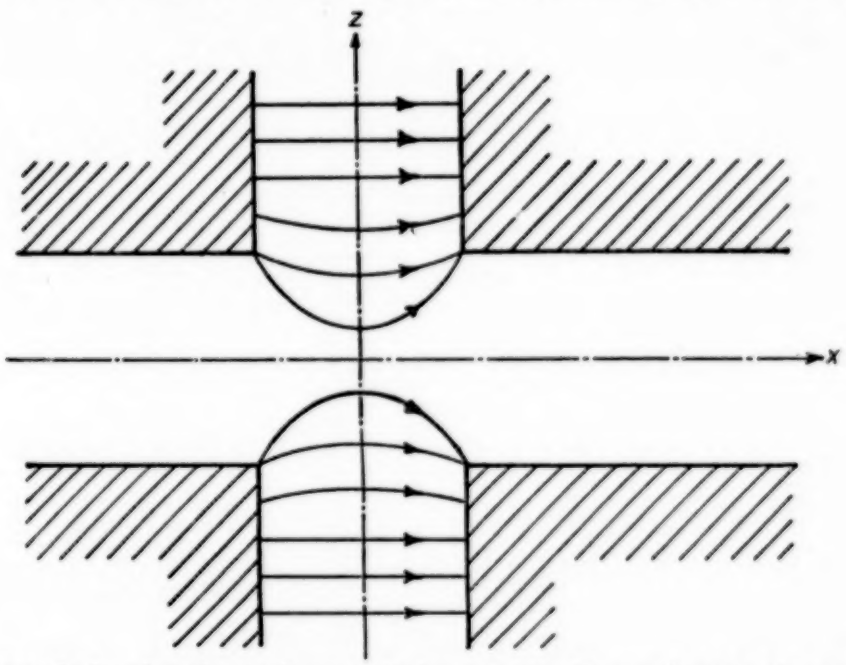

Fig. 4. Schematic drawing of a single magnetic lens showing the coordinate system used in the focal length calculation. The electrons travel in the x-direction.

xz-plane. This happens in this apparatus because — even though the cylinder lens is bent to have rotational symmetry — the sources are not point sources. The velocity component perpendicular to the xz-plane causes a smearing out of the image, in effect, producing a rotation in the yz-plane. It is this same effect which causes a rotation of the image in the standard thin circular magnetic lens. In that case, however, the symmetries of the fields keep the image itself sharp. Fortunately, however, it is possible to correct for this effect in the cylindrical case. It can be shown, again to first order, that the change in z due to an initial velocity component v_y, perpendicular to the xz-plane is directly proportional to

$$v_y(e/pc) \int_{-\infty}^{\infty} H_0(x)\mathrm{d}x.$$

Hence, by the construction of a second magnetic lens similar to the first except that the field has the opposite sign, it is possible to cancel this rotation effect (provided the two lenses are placed close together). It should be noted that the focussing property is left unaffected (because the focal length is proportional only to the absolute value of the field and not to its sign).

The strong curvature of the field near the edges of the iron prevented making use of the full possible aperture. The strongly curving field requires that higher order terms be taken into consideration, which in turn affects the focussing properties of the lens. A diaphragm was therefore constructed to vary the lens opening and it was located close to the two lenses (not shown in fig. 3). For our purposes, an aperture of 60 % (0.6 mm) of the maximum possible was found to be quite satisfactory with an object distance of about 10 mm.

Because of the double lens feature, it was most expedient to generate the fields by means of a permanent magnet. Field variation was made possible by inserting an iron yoke in the magnetic circuit whose position could be controlled from the outside with a wormgear. This system was found to work quite well and no appreciable change in the magnetomotive force was observed during the measurements. The lens gaps were 1.0 mm each and were 3.0 mm apart.

5. The Electron Spectrometer

The electrons coming from the source after passing through the magnetic lens system were focussed on an analyzing slit (shown in fig. 1) about 26 cm away from the microscope. The opening of the analyzing slit was variable; for most purposes, runs were made with openings of 1.0 or 2.0 mm. By means of a shield controlled from outside it was possible to open various parts of the slit and in this manner to study the properties of the electron spectrometer located behind the slit.

It was necessary to build this electron spectrometer because it seemed to be the best way to collect the electrons in a scintillator after passing through the slit. A long GM counter would be impractical because of the fast coincidence required between electron and recoil pulses. The presence of a crude spectrometer gave furthermore some additional energy selection. In the sources used, there was always some gamma activity present as well as shortlived emanation products. The spectrometer arrangement had the advantage that it made it rather easy to shield against this background.

The construction and properties of the spectrometer are indicated in fig. 1. The drawing shows two magnetic fields, the first a homogeneous region where the electrons will have circular orbits, and the second an inhomogene-

ous field falling off in intensity, which "guides" the electrons into the scintillator. Typical electron orbits are shown in fig. 1 to illustrate the properties of such a "varying resolution" spectrometer.

One of the difficulties in a spectrometer of this type is the strong focussing action (or defocussing as far as the electron counter is concerned) in the z (up and down) direction due to the fringing field. The electron, after its first rather large deflection in the strong homogeneous magnetic field, spends a considerable amount of time in a region where the fields also have radial components. This effect was studied with baffles and, with a 2 mm entrance beam, it was found that for the worst case where the electron spent most time in the fringing field the spread out was about 8 mm. A plastic phosphor of 2 cm width is thus more than sufficient to collect all the electrons in the z-direction. The length of the phosphor was 35 mm because the electrons from different parts of the slit are not focussed in a spot by this spectrometer.

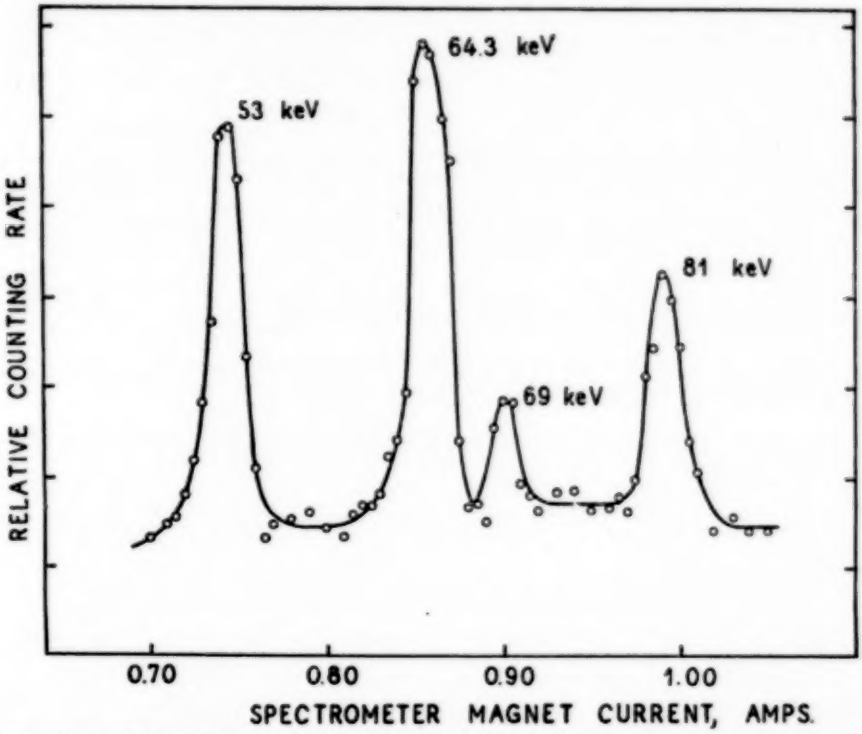

Fig. 5. A portion of the beta spectrum observed through the electron spectrometer from a $Pa^{233}(\beta^-)U^{233}$ source. Microscope removed from the apparatus. The four peaks are well-known conversion lines observed in this decay. Only that half of the spectrometer furthest away from the counter was used.

A curve was taken of a portion of the Pa^{233} electron spectrum with the microscope removed from the system. This curve, shown in fig. 5. depicts four of the well-known conversion lines found in the de-excitation of states in U^{233}. The background comes from the continuous beta radiation of the Pa^{233} beta disintegrations. To get this curve with this rather good resolution it was

necessary to use that half of the available spectrometer entrance slit which was furthest away from the detector. Otherwise the resolution would have been much worse.

The entrance slit was divided into four equal sections and the average resolution measured for each. The results are listed below, gap 1 denoting the sector closest to the detector:

gap	1	2	3	4
resolution dp/p (%)	9.2	4.4	2.6	1.7

6. The Recoil Counter and Electronics

The recoil counter consisted of a secondary emission multiplier of the venetian blind type with Ag-Mg dynode surfaces. This material was chosen so that the counter could be exposed to room air for shorter periods without damaging its secondary emission properties. It was made especially for this experiment by the EMI Corporation. The surface area presented to the incoming recoils was about 6 cm^2. Even though the multiplier had 15 stages it was impossible to get pulses out bigger than about 10 mV. The recoils do not produce any discrete pulse heights in the spectrum. The counter was tested with different energy recoils from 50—150 keV (from thin ThB sources) but no correlation between pulse height and energy was observed; in fact, no difference in pulse height was observed between 5 MeV alpha particles and recoil nuclei. This is attributed to the fact that the alphas produce the same number of secondary emission electrons as does the entire recoil. Insertion of a thin 50$\mu g/cm^2$ foil to stop the recoils while allowing all alphas to go through does indeed lower the counting rate roughly by the expected factor of two. The noise was about 1 mV. The vacuum was roughly 10^{-4} mm Hg; a better vacuum should be helpful in reducing the noise.

The coincidence circuit used was the ordinary Bell, Graham, and Petch fast-slow circuit. Because some of the recoil pulses were very small, it was necessary to use an amplification of 4000$\times$ to get pulses large enough to saturate the limiter tubes. This was done by connecting four commercial wide band amplifiers in cascade. The coincidence resolving times used were from 20 to 40 ns, and were chosen this long in order to accept a fairly wide channel of the recoil velocity distribution.

7. Testing the System

One of the first tests made was to check the focussing properties of the microscope. A Pa^{233} source beta-decaying to states in U^{233} was used in many of the calibration measurements because it has several strong conversion lines in the region of interest. The sources used were thick with respect

to the recoils but "thin" for the electrons and the conversion lines were in most cases believed to be coming from M1 transitions. These facts, plus the fact that the recoil energy in a beta disintegration is small, make Pa^{233} a safe calibration, "no measurable lifetime" source. The source was monted carefully in the central position of the lens system and the spectrometer fields adjusted so as to accept one of the conversion lines. The counting rate in the electron counter was then measured while the magnetic field strengths in the microscope lens were varied. The results are plotted in fig. 6. Two analyzing slit openings were used; the 64.5 keV line with a 1.0 mm opening, the 53.0 keV a 2.0 mm. Hence the difference in shapes.

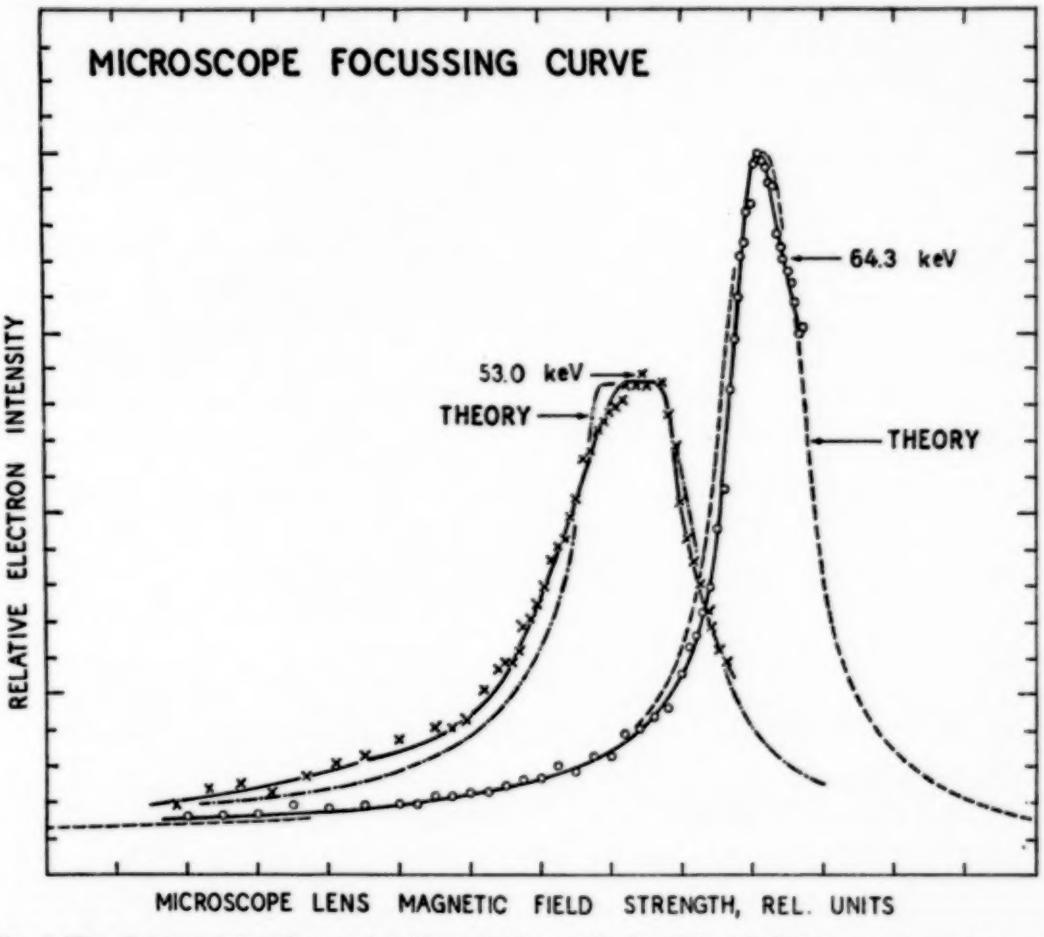

Fig. 6. The electron intensity coming through the analyzing slit and electron spectrometer as a function of the field strengths in the magnetic lens system with fixed electron spectrometer settings. The focussing effect is shown for two U^{233} conversion lines and the experimental results are compared with a theoretical curve, assuming a monoenergetic source. The depth-of-focus effect is included in the calculation. The field strengths available did not allow focussing above about 70 keV. The two curves are not normalized to each other. The 64.5 keV line was measured with a 1.0 mm wide analyzing slit; the 53.0 with a 2.0 mm.

The scale of fig. 6 represents the field strength in the microscope lens as determined by the displacement of the iron yoke in the magnetic circuit (see above). From the design it was concluded that the yoke displacement

(varied with a screw) changed the field linearly. This was roughly shown to be so from measurements with different energy conversion lines.

As can be seen from the curve, the lens works quite well up to electron energies of about 70 keV. Unfortunately, the lens was underdesigned and the maximum field strengths available allowed focussing only up to this energy. There is no fundamental reason, however, why it should not be possible to focus higher energies. The theoretical curves shown were calculated, assuming a monochromatic electron source with a "depth of focus" effect due to a source diameter of 1 mm, also taken into account.

A more critical test is to set the microscope field for the best focussing and then to vary the source position by means of the calibrated screw. If the image is indeed a sharp line (i.e., in the case of "no measurable" lifetime) then, as this image is swept across the analyzing slit, one should observe a rectangular intensity distribution. The width of this distribution is equal to the displacement of the source times the magnification. This should in turn be equal to the slit width used. It can be shown that of those factors that contribute to making the sides of this rectangle less steep the finite source extension is by far the most important because it affects the "depth of focus". A calculation was made of this, assuming a monochromatic source of electrons, and the results were plotted against the observed points. This is shown in fig. 7. The small discrepancy at the peak of the curve is attributed to the fact that monochromatic electrons were used in the calculation, whereas, in the sources used, there was always a continuous beta background present. The reason the intensity does not drop-off to zero at large source displacements is mainly that a background of source gamma rays was not completely shielded out. The 78 micron half-width corresponds to a magnification factor of 25.5.

It is difficult to determine the magnification factor accurately from the source and image distances because of the double lens used. However, to a good approximation, the observed and calculated magnification factors agree. The steepness of both curves is indicated in terms of time by assuming a recoil velocity of 2.8×10^7 cm/sec, which is a representative value for alpha disintegrations. It can be seen from the curves that, with the present arrangement and magnification, it is possible to measure directly half lives down to about 2×10^{-11} sec. The theoretical curve predicts a limit of 1.2×10^{-11}. The discrepancy between these two values lies probably in a slight misalignment and aberrations such as chromatic, spherical, etc. which were not taken into the calculation. Better resolution can be obtained at higher magnification if, at the same time, the source dimensions (or lens aperture) are reduced. One can roughly say that in order to double the resolution it will be necessary to halve the source diameter; in the present case 1.0 mm. This does indeed set a serious upper limit to the practical application of the

instrument. Because of the small solid angles involved it is necessary to have sources of several μC strengths, which is, however, not always compatible with a thin source. For measurements of lifetimes $> 3\times10^{-11}$ sec the present apparatus should, however, be quite satisfactory. One of the advantages inherent in this setup is that it can also be used for low energy conversion electrons (i.e., < 30 keV), a region where the delayed electronic

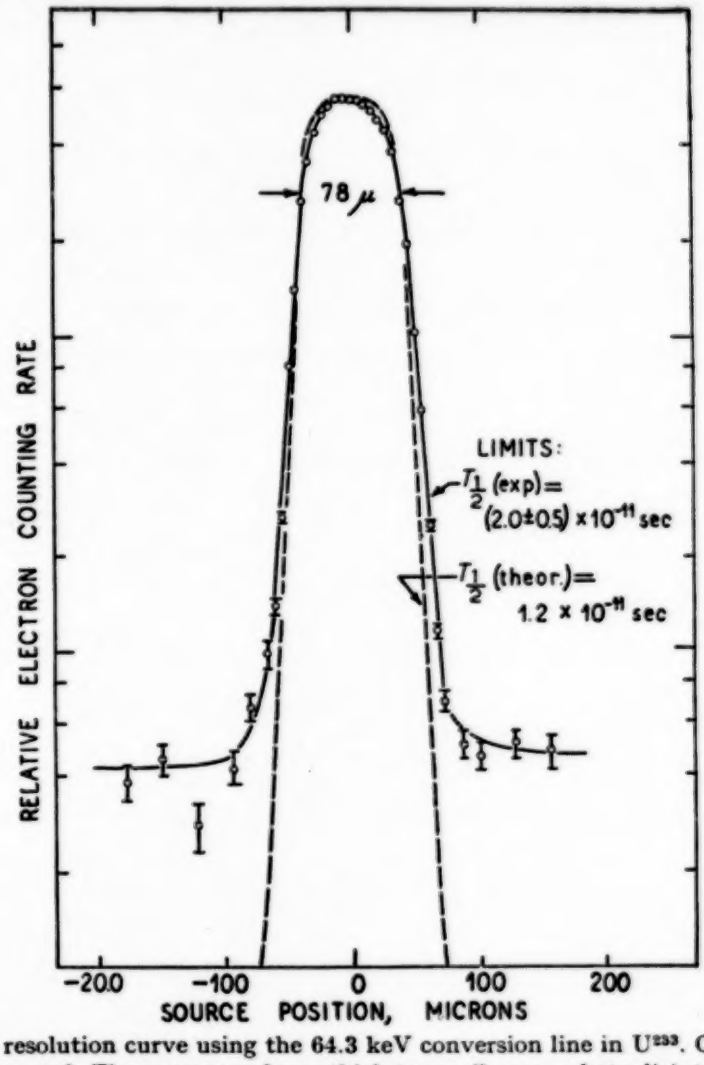

Fig. 7. Prompt resolution curve using the 64.3 keV conversion line in U^{233}. Only the electron counts were measured. The source used was thick to recoils, was a beta disintegration, and the 64.3 keV an M1 transition. Hence no lifetime effect is expected. A theoretical curve is shown based on the assumption of a monoenergetic source and the presence of the depth-of-focus effect. The limits are assigned on the basis of a "fictitious" recoil velocity of 2.8×10^{7} cm/sec.

coincidence technique is limited by the small light output of the scintillating phosphors.

8. The Ra^{224} Lifetime Measurements

The Th^{228} alpha decay to the first excited state in Ra^{224} was used to test the instrument and at the same time to check some earlier measurements.

The state in question is the 84.4 keV first excited state in Ra^{224}. This source has the advantage that the half-life of the Th^{228} alpha decay is 1.9 years and, thus, it should be possible to produce relatively thin sources with activities of 5 to 10 μC. A simplified decay scheme showing only the more intense radiation is given in fig. 8.

The sources were produced † by an ion exchange method utilizing a cation exchange column of very small dimensions (the free volume being about 0.2 μl). Th^{228} together with its daughter products was adsorbed on the ion exchanger in a band on top of the resin filling by passing a solution of the activity through the column. Thereafter, the daugthers were eluted from the column and, finally, the cleaned thorium taken out with a lactate solution. The activity was collected in small drops (diameter roughly 0.6 to 1.0 mm) on the ends of flat, polished high purity gold source holders (see, e.g. fig. 3). In this way it was possible to get source areas less than 1 mm in diameter. They were thereupon quickly dried at high temperatures and inserted in the

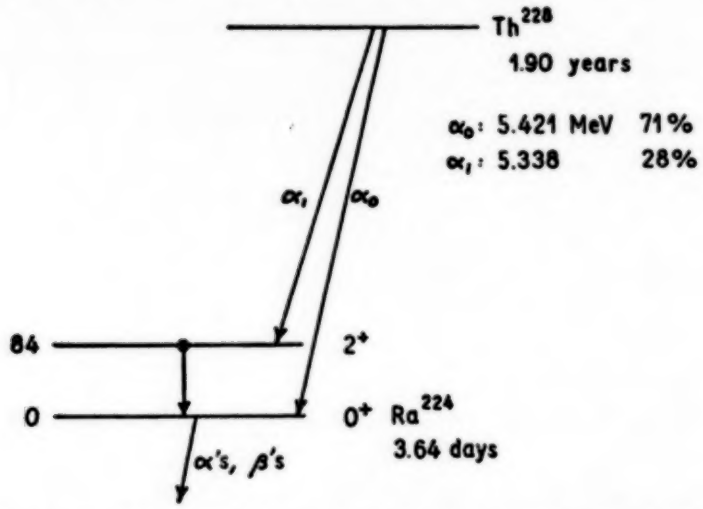

Fig. 8 Simplified Th^{228} decay scheme showing only the two prominent alpha groups. Those alphas leading to higher excited states in Ra^{224} add up to less than 1 %.

apparatus. This technique successfully produced some thin sources, although several of the sources made turned out to be too thick. It should be noted here that the average recoil range at these energies is only a few $\mu g/cm^2$ in its own material. Hence, source preparation is very critical.

The L-conversion electrons were used to study the decay of the 84.4 keV state. The energies are roughly 66 and 69 keV for the L_{II} and L_{III} conversion electrons, respectively. Since they occur in an intensity ratio of about 5 to 4 it was decided that the best results would be obtained if the instrument were set for an average energy of 67.5 keV. It can be inferred from fig. 6 that, with a 2 mm analyzing slit as was used here, this means that most of

† We are very much indebted to civ. ing. S. Bjørnholm for preparing these sources.

both L-conversion electron groups was accepted and counted by the spectrometer. The 84.4 keV state is populated in 28 % of all Th^{228} alpha decays. Taking the total conversion coefficient and the L/M, N, . . . ratio into consideration, this means that about 20 % of all Th^{228} decays produce L-conversion electrons.

After adjusting the various fields, a coincidence curve was measured between the recoil pulses and the delayed conversion electron pulses. The results are shown in fig. 9. It can be seen here that there is a definite peak at delays of about 180 ns, which corresponds to the time taken for a recoil of velocity 2.3×10^7 cm/sec to traverse the source to recoil counter distance. The curve shows that there is not one characteristic recoil velocity, but rather a smeared-out distribution. This is evidence that the source is not infinitely thin and that energy losses occur in the source surface. The maximum velocity available, computed from the alpha particle energy, is 2.8×10^7 cm/sec, corresponding to a delay of 145 ns. Indeed, at this point

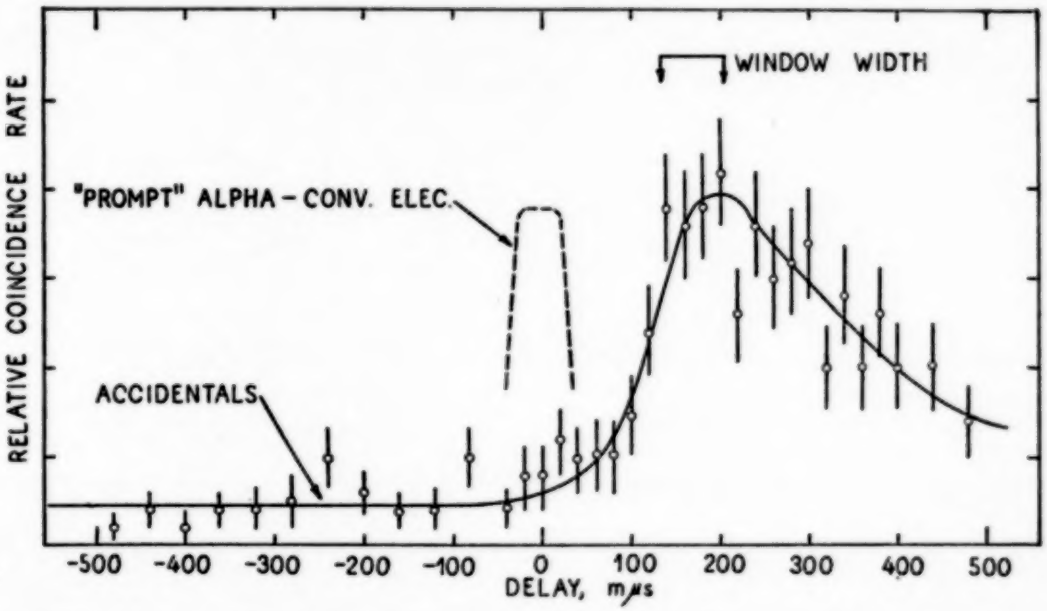

Fig. 9. Delayed coincidence curve between recoil and electron pulses. The source was tilted here slightly (2–3 degrees) so that electrons coming directly from the surface could not enter the analyzing slit. This was done to minimize chance coincidences. Hence, coincidences between alphas and electrons were not observed simultaneously with recoil-electron coincidences. The dashed curve, taken with the source *not* tilted, shows the alpha-electron coincidence curve. The two curves are not normalized to each other. Positive delay means delay inserted on the electron side. The window indicated refers to the setting used to measure the recoil spatial distribution curves (fig. 10).

the curve begins to rise, if allowance is made for the wide window width used in the measurement. It should be pointed out that this delay curve was obtained with the source slightly tilted (about 2–3 degrees away from being perfectly horizontal) so that the actual surface of the source could not be

seen through the microscope. The coincidences that are then observed can only come from recoils that have actually left the source surface and are moving towards the recoil counter. Had this not been the case, then one should also observe a coincidence peak around zero delay corresponding to alpha-electron coincidences (i.e., the recoil counter is also sensitive to alpha particles). These coincidences, which can be used to define the real zero on the time scale, should all come from the source surface since they represent the case where the recoil moves into the surface and the alpha out of the source. The tilting was done solely to reduce the accidental coincidence rate and does not influence the lifetime measurements, since these are made on recoils that have left the surface. To determine experimentally the position for zero delay, the alpha-electron delayed-coincidence curve was thus measured with the source so tilted as to permit this. The results are shown in the dashed line in fig. 9. Surface effects made it impossible to normalize the areas of these two curves together. The "prompt" alpha curve is also an indication of the resolving time used in the electronics, about 40 ns. The constant intensity observed in the left part of the curve is due to accidentals.

The determination of the spatial distribution of recoils in the first excited state was made at a fixed value of delay indicated by the window shown in fig. 9. The average recoil velocity selected by the delay and the source-to-counter distance was set to be 2.40×10^7 cm/sec. This represents an average recoil velocity of about 85 % of the maximum available. The results obtained with a 2 mm slit are shown in fig. 10. This curve is a compilation (normalized and weighted) of data obtained from 7 runs made with 3 sources of different strength, the individual runs agreeing within statistics. The figure shows two curves (both with the background subtracted); one, the recoil distribution curve with the electronic delay set so as to accept only recoils of velocity of 2.40×10^7 cm/sec, and the other, a prompt curve with the delay set at zero to accept alpha-electron coincidences. This latter curve thus represents the case where all the recoils radiate from the source surface. It serves to locate the central position of the source which, however, does not enter into the lifetime measurement, since that is made from the slope of the delayed curve. It does, however, demonstrate the sensitivity of the method in that the prompt curve has slopes of the order of 2×10^{-11} sec for a change in intensity of a factor 2. Using a weighted analysis of the least squares, one gets a value of 144 ± 30 microns for the distance needed to obtain half intensity. Coupled with an average recoil velocity of 2.40×10^7 cm/sec, this yields a half life of

$$T_{\frac{1}{2}} = (6.0 \pm 1.6) \times 10^{-10} \text{ sec}$$

for the first excited state of Ra^{224}.

The errors in this value come from two uncertainties. The first is the statistical error which is estimated to be ± 20 %. The second error is that in

the velocity measurement. Because of counting rate considerations, it is necessary to use a fairly wide window in the recoil velocity selection. Furthermore, one does not know accurately the velocity distribution within this window. Taking these two facts into consideration, it is felt that a mean error of ± 25 % can be assigned, although this error is perhaps somewhat less on the lower side of the value.

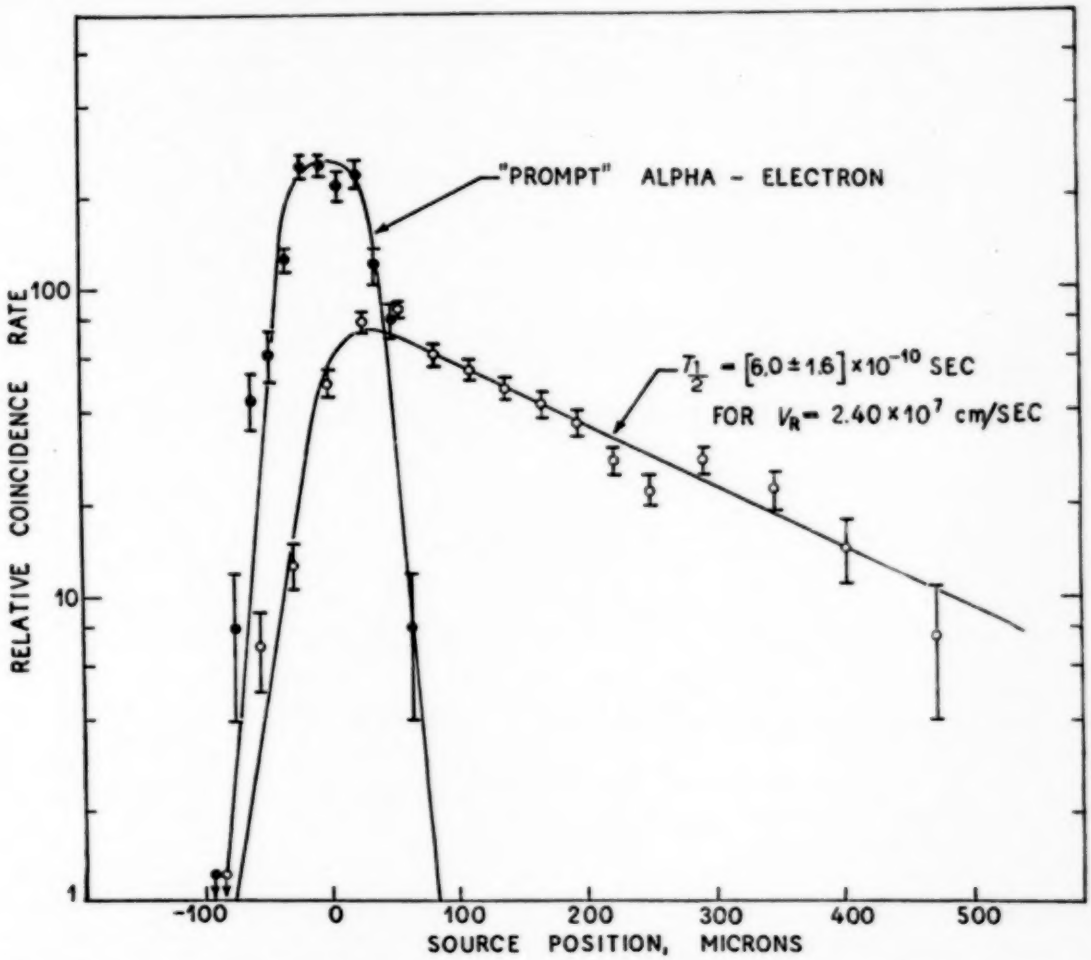

Fig. 10. Curve showing the spatial distribution of recoiling Ra^{224} nuclei in the first excited state. This curve is the composite of several runs which were made with a 2 mm slit. The value for the recoil velocity, V_R, represents about 85 % of the maximum available. The prompt alpha-electron curve was taken with the delays set to accept only alpha-electron coincidences (i.e., recoils going into the surface) and hence represents a source without a measurable lifetime. The chance coincidence background has been subtracted.

9. Discussion

The result given above is in fair agreement with the average half lives of (7.0 ± 1.0) and $(7.4 \pm 1.5) \times 10^{-10}$ sec given by Siekman and de Waard [3, 4])

and of $(8.4 \pm 0.7) \times 10^{-10}$ sec given by Vartapétain [5]). A recent delayed coincidence measurement by Bell *et al.*[6]) gave 7.6×10^{-10} sec with an error of about 5 %. The value obtained with the present apparatus is thus a little on the low side, although still within the experimental limits.

From the measured half life and using a total conversion coefficient [7]) of 21, we get a Q_0-value of 7.2×10^{-24} cm^2, in agreement with what is expected on the basis of an E2 transition from the first rotational level to the ground state in the spheroidal nuclear model [8]).

10. Conclusion

In conclusion it can be said that the present instrument has two basic advantages over the other means of determining the mean recoil distance in an excited nuclear state. One is the requirement that the de-exciting radiation is counted only in a delayed coincidence with the actual recoil which produced the radiation. The other is that it has become possible to measure shorter distances by means of the microscope lens while still keeping a reasonable solid angle.

The lower limit can probably be pushed down quite a bit by using smaller sources, smaller lens openings, and higher magnification. The latter means also that alignment problems become more severe. It should be possible, however, with further developments to measure in the 10^{-12} sec range.

Another advantage is that the method is equally good for lower energy electrons (e.g., those in the transuranic elements) where the delayed electronic coincidence method may fail.

The solid angles involved in this apparatus set a practical lower limit of about 1 μC to the source strength that can be used profitably. This, in turn, means that the half-life of the parent activity should not be much longer than 50 years if one keeps in mind that the source must be thin enough to permit a reasonable fraction of the recoils to leave the surface. The lower limit for the parent activity half-life is set by the time needed to collect the data, which is about one day.

It is a disadvantage that the excited nuclei must have sufficient recoil energy. This essentially limits one to alpha disintegrations.

Another disadvantage is of course the high requirements placed on source preparation. In practice, this will probably be the limiting factor.

The authors are very grateful to Professors Niels Bohr and Aage Bohr for the hospitality granted at the Institute. They want to thank Dr. Torben Huus for his interest in the work and in particular for his contribution to the design of the magnetic lens. Civ. ing. S. Bjørnholm has kindly provided the thin sources which are so essential for this experiment. Stimulating discussions

with and technical assistance from the staff members and guests of the Institute have been of greatest value in the various phases of the work.

Stipends from the Ford Foundation which enabled both authors to carry out this work are gratefully acknowledged. One of us (F. W. R.) is also indebted to the Rask-Ørsted Foundation for a study grant.

References

1) See, for example, the review by S. Devons in Proc. Rehovoth Conf. on Nuclear Structure (North-Holland Publ. Co., Amsterdam 1958)
2) J. Burde and S. G. Cohen, Phys. Rev. **104** (1956) 1093
3) J. G. Siekman and H. de Waard, Nuclear Physics **8** (1958) 402
4) J. G. Siekman, thesis (Groningen, 1959, Holland)
5) Vartapétain, Compt. Rend. **246** (1958) 1846
6) R. E. Bell, S. Bjørnholm and J. C. Severiens (to be published)
7) M. E. Rose, Internal Conversion Coefficients (North-Holland Publ. Co., Amsterdam, 1958)
8) Alder *et al.*, Revs. Mod. Phys. **28** (1956) 432

2.D *Nuclear Physics* **13** (1959) 258—280; © *North-Holland Publishing Co., Amsterdam*
Not to be reproduced by photoprint or microfilm without written permission from the publisher

NUCLEAR INTERACTIONS OF 660 MeV PROTONS AND THE MOMENTUM DISTRIBUTION OF NUCLEONS IN NUCLEI

L. S. AZHGIREY, I. K. VZOROV, V. P. ZRELOV, M. G. MESCHERYAKOV, B. S. NEGANOV, R. M. RYNDIN and A. F. SHABUDIN
Joint Institute for Nuclear Research, Dubna

Received 28 January 1959

Abstract: An investigation is carried out of the angular distributions and, by magnetic analysis, of the energy spectra of secondary charged particles (mainly protons with energies $\gtrsim$ 60 MeV) emitted at angles of 7°, 12.2°, 18°, 24° and 30° in interactions of 660 MeV protons with nuclei of Be, C, Cu and U. The cross sections for emission of such secondary charged particles increase with decrease of the angles. In the order of decreasing energy the various spectral regions of all investigated elements correspond to diffraction scattering of protons on nuclei (in the small angle region), single quasi-elastic proton-nucleon collisions, π-mesons production on bound nucleons and nuclear cascade.

The experimental energy spectra for single quasi-elastic proton-nuclear scattering are compared with the spectra computed in the impulse approximation under various assumptions regarding the momentum distributions of the nucleons in the nuclei. The Be and C data are consistent with a Gaussian nucleon momentum distribution falling to 1/e at an energy of approximately 20 MeV. This means that the mean square value of the nucleon momentum in Be and C nuclei corresponds to an energy of $\approx$ 30 MeV.

1. Introduction

Information on momentum distributions of nucleons in the ground nuclear state is drawn from energy and angular distributions of the products of nuclear reactions induced by high energy particles. Chew and Goldberger [1]) have shown in their analysis of the data of Hadley and York [2]) on pickup of protons from C nuclei by 90 MeV neutrons that the energy and angular distributions of deuterons fit a momentum distribution of the form $\alpha/\pi(\alpha^2+s^2)^2$ with $\alpha^2/2M = 18$ MeV, but not a distribution corresponding to a Fermi gas model for noninteracting particles. Selove [3]) has found that for neutron pickup from C nuclei by 95 MeV protons the experimental data can be satisfactorily explained if the nuclear momentum distribution of neutrons is approximated by the sum of two Gaussian distributions of the form $\exp(-s^2/s_1^2)+0.15\exp(-s^2/s_2^2)$, where $s^2/2M$ is the bound neutron energy, $s_1^2/2M = 7$ MeV and $s_2^2/2M = 50$ MeV. One is compelled to assume the existence of a significant impurity of high momentum components in the ground state wave function of light nuclei in order to explain qualitatively the direct knockout of deuterons from Li, Be, C and O nuclei by 670 MeV protons [4]) as well as the strong smearing out in the high energy region of the

spectra of π^+ and π^- mesons produced in p+C collisions at the same energy [5]). According to Henley [6]) the Gaussian momentum distribution corresponding to a mean kinetic energy of 19.3 MeV yields the best fit with such aspects of π-meson production in p+C-collisions at 340 MeV [7]) as the threshold value of proton energy, excitation curve and π-meson energy and angular distributions.

The nature of the nucleon momentum distribution in the ground state is most pronounced in quasi-elastic scattering of fast protons on light nuclei. This process has been experimentally studied at 340 MeV by Cladis, Hess and Moyer [8]), who found that within the framework of the impulse approximation the energy spectra of protons quasi-elastically scattered on C and O nuclei satisfy a Gaussian nucleon momentum distribution falling to a 1/e value at 16 ± 3 MeV. Wilcox and Moyer [9]) measured the energy spectrum of protons from pp-collision at 340 MeV by recording coincidences from both scattered protons and showed that a Gaussian momentum distribution for protons in Be nuclei yields good agreement with a 1/e value of 20 MeV. Observation of the angular correlations in 925 MeV quasi-elastic pp-collision (mainly in the light nuclei of the photographic emulsion) led McEwen, Gibson and Duke [10]) to the conclusion that the proton momentum distribution can be approximated by a Gaussian distribution with 1/e value of 11 ± 3 MeV; however, somewhat better agreement was obtained by using the sum of two Gaussian distributions of the form $\exp(-s^2/s_1^2)+0.05\exp(-s^2/s_2^2)$ with $s_1^2/2M = 7$ MeV and $s_2^2/2M = 40$ MeV. Finally, nuclear photoeffect experiments indicate that a Gaussian distribution with a 1/e value of 19 MeV is a good approximation of the momentum distribution of quasi-deuteron groups in C and O nuclei [11]).

Thus, from the set of the data on various types of high energy nuclear reactions it can be concluded that in contrast to the Fermi model with its sharp upper boundary of the nucleon momentum distribution, a good fit is obtained with models yielding a smeared-out distribution in the high momentum region.

The present paper contains the main results of investigation of the interaction between 660 MeV protons with Be, C, Cu and U nuclei. The experiments consisted primarily in magnetic deflection measurements of the energy spectra of secondary particles and in particular of quasi-elastically scattered protons. Since the validity of the impulse approximation improves with increase of the energy of the incident proton, it should be expected that the high energy regions of spectra measured at large angles should mainly contain protons emitted as a result of single collisions between the protons and nucleons of the nuclei. The quasi-elastically scattered proton spectra thus obtained were compared with the calculated spectra in which account was taken of relativistic kinematics and which were based on various assumptions

regarding the momentum distribution of the nucleons in the nuclei. The angular distributions of secondary charged particles emitted in the collisions under investigation were also measured.

The experiments were performed on the six-meter synchrocyclotron of the Joint Institute for Nuclear Research.

2. Calculation of the Momentum Distribution in Quasi-Elastic Proton-Nucleon Scattering

In the case of light nuclei it may be considered that a fast incident nucleon is scattered once by a nucleon of the nucleus. If the collision time of the two nucleons is much smaller than the nuclear periods one may assume, in the spirit of the impulse approximation, that the nuclear state does not change appreciably during the collision. The role of the interaction between the struck nucleon and the remaining nucleons in the nucleus reduces to the establishment of a momentum distribution of the nucleons participating in the collision. Thus the collision between the incident nucleon and nucleons of the nucleus can be regarded as a collision between free particles with the difference that the nuclear particles are in motion during the time of the collision. The amplitude of such "quasi-elastic" collisions with the nucleus can be obtained by summation of the scattering amplitudes on separate nucleons of the nucleus. In the large angle region in which interference of the waves scattered by separate nucleons can be neglected, the problem of scattering on the nucleus essentially reduces to the problem of scattering on a classical ensemble of independent particles, with a given momentum distribution. The distribution function is determined by the squares of the moduli of the Fourier components of the nuclear wave function. We consider below, in the indicated approximation, the problem of the energy distribution of nucleons scattered "quasi-elastically" through a given angle, relativistic kinematics effects being accounted for.

The differential cross section $d\sigma_c = \sigma_c(E_c, \cos\vartheta_c)d\omega_c$ for elastic collision of two free neutrons in their c.m.s. and the momentum distribution function $f(\mathbf{s})d\mathbf{s}$ of the nuclear particles will be assumed known. We shall denote the momenta of the incident and scattered nucleon in the laboratory system by $\mathbf{p}$ and $\mathbf{q}$, while $\mathbf{s}$ will denote the momentum of the nucleon in the nucleus. The energy of a particle with momentum $\mathbf{p}$ will be denoted by E_p etc. The corresponding quantities in the c.m.s. will be indicated by the subscript c; four-dimensional momenta are denoted by $\mathbf{p}$, $\mathbf{q}$ etc.

In order to find the number of collisions yielding a given momentum $\mathbf{q}$ (or more precisely momenta contained in an element $d\mathbf{q}$ of momentum $\mathbf{q}$) we shall assume that the incident nucleons as well as the nucleons of the target are distributed in accord with a certain law. We introduce the

distribution functions $f(\mathbf{r}, \mathbf{p}, t)\, \mathbf{dr dp}$ and $f_n(\mathbf{r}, \mathbf{s}, t)\mathbf{drds}$ which define the probable number of incident particles and nuclear particles in phase space volume elements $\mathbf{drdp}$ and $\mathbf{drds}$ respectively; the functions f and f_n are scalar functions with respect to Lorentz transformations [12]). Consider collisions between particles with momenta $\mathbf{p}$ and $\mathbf{s}$. Changing to the rest system of particles with momentum $\mathbf{p}$ we can express the number of collisions per unit volume and unit time, that is, per unit of four-dimensional volume, in the form

$$dN = f^0 f_n{}^0 d\mathbf{p}^0 d\mathbf{s}^0 d\sigma v, \tag{1}$$

where $d\sigma$ is the invariant differential cross section [13]), and v is the relative velocity. The superscript ^{0} signifies that the corresponding quantities refer to the rest system of the impinging particles. Since v and $d\mathbf{p}^0 d\mathbf{s}^0$ are invariant, we can use their expression in terms of velocity †

$$v = \frac{\left[|\mathbf{v}_p - \mathbf{v}_s|^2 - \frac{(\mathbf{v}_p \times \mathbf{v}_s)^2}{c^2}\right]^{\frac{1}{2}}}{1 - \frac{\mathbf{v}_p \cdot \mathbf{v}_s}{c^2}}, \tag{2}$$

$$d\mathbf{p}^0 d\mathbf{s}^0 = d\mathbf{p} d\mathbf{s} \left(1 - \frac{\mathbf{v}_p \cdot \mathbf{v}_s}{c^2}\right),$$

where

$$\mathbf{v}_s = \frac{c^2 \mathbf{s}}{E_s} \quad \text{and} \quad \mathbf{v}_p = \frac{c^2 \mathbf{p}}{E_p},$$

and, by integrating over $d\mathbf{p}$ and $d\mathbf{s}$, obtain an expression for the total number of collisions per unit of 4-volume which yields the prescribed result

$$N = \int d\mathbf{p} d\mathbf{s} f(\mathbf{r}, \mathbf{p}, t) f_n(\mathbf{r}, \mathbf{s}, t) \sqrt{|\mathbf{v}_p - \mathbf{v}_s|^2 - \frac{(\mathbf{v}_p \times \mathbf{v}_s)^2}{c^2}}\, d\sigma. \tag{3}$$

If the incident nucleons form a rectilinear monochromatic beam, the distribution $f(\mathbf{r}, \mathbf{p}, t)$ should be chosen in the form

$$f(\mathbf{r}, \mathbf{p}, t) = \frac{\rho^0}{\sqrt{1 - \beta_p{}^2}} \delta(\mathbf{p} - \mathbf{p}_0),$$

where ρ^0, the density of the incident particles in the rest system, is an invariant. Thus ††,

$$N = \frac{\rho^0}{\sqrt{1 - \beta_p{}^2}} \int d\mathbf{s} f_n(\mathbf{r}, \mathbf{s}, t) \sqrt{|\mathbf{v}_p - \mathbf{v}_s|^2 - \frac{(\mathbf{v}_p \times \mathbf{v}_s)^2}{c^2}}\, d\sigma. \tag{4}$$

† The relation between $d\mathbf{s}^0 d\mathbf{p}^0$ and $d\mathbf{p}\, d\mathbf{s}$ follows from the fact that $d\mathbf{p}$ can be considered as the four-component of an infinitely small 4-vector $d\mathbf{p}\, \mathbf{v}_p,\ icd\mathbf{p}$.

†† Chernikov [14]) earlier obtained a formula similar to (4).

The cross section $d\sigma(\mathbf{q}_c)$ for scattering into a given momentum interval $d\mathbf{q}_c$ in the c.m.s. can be written in the form

$$d\sigma(\mathbf{q}_c) = \sigma_c \frac{\delta(q_c - p_c)}{p_c^2} d\mathbf{q}_c = \sigma_c \left| \frac{\partial E'_c}{\partial q_c} \right| \frac{\delta(E'_c - E_c)}{p_c^2} d\mathbf{q}_c, \tag{5}$$

where E_c and E'_c are the total energies in the c.m.s. before and after the collision and $\sigma_c = d\sigma_c/d\omega$. The law of conservation of momenta is assumed to hold in eq. (5). Making use of the fact that $\partial E'_c/\partial q_c = 2c^2 q_c/E_{q_c}$ for equal masses of the colliding particles, and also of the invariance of $d\mathbf{q}_c/E_{q_c} = d\mathbf{q}/E_q$ and $d\sigma$, we obtain for the cross section for scattering into a prescribed momentum interval $d\mathbf{q}$ in the laboratory system

$$d\sigma(\mathbf{q}) = \sigma_c \frac{2c^2}{p_c} \delta(E'_c - E_c) \frac{d\mathbf{q}}{E_q}, \tag{6}$$

where quantities referring to the c.m.s. are assumed to be expressed in terms of the corresponding quantities in the laboratory system.

Inserting (6) in (4), assuming $f_n = \rho_n/(\mathbf{s})$ and dividing N by $\rho^0 \rho_n{}^0 v_p$, we find for the effective cross section for scattering on a nucleon of the nucleus

$$\begin{aligned} d\sigma_{eff} = \frac{2Mc^2}{p} \cdot \frac{d\mathbf{q}}{E_q} \int d\mathbf{s} f(\mathbf{s}) \sqrt{|\mathbf{v}_p - \mathbf{v}_s|^2 - \frac{(\mathbf{v}_p \times \mathbf{v}_s)^2}{c^2}} \sigma_c \\ \times \frac{\delta(E'_c - E_c)}{p_c} \frac{1}{\sqrt{1-\beta_p{}^2}} = \frac{N}{\rho^0 \rho_n{}^0 v_p}. \end{aligned} \tag{7}$$

To evaluate the integral in eq. (7) it is convenient to introduce in $\mathbf{s}$-space a polar coordinate system (s, Θ, Φ) with the polar axis directed along the direction of momentum transfer $\mathbf{x} = \mathbf{p} - \mathbf{q}$. We first transform the δ-function. Since

$$E_c = 2E_{p_c} = 2 \frac{E_p - \mathbf{v} \cdot \mathbf{p}}{\sqrt{1 - v^2/c^2}},$$

where $\mathbf{v}$ is the velocity of centre of mass of the colliding nucleons (and similarly for E'_c), we get

$$\delta(E'_c - E_c) = \tfrac{1}{2} \sqrt{1 - \frac{v^2}{c^2}} \delta(E_q - \mathbf{v} \cdot \mathbf{q} - E_p + \mathbf{v} \cdot \mathbf{p}) = \frac{1}{2c} \delta(\mathbf{x} \cdot \mathbf{P}) \sqrt{\mathbf{P}^2}, \tag{8}$$

where $\mathbf{P}$ and $\mathbf{x}$ are four-dimensional vectors of the total momentum and momentum transfer, and the scalar product of the two vectors $\mathbf{a}$ and $\mathbf{b}$ is defined as $\mathbf{a} \cdot \mathbf{b} = -(a_4 b_4 + \mathbf{a} \cdot \mathbf{b}) = a_0 b_0 - \mathbf{a} \cdot \mathbf{b}$. For integration over the polar angle Θ the well known formula

$$\delta(f(\Theta)) = \sum_{\Theta_0} \frac{\delta(\Theta-\Theta_0)}{\left|\frac{\partial f(\Theta)}{\partial(\Theta)}\right|_{\Theta=\Theta_0}},$$

was employed, where summation is carried out over all roots of the equation $f(\Theta_0) = 0$. In the case under consideration the role of $f(\Theta)$ is played by the function

$$\mathbf{x}\cdot\mathbf{P} = \frac{(E_q-E_p)(E_s+E_p)}{c^2} - (\mathbf{p}+\mathbf{s})\cdot\mathbf{x}.$$

Equating it to zero we get

$$\cos\Theta_0 = \frac{\frac{1}{c^2}(E_q-E_p)(E_s+E_p) - \mathbf{p}\cdot\mathbf{x}}{s|\mathbf{x}|}. \tag{9}$$

Together with eq. (9), the condition $|\cos\Theta_0| \leqq 1$ leads to the result that allowed values of s possess a lower limit $s = s_0$:

$$s_0 = \frac{1}{\mathbf{x}^2 - \frac{(E_q-E_p)^2}{c^2}}\left| x\left\{\frac{E_p(E_q-E_p)}{c^2} - \mathbf{x}\cdot\mathbf{p}\right\}\right.$$
$$\left. + \frac{(E_q-E_p)}{c}\sqrt{\left[\frac{E_p(E_q-E_p)}{c^2} - \mathbf{p}\cdot\mathbf{x}\right]^2 - \left[\frac{(E_q-E_p)^2}{c^2} - \mathbf{x}^2\right]M^2c^2}\right|. \tag{10}$$

The root under the absolute value sign is always real since $\mathbf{x}$ is either space-like or a zero vector. The derivative $|\partial f(\Theta)/\partial\Theta|_{\Theta=\Theta_0}$ is equal to $|\partial(\mathbf{x}\cdot\mathbf{P})/\partial\Theta|_{\Theta=\Theta_0} = xs\sin\Theta_0$.

Thus,

$$\delta(E'_c - E_c) = \frac{1}{2c}\sqrt{\mathbf{P}^2}\cdot\frac{\delta(\Theta-\Theta_0)}{xs\sin\Theta_0}. \tag{11}$$

Inserting (11) in (7) and taking into account that

$$p_c = \frac{\sqrt{(\mathbf{P}\cdot\mathbf{p})^2-\mathbf{P}^2\mathbf{p}^2}}{\sqrt{\mathbf{P}^2}} = \frac{1}{\sqrt{\mathbf{P}^2}}\cdot\frac{M^2c^2}{\sqrt{1-\beta_\rho^2}\sqrt{1-\beta_s^2}}\cdot\frac{1}{c}\sqrt{|\mathbf{v}_p-\mathbf{v}_s|^2 - \frac{(\mathbf{v}_p\times\mathbf{v}_s)^2}{c^2}}$$

(this equality can be obtained by applying the general Lorentz transformation and expressing p_c in terms of laboratory quantities), we obtain after integration over Θ

$$d\sigma_{eff} = \frac{c^2}{px}\cdot\frac{d\mathbf{q}}{E_q}\int_{s_0}^{\infty}\int_0^{2\pi} d\Phi\,\frac{sds f(s)}{E_s}\sigma_c(E_c, \cos\vartheta_c)(\mathbf{P})^2. \tag{13}$$

Summation over all nuclear nucleons yields

$$\frac{d^2\sigma}{d\omega dq} = \frac{1}{p|\mathbf{q}-\mathbf{p}|}\frac{q^2}{\sqrt{c^2q^2+M^2c^4}}\sum_{i=1}^{A}\int_{s_0(q)}^{\infty}\int_0^{2\pi} d\Phi\,\frac{sds f(s)}{\sqrt{c^2s^2+M^2c^4}}E_c^2\sigma_{ci}(E_c,\vartheta_c). \tag{14}$$

The quantities E_c and $\cos\vartheta_c$ can easily be expressed in terms of the laboratory quantities and equal respectively

$$E_c = c\sqrt{(\mathbf{P})^2} = c\left[2(M^2c^2 + \frac{E_p E_s}{c^2} - \mathbf{p}\cdot\mathbf{s}\right]^{\frac{1}{2}},$$

$$\cos\vartheta_c = 1 + \frac{\frac{E_s(E_q - E_p)}{c^2} - \mathbf{x}\cdot\mathbf{s} - \left(\frac{E_p E_q}{c^2} - \mathbf{p}\cdot\mathbf{q}\right) + M^2c^2}{\frac{E_s E_p}{c^2} - \mathbf{s}\cdot\mathbf{p} - M^2c^2} \qquad (15)$$

$$= 1 + \frac{2\left[M^2c^2 - \frac{E_p E_q}{c^2} + \mathbf{p}\cdot\mathbf{q}\right]}{\frac{E_c^2}{2c^2} - 2M^2c^2},$$

where

$$\mathbf{x}\cdot\mathbf{s} = xs\cos\Theta_0,\ \mathbf{p}\cdot\mathbf{x} = px\cos\Theta_1,\ \mathbf{p}\cdot\mathbf{q} = pq\cos\vartheta,$$

$$\mathbf{p}\cdot\mathbf{s} = ps\cos(\mathbf{p},\hat{\mathbf{s}}),\ \cos(\hat{\mathbf{p}},\mathbf{s}) = \cos\Theta_0\cos\Theta_1 + \sin\Theta_0\sin\Theta_1\cos\Phi.$$

In the non-relativistic limit

$$s_0 \to \frac{q(q - p\cos\vartheta)}{|\mathbf{q}-\mathbf{p}|}.$$

If σ_c is assumed to depend only upon the momentum transfer, a formula is obtained which is analogous to that previously derived by Wolff [15]:

$$\frac{d^2\sigma}{d\omega dq} = \frac{8\pi q^2}{p|\mathbf{q}-\mathbf{p}|}\sum_{i=1}^{A}\sigma_c{}^i(\mathbf{q}-\mathbf{p})\int_{s_0}^{\infty} sf(s)ds. \qquad (16)$$

3. Experimental

The measurements of the energy spectra of the secondary particles emitted in p+Be, p+C, p+Cu and p+U collisions were carried out in the energy range approximately between 100 and 700 MeV at angles of 7°, 12.2°, 18°, 24° and 30°. The magnetic analyzer previously used to investigate the momenta spectra of the products of the $pp \to np\pi^+$, $pp \to pp\pi^0$ and $pp \to d\pi^+$ reactions [16]) and in experiments on direct knockout of deuterons from light nuclei by 670 MeV protons [4]) was used. Details concerning the analyzer, its position with respect to the primary proton beam and the concrete shield of the synchrocyclotron can be found in the papers cited above [16, 4]); the method of treatment of the results of the measurements and the corrections introduced are also described in the above-mentioned papers. The observation angle was varied by shifting target R(see fig. 1. ref.[10])) along the primary proton beam passing near the pole faces of the analyzer magnet. In all cases

entrance and exit of the particles took place normal to the boundary of the magnetic field. In table 1 is shown the dependence on the observation angle of the distance between the target and the front pole face, the angle of deflection of the particles in the magnetic field, radius of curvature of the central trajectory, angular divergence of the secondary particle beam defined in the horizontal plane and the instrumental resolution $\Delta(H\rho)/H\rho$ computed with account of only geometrical factors ($\Delta(H\rho)$ is the peak half-width).

TABLE 1

Observation angle Φ (degrees)	7	12.2	18	24	30
Distance between target and pole face (cm)	410	218	138	94	64
Deflection angle (degrees)	18.3	24	29.5	19.5	25.7
Radius of curvature ρ of the central trajectory (cm)	360	284.8	222	350	265
Angular divergence of secondary beam in horizontal plane (degrees)	0.10	0.14	0.17	0.20	0.22
Calculated resolution $\Delta(H\rho)/H\rho$(%)	1.9	1.5	1.2	2.6	1.9

The energy of the primary protons immediately in front of the target was 661 MeV; the mean square spread of the proton energies in the beam was about 1 %. A telescope consisting of four scintillation counters (total thickness 3.1 g/cm² tolan) connected in coincidence were employed to detect the particles of the analyzer exit. The proton detection threshold of the telescope was 60 MeV. Throughout the investigated energy range the counting efficiency was practically 100 %. The particles moved in vacuum in the analyzer before entering the telescope. The 2.5×1 cm targets were prepared from chemically pure Be, C, Cu and U. They were respectively 3.26, 1.09, 3.45 and 7.62 g/cm² thick.

The absolute values of the differential cross sections in the spectra, $d^2\sigma/d\omega dE$ were determined by measuring the differential cross sections $d\sigma/d\omega$ for emission of secondary charged particles between 7 and 40° in the investigated collisions. In these experiments, which were performed with an angular resolution of $\pm 0.8°$ at angles of 24°, 30° and 40° and with a resolution of about $\pm 0.4°$ at smaller angles, the counting threshold was the same as in the spectrum measurements. The charged π-mesons contribution was subtracted from the observed charged particle yield; this contribution was estimated from data on π^+-mesons produced in 670 MeV p+C collisions [5]) under the assumption that the cross section of this process increased as $A^{\frac{2}{3}}$. The contribution of charged π-mesons to the total secondary charged particle yield did not exceed 7 %. The areas under the curves of the secondary particle energy spectra were normalized to the corresponding experimental values of $d\sigma/d\omega$. The spectra were linearly extrapolated from the last experimental point to the energy threshold for proton detection. The

accuracy of this method of estimation of the values of $d^2\sigma/d\omega dE$ is about 20 %.

The experimental spectrum $F(E)$ is related to the true spectrum $G(E)$ by the linear integral relation

$$F(E) = \int_0^\infty G(E')K(E, E')dE', \tag{17}$$

where $K(E, E')$ is the experimental resolution curve of the apparatus. The function $K(E, E')$ was determined for each observation angle from the results of measurement of the shape of the peak corresponding to protons elastically scattered in pp-collisions. The peaks were observed under the same conditions as $F(E)$. The resolution curves could be best approximated by the function

$$K(E, E') = \frac{1}{2a}\exp\left(-\frac{|E-E'|}{a}\right), \tag{18}$$

where E is the energy in the middle of the elastic pp-scattering peak. With sufficient accuracy the solution of equation (17) can be written down as

$$G(E) \approx F(E) - a^2\frac{d^2F(E)}{dE^2}, \tag{19}$$

since $E \gg a$ and the value of a corresponding to the given observation angle was approximately constant on that part of the spectrum which was occupied by the quasi-elastic scattering peak. The values of E, a and $\Delta E/E$ corresponding to the observation angles under consideration are presented in table 2; ΔE is the half-width of the elastic pp-scattering peak. It should be noted that in the vicinity of the quasi-elastic scattering peak at 30°,

TABLE 2

Scattering angle Φ (degrees)	7	12.2	18	24	30
E(MeV)	647	621	578	521	455
a(MeV)	14.4	9.3	6.3	15.0	10.3
$\Delta E/E$(%)	4.7	2.9	1.6	4.4	4.0

the magnitude of the correction $a^2d^2F(E)/dE^2$ which accounts for instrumental distortions of the spectrum does not exceed 2—3 %.

4. Experimental Results

4.1. ANGULAR DISTRIBUTION DATA

The differential cross sections per nucleus for emission of a secondary charged particle recorded under the conditions of our experiments are collected in table 3 and represented in fig. 1 as a function of the emission angle in the laboratory system.

TABLE 3

Φ (degrees)	$d\sigma/d\omega(10^{-24}$ cm^2/sr)			
	Be	C	Cu	U
7	0.660±0.033	1.100±0.055	1.168±0.058	3.650±0.182
10	0.376±0.019	0.492±0.015	1.052±0.053	1.544±0.077
12.2	0.298±0.015	0.336±0.017	0.765±0.039	1.180±0.059
15	0.227±0.011	0.276±0.014	0.642±0.032	0.998±0.050
18	0.195±0.010	0.230±0.011	0.556±0.028	0.900±0.045
24	0.125±0.006	0.158±0.008	0.400±0.020	0.716±0.036
30	0.089±0.004	0.114±0.006	0.335±0.017	0.592±0.030
40	0.054±0.003	0.074±0.004	0.228±0.011	0.443±0.022

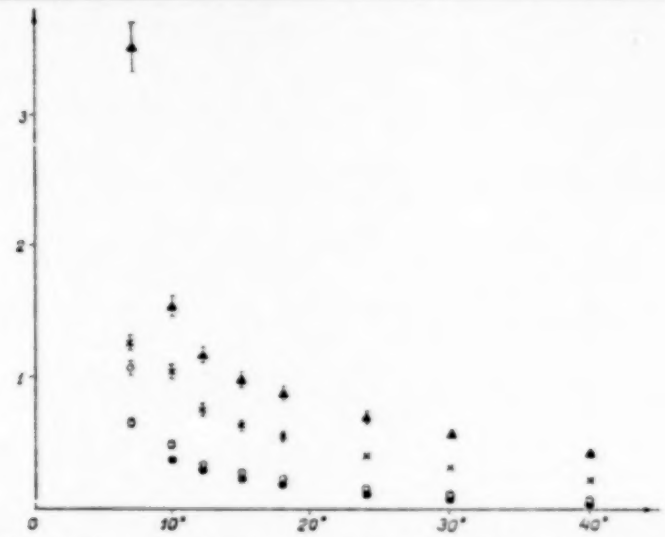

Fig. 1. Angular distributions of secondary charged particles possessing ranges of more than 3.18/cm^2 in tolane and emitted in 660 MeV p+Be, p+C, p+Cu and p+U collisions. ●-beryllium, ○-carbon, ×-copper, ▲-uranium.

Uncertainties due to statistical errors in measurement of the number of secondary particles and errors in determination of the intensity of the primary proton beam are indicated.

Between 40° and 18° where diffractional scattering is negligible (see figs. 3—7) the values of $d\sigma/d\omega$ for all investigated nuclei smoothly increased with decrease of the emission angle. In this case $d\sigma/d\omega$ as a function of A could be approximated by a function of the form KA^r. The result of this method of treatment of the experimental data is represented in fig. 2. Between Be and Cu the values of $d\sigma/d\omega$ increased in approximately the following way (in units of 10^{-26} cm^2/sr)

$$\left(\frac{d\sigma}{d\omega}\right)_{40^\circ} \approx 1.20\,A^{0.71}; \quad \left(\frac{d\sigma}{d\omega}\right)_{30^\circ} \approx 2.12\,A^{0.67}$$

$$\left(\frac{d\sigma}{d\omega}\right)_{24^\circ} \approx 3.62\,A^{0.58}; \quad \left(\frac{d\sigma}{d\omega}\right)_{18^\circ} \approx 6.12\,A^{0.53}.$$

These results indicate that with decrease of angle the dependence of $d\sigma/d\omega$ on A becomes less pronounced. Proceeding from data obtained for U, the dependence of $d\sigma/d\omega$ on A becomes weaker near the end of the periodic table. One, of course, cannot estimate the differential cross sections of the nuclear interactions under consideration or establish their dependence on A from the results presented above since the mean number of secondary particles emitted in each collision and recorded in the experiments is unknown.

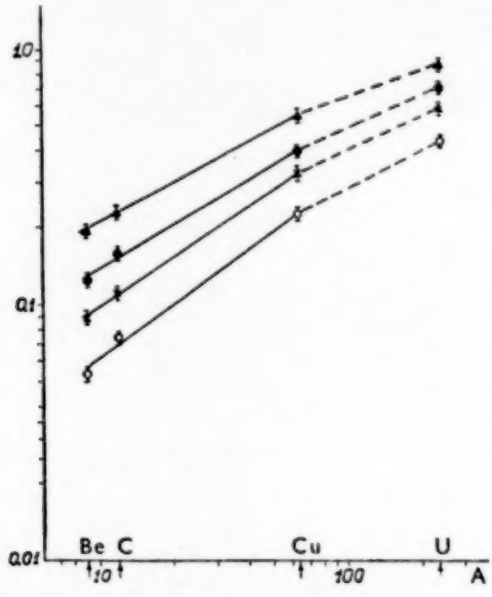

Fig. 2. Differential cross sections for ejection by 660 MeV protons of secondary charged particles with ranges exceeding 3.18/cm² in tolane as a function of mass number. In the laboratory system: ▲ −18°, ● −24°, × −30°, ○ −40°.

For angles below 18° the differential cross sections for the investigated nuclei vary rapidly and nonuniformly due to the significant contribution of diffractional scattering to the secondary particle yield.

4.2. ENERGY SPECTRA

By measuring the number of particles at the spectrometer exit as a function of the magnetic field strength, introducing the required corrections and normalizing the result to unit counting rate of the monitor, one can represent the relative secondary particle momentum spectrum in equal units of H_ρ. The transformation from the momentum spectrum to the energy spectrum was performed under the assumption that the secondary particles are protons. This assumption should be checked for that part of the spectra which corresponds to cascade protons since there may be a relatively small admixture of deuterons produced as a result of nucleon pickup in the surface layer of the nucleus by secondary nucleons [17]). This indirect pickup process may also lead to emission of small amounts of fast tritium nuclei. According to the data of Hess and Moyer [18]) the ratio of the yields of secondary protons,

deuterons and tritons emitted at angles of 26°, 40° and 60° as a result of proton bombardn.ent of C, Cu and U is approximately 1000 : 50 : 2. The deuteron energy spectrum in this case varies with the energy as E^{-3} and extends almost up to 150 MeV. Since properties of the internal nuclear cascade process weakly vary with the energy of the incident nucleon it may be assumed that with increase of the energy from 330 MeV to 670 MeV the relation between the secondary proton, deuteron and triton yields will not change significantly.

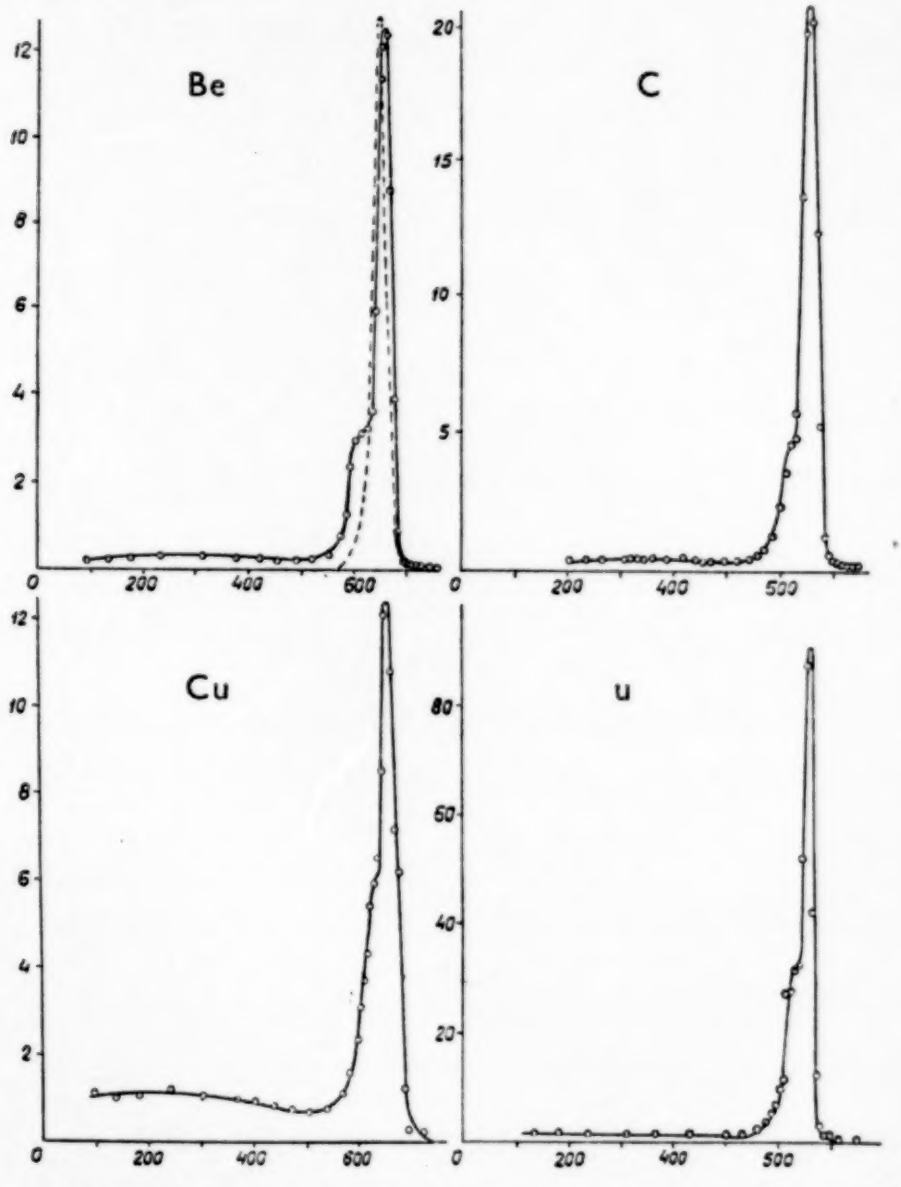

Fig. 3. Energy spectra of secondary charged particles ejected by 660 MeV protons in p+Be, p+C, p+Cu and p+U collisions. The dashed line is the resolution curve. Observation angle 7°.

Among the secondary charged particles observed at small angles there may be deuterons from the reactions $pp \rightarrow d\pi^+$ and $pn \rightarrow d\pi^0$ which may occur

on bound nucleons. At 660 MeV the contribution of these reactions to the total cross section for free pp and pn collisions is respectively ≈ 7.3 % and ≈ 4 %. It may be expected, however, that deuteron emission from the nuclei will be strongly inhibited due to the fact that the deuteron mean free path in nuclear matter is small compared with the size of the nucleus.

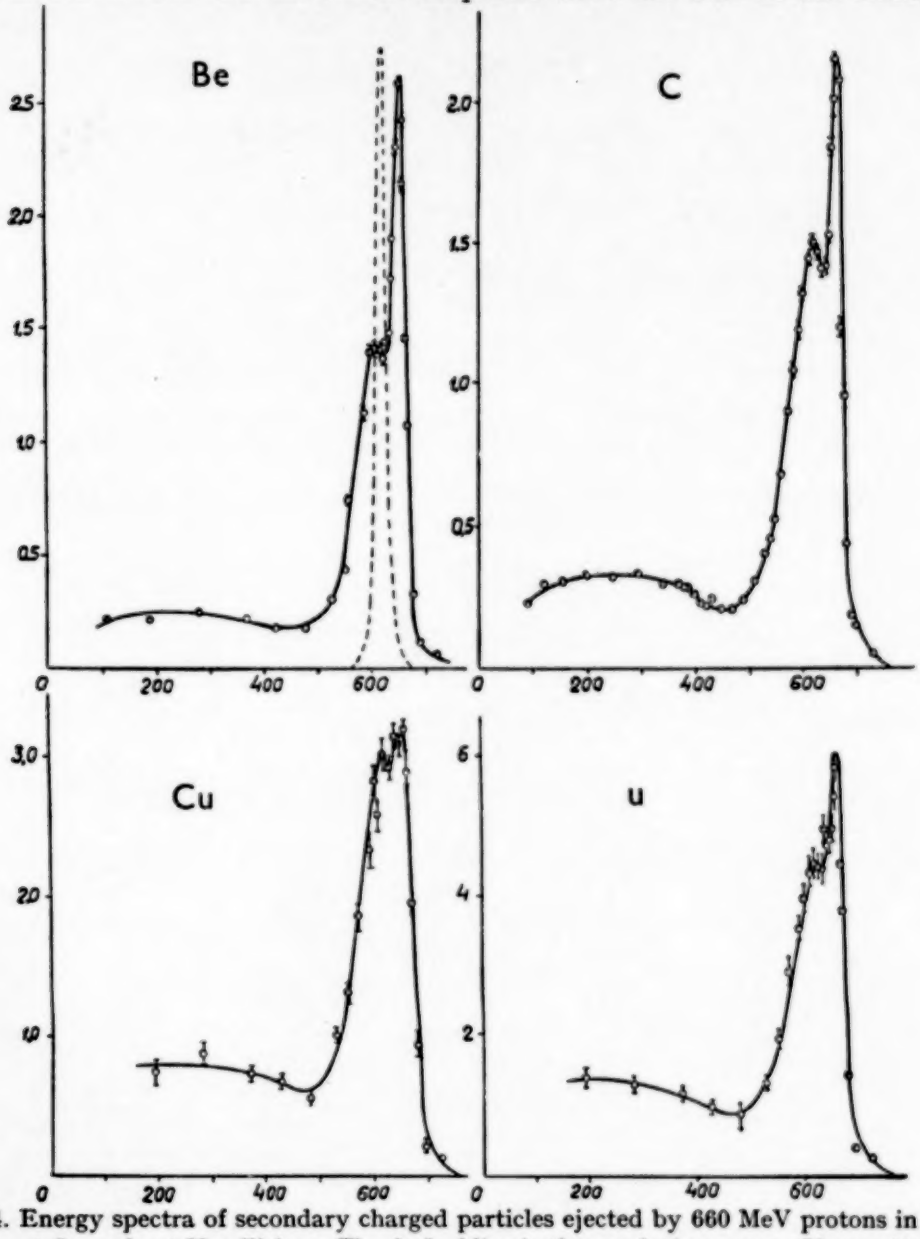

Fig. 4. Energy spectra of secondary charged particles ejected by 660 MeV protons in p+Be, p+C, p+Cu and p+U collisions. The dashed line is the resolution curve. Observation angle 12.2°.

The energy spectra of secondary protons produced in p+Be, p+C, p+Cu and p+U collisions are presented in figs. 3—7 by the solid lines which were drawn visually through the experimental points; the verticle lines represent the statistical errors of the measurements. The observed elastic pp scattering peaks are shown by the dashed lines. The heights of those

peaks which represent the spectrometer resolution curves are not connected with the scale of the ordinates.

At angles of 7° the high energy parts of the spectra of all investigated nuclei consist of intense peaks due in the main to protons scattered diffractionally on the nuclei. These peaks are superimposed on the right hand slopes

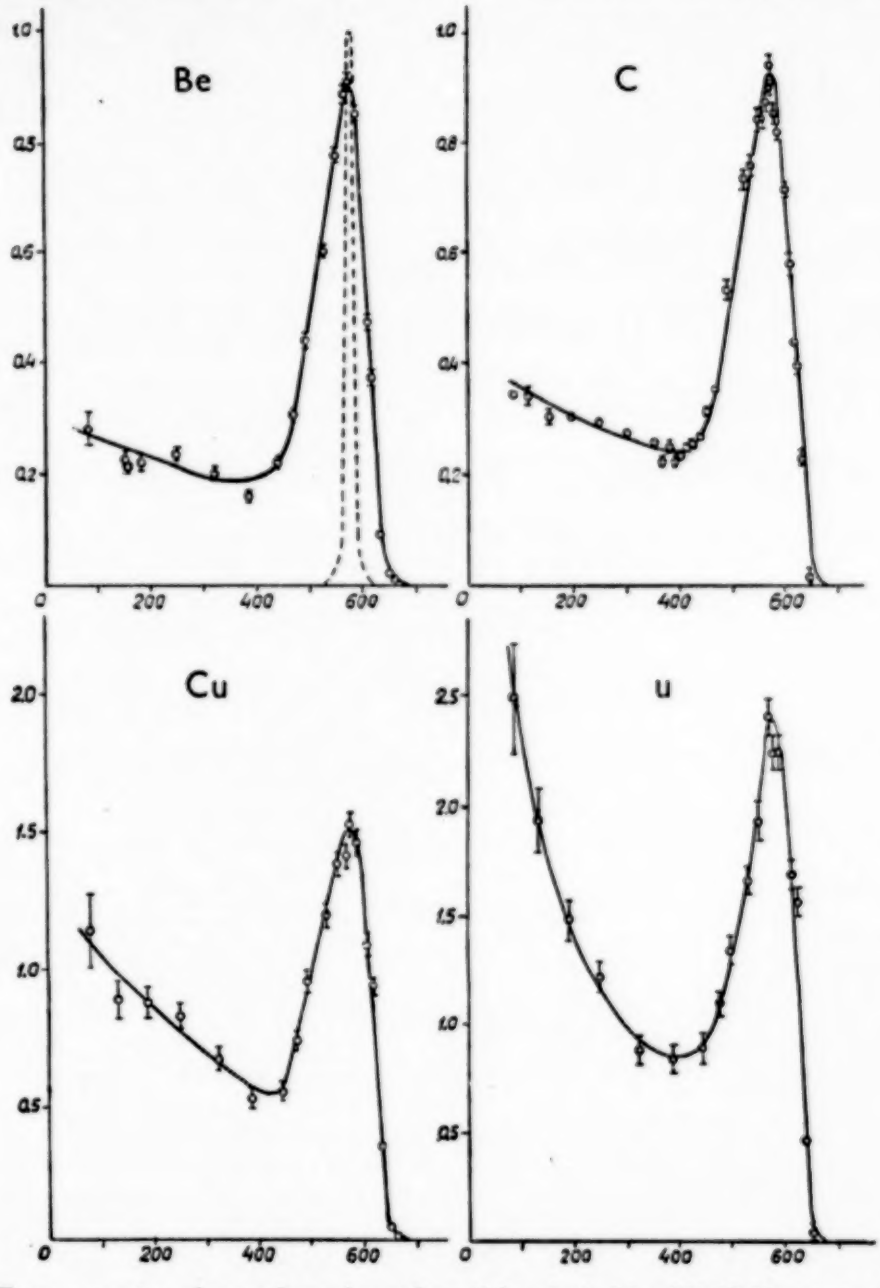

Fig. 5. Energy spectra of secondary charged particles ejected by 660 MeV protons in p+Be, p+C, p+Cu and p+U collisions. The dashed line is the resolution curve. Observation angle 18°.

of the proton quasi-elastic scattering peaks. The magnitude of the shift of the diffraction scattering peaks towards larger energies relative to the elastic pp scattering peaks corresponds to the energy difference of the corresponding

recoil nuclei. It can be seen that at 7° the yield of secondary protons with $E > 500$ MeV is mainly due to diffraction scattering. The contribution of diffraction scattering through 12.2° to the total secondary proton yield is much less, especially for p+Cu collisions. This property of the 12.2° spectra is consistent with the well-known values of the nuclear radii. Thus if in

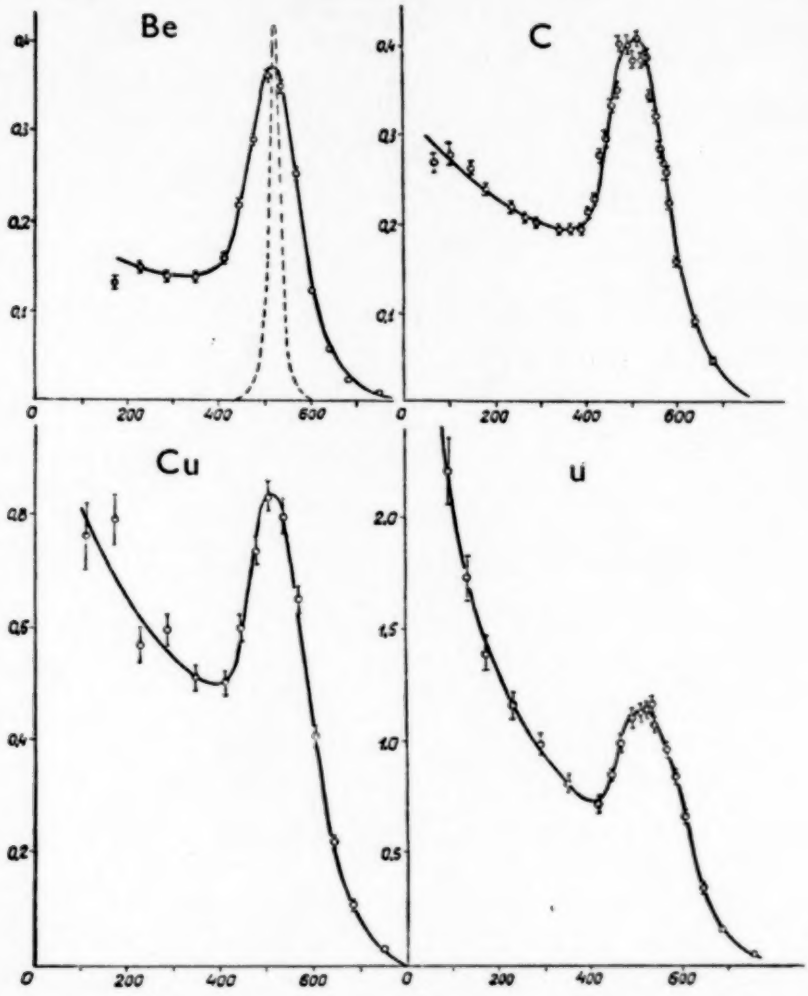

Fig. 6. Energy spectra of secondary charged particles ejected by 660 MeV protons in p+Be, p+C, p+Cu and p+U collisions. The dashed line is the resolution curve. Observation angle 24°.

accordance with the results of determination of the nuclear radii from the cross sections for absorption of 1400 MeV neutrons [19]) and 860 MeV and 900 MeV protons [21]) we insert the value $R = 1.26\, A^{\frac{1}{3}} \times 10^{-13}$ cm (R is the radius of the scattering nucleus) into the expression for the diffraction scattering angular distribution

$$\frac{\mathrm{d}\sigma}{\mathrm{d}\omega} = k^2 (R')^4 \left[\frac{J_1(2kR' \sin \frac{1}{2}\Theta)}{2kR' \sin \frac{1}{2}\Theta}\right]^2, \qquad (20)$$

where Θ is the scattering angle, $k = 2\pi/\lambda$, λ is the wave length of the incident proton, $R' = R+1/k$ and J_1 is a Bessel function of the first kind, we find that near 12.2° there should be a fourth maximum for U, whereas for Cu this scattering angle approximately corresponds to the position of a second minimum.

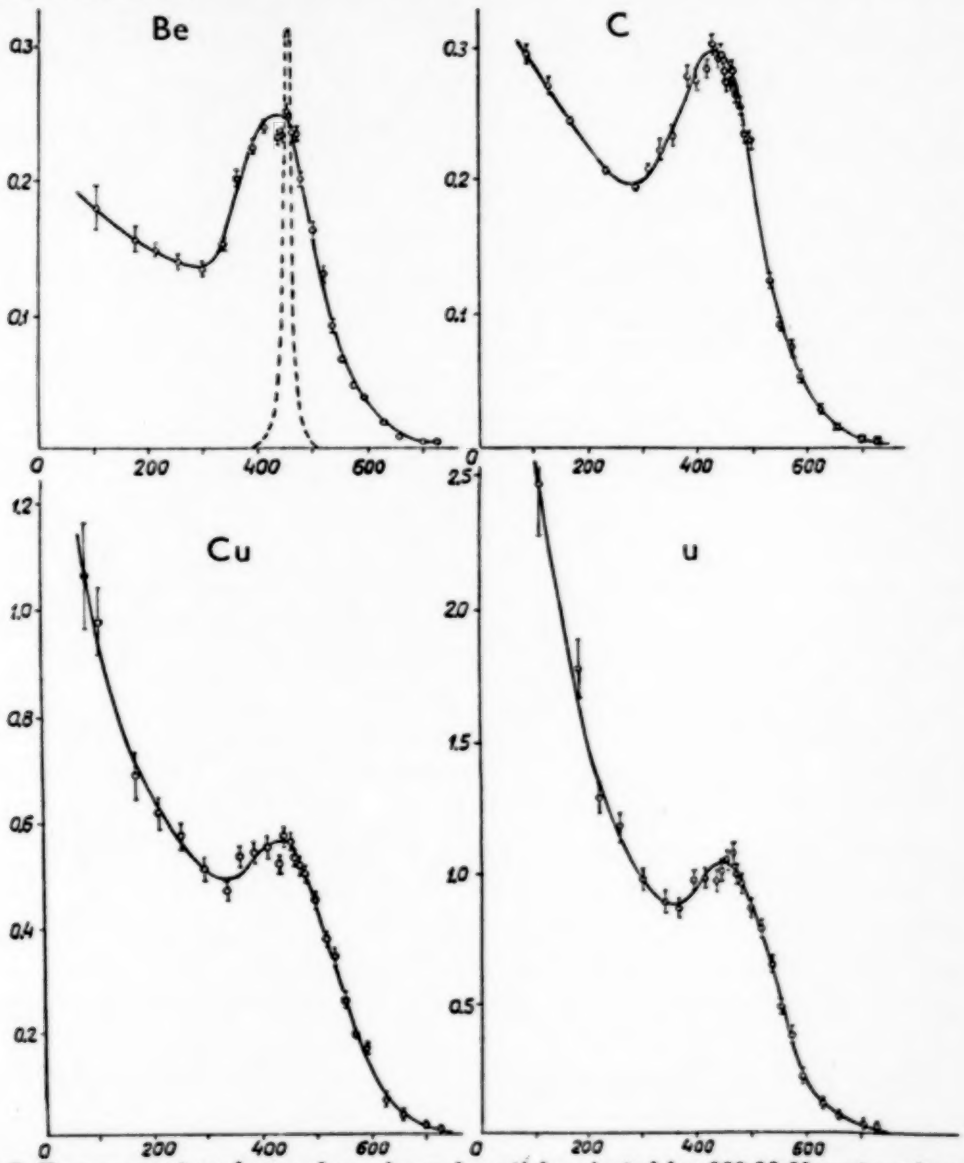

Fig. 7. Energy spectra of secondary charged particles ejected by 660 MeV protons in p+Be, p+C, p+Cu and p+U collisions. The dashed line is the resolution curve. Observation angle 30°.

A characteristic feature of the spectra measured at 18° is the absence of typical diffraction peaks and the sharp cut-off of the quasi-elastic scattering peaks near the upper limit of the energy region defined by the conservation laws. At 24° and 30° distinct maxima are observed in the high energy regions of the spectra of all investigated elements, these maxima correspond to

single quasi-elastic collisions between the protons and nucleons of the nuclei. Assuming that the quasi-elastic scattering peaks are symmetric, it was possible to estimate the differential quasi-elastic scattering cross-section by measuring the areas under them and comparing the values with the sum

$$Z\frac{d\sigma_{pp}}{d\omega}+(A-Z)\frac{d\sigma_{pn}}{d\omega}$$

where $d\sigma_{pp}/d\omega$ and $d\sigma_{pn}/d\omega$ are the pp and pn elastic scattering cross sections †. Thus it was found that quasi-elastic scattering in Be, C, Cu and U through an angle of 30° comprises respectively ≈ 60, ≈ 53, ≈ 22 and ≈ 9 % of free scattering. It is important that after the first collision with one of the nucleons of the nucleus the proton can be ejected from the heaviest nuclei with an appreciable probability without experiencing any other interactions. This may be regarded as indication that the observed nucleon collisions occur primarily in the surface layer of the nucleus. In this connection it might be mentioned that the nuclear cascade computations carried out by Metropolis *et al.* [23]) for a nuclear model with a sharp boundary predict that when Al and U are bombarded by 460 MeV and 1840 MeV protons the secondary proton energy spectrum should not possess a peak due to protons which experienced only single collision. It may be expected that use of a nuclear model with diffuse edge for cascade calculations should lead to an increase of the relative frequency of emission of protons after the first collision and thus yield better agreement with the experimental secondary proton spectrum.

The strong smearing out of the quasi-elastic scattering peaks compared to the elastic pp scattering peak is a direct reflection of the momentum distribution of the nucleons in the nuclei. The quasi-elastic scattering peaks are somewhat shifted towards smaller energies with respect to the elastic pp scattering peaks. A similar decrease of the mean proton energy in quasi-elastic scattering was also detected at 340 MeV and interpreted as being the result of collisions of nucleons in the potential well, energy losses on excitation of the residual nuclei and increase of the scattering cross sections at relatively smaller collision energies [8]).

The continuous spectra observed below the quasi-elastic scattering peaks are due to inelastic processes. In the case of p+Be and p+C collisions the shapes of the continuous spectra closely resemble those of recoil protons from the reactions $pp \rightarrow np\pi^+$ and $pp \rightarrow pp\pi^0$ (see fig. 2 and 3 in ref. [16]). It may thus be concluded that in collisions between protons of a given energy and light nuclei the continuous spectra are mainly due to π-meson production in single proton-nucleon collisions but not to nuclear cascade process. On the

† In these calculations the values of $d\sigma_{pn}/d\omega$ for 660 MeV were assumed to equal the corresponding differential cross sections for elastic np-scattering obtained by Kazarinov and Simonov at an energy of 580 MeV [22]).

contrary, in p+Cu and p+U collisions the continuous spectra are mainly due to the cascade process. This is substantiated by the fact that the rate of growth of the number of particles in the continuous spectra with decreasing energy is the higher the larger the size of the nucleus and hence the cascade process in it develops much more intensively. This feature of the continuous spectra becomes more pronounced with increase of the observation angle.

5. Comparison of the Experimental and Calculated Quasi-Elastic Scattering Energy Spectra

The quasi-elastic scattering spectra of Be and C measured at 30° were employed in the comparison since the influence of interference effects should be smallest in this case. Two types of momentum distributions were tested:

a) Gaussian distribution

$$f(s) \propto \exp\left(-\frac{s^2}{{s_0}^2}\right)$$

for four values of s_0 corresponding to 16, 18, 20 and 22 MeV;

b) a three-parameter sum of two Gaussian distributions

$$f(s) \propto \exp\left(-\frac{s^2}{{s_1}^2}\right) + \alpha \exp\left(-\frac{s^2}{{s_2}^2}\right)$$

with $s_1^2/2M = 16$ MeV and $s_2^2/2M = 50$ MeV and also a similar Selove [3]) distribution with $s_1^2/2M = 7$ MeV and $s_2^2/2M = 50$ MeV and $\alpha = 0.15$. The parameter α was chosen by making the best fit between the calculations and the experimental high energy tail of the quasi-elastic scattering peak.

Evaluation of E_c and $\cos\vartheta_c$ by formulas (15) for prescribed values of s and E_q and subsequent evaluation of the integrals in expression (14) were carried out on the "Ural" electronic computer of the Joint Institute for Nuclear Research. The pp- and pn-differential scattering cross sections corresponding to each pair of values of E_c and $\cos\vartheta_c$ were determined from plots of $d\sigma_{pp}/d\omega$ and $d\sigma_{pn}/d\omega$ as a function of energy and scattering angles $20° \leqq \vartheta_c \leqq 160°$.

Intermediate values of $d\sigma_{pp}/d\omega$ and $d\sigma_{pn}/d\omega$ were determined by graphical interpolation from the experimental data on pp and pn differential scattering cross sections compiled by Hess [24]). In a similar manner the values of $d\sigma_{pn}/d\omega$ for energies exceeding 580 MeV were derived from results of measurement of the differential cross sections for elastic np scattering at 580 MeV [22]) and quasi-elastic pn scattering at 970 MeV [25]).

The final result of the calculations was obtained on the sum of the momentum distributions of the emitted protons

$$Z\frac{d^2\sigma_{pp}}{d\omega dq} + (A-Z)\frac{d^2\sigma_{pn}}{d\omega dq};$$

this sum depended only on q and could easily be transformed to the energy spectrum of protons which suffered a single quasi-elastic collision. Some of the computed quasi-elastic scattering energy spectra in Be and C are reproduced in figs. 8 and 9 together with the experimental data. The horizontal lines through the experimental points represent the energy resolution which decreased from 3.8 % at 300 MeV to 4.1 % at 660 MeV. In order to fit the peak of the theoretical curves with the quasi-elastic peak it was necessary to

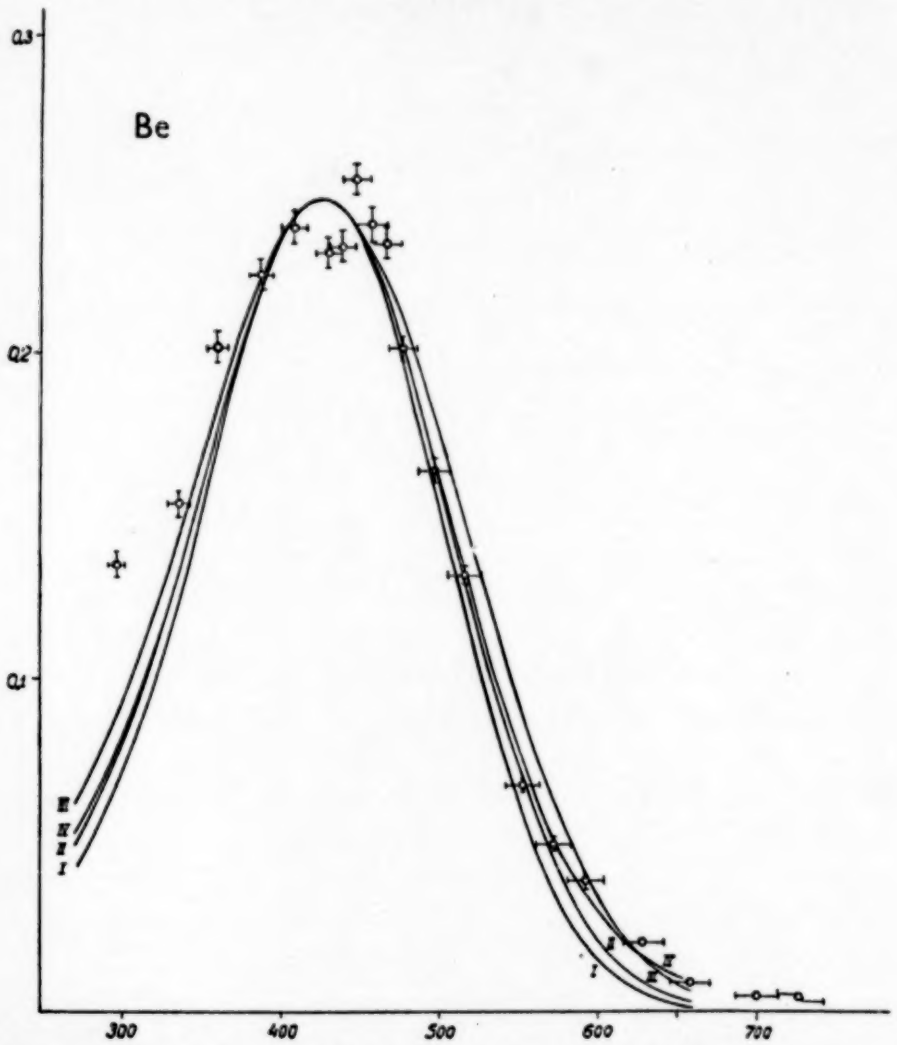

Fig. 8. Energy spectrum of quasi-elastically scattered protons; theoretical curves and experimental data for Be at incident proton energy of 660 MeV. Observation angle 30°. I, II, III; Gaussian distribution with 1/e value of respectively 16, 18 and 22 MeV; IVe sum of two Gaussian distributions of the form $\exp(-s^2/s_1^2)+\alpha\exp(-s^2/s_2^2)$ with $s_1^2/2M = 16$ MeV, $s_2^2/2M = 50$ MeV and $\alpha = 0.06$.

shift the theoretical curves towards smaller energies since the calculations did not account for the presence of a potential well or excitation effects in the residual nuclei. For the spectra under consideration this shift was about 30 MeV.

It can be seen from figs. 8 and 9 that at energies lying below that of the quasi-elastic scattering peak, the theoretical curves lie below the experimental points. This discrepancy may be due to the smeared out spectrum of protons multiply scattered in nuclei, this spectrum being superimposed on the left hand part of the quasi-elastic peak. The theoretical curves and experimental data were compared in the high energy region of the spectrum in which the effect from multiple nuclear scattering should be insignificant.

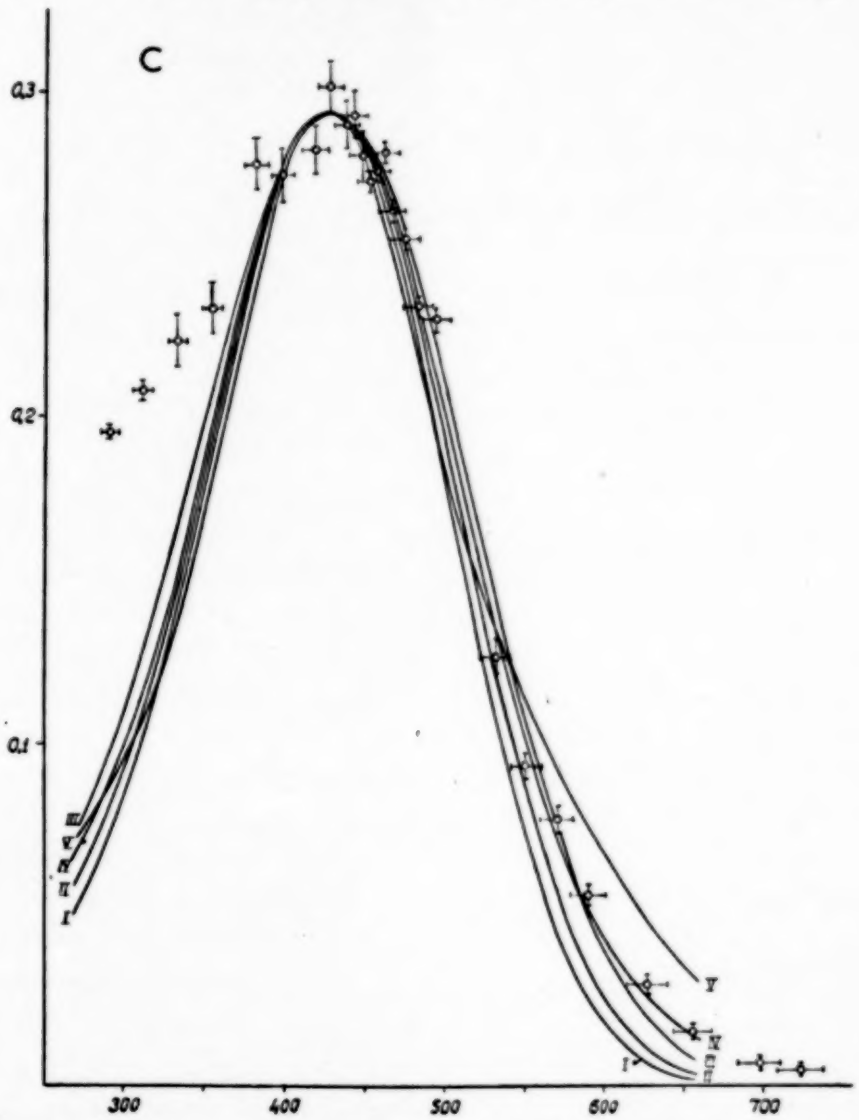

Fig. 9. Energy spectra of quasi-elastically scattered protons; theoretical curves and experimental data for C at incident proton energy of 660 MeV. Observation angle 30°. I. II, III: Gaussian distribution with 1/e value of respectively 16, 18 and 22 MeV. IV, V: sum of two Gaussian distributions of the form $\exp(-s^2/s_1^2)+\alpha\exp(-s^2/s_2^2)$ with

$$\text{IV:}\ \frac{s_1^2}{2M} = 16\ \text{MeV},\quad \frac{s_2^2}{2M} = 50\ \text{MeV},\quad \alpha = 0.09;$$

$$\text{V:}\ \frac{s_1^2}{2M} = 7\ \text{MeV},\quad \frac{s_2^2}{2M} = 50\ \text{MeV},\quad \alpha = 0.15.$$

In a first approximation the observed spectra are consistent with a Gaussian momentum distribution with a 1/e value of about 20 MeV. This means that the mean square value of the nucleon momentum in Be and C nuclei corresponds to an energy of about 30 MeV. Evidently, somewhat better agreement with experiment can be obtained near the upper boundary of the carbon spectrum by taking a three-parameter sum of two Gaussian distributions with $s_1^2/2M = 16$ MeV, $s_2^2/2M = 50$ MeV and $\alpha = 0.09$. However, the experimental data are not exact enough to permit one to state with certainty that this distribution is preferable to a simple Gaussian distribution. In the Selove distribution [3]), on the other hand, high momenta are too abundant, and far away from the quasi-elastic scattering peak the cross sections are too large.

The results obtained here seem to indicate that a theory based on the concept of two-particle collisions between fast nucleons in nuclei in general yields a correct shape of the high energy tail of the quasi-elastic peak. However, one should not attach too much importance to this circumstance, since the result of comparison of theory and experiment depends entirely on the shape of the highest energy part of the spectrum; this in turn depends on collisions between the incident protons and high momentum nucleons, that is, nucleons which strongly interact with other particles during the collision; and it is clear that for such collisions it is especially difficult to meet the requirements of applicability of the impulse approximation. It should be mentioned in this connection that scattering of protons on compact two-nucleon units and possibly on α-particles which exist in nuclei as substructural units, should undoubtedly distort somewhat the high energy part of the quasi-elastic scattering spectrum. On the other hand, the background observed at energies exceeding that of a proton after its first quasi-elastic scattering may partly be due to deuterons knocked out of the nuclei by protons colliding with compact two-nucleon units.

These conclusions do not contradict the fundamental fact that distributions containing large momentum values are required in order to explain the observed quasi-elastic scattering spectra. If the momentum distribution of nucleons were a Fermi distribution with an upper limit corresponding to $E \approx 30$ MeV (degenerate gas model), no elastically scattered protons with energies above ≈ 525 MeV would be observed at an angle of 30° in the present experiments. High momentum states of nucleons in nuclei are probably due to strong two-nucleon interactions which nucleons are sometimes subjected to when they move independently in the average field of the nucleus, and which are conditioned by a short range potential.

6. Conclusion

The energy spectra of secondary charged particles (mainly protons) obtained in the present experiments yield information on the relative role of

various processes occurring during the interaction of 660 MeV protons with light and heavy nuclei. The relevant processes are diffraction scattering of protons on nuclei and quasi-elastic scattering on individual nucleons, the nuclear cascade process and π-meson production in nucleon collisions. Collisions between protons and compact two-nucleon units also yield a relatively small contribution to the secondary proton yield, a proof of which is direct ejection of deuterons from light nuclei by protons [4]) and the strong smearing out of the π-meson spectrum at high energies [5]).

The nucleon momentum distribution in Be and C nuclei obtained in the present experiments (a Gaussian distribution with a 1/e value of about 20 MeV) is in fairly good agreement with the results obtained by the Berkeley group at 340 MeV [8, 9]). Thus, an analysis of quasi-elastic scattering of protons in light nuclei in a broad range of collision energies leads to approximately the same momentum distribution of the nucleons. Evidently this means that it is quite legitimate to study quasi-elastic scattering in Be and C nuclei from the viewpoint of the impulse approximation. It should be emphasized that within the present accuracy of measurements the quasi-elastic scattering spectra in Be and C can, in a first approximation, be reproduced by using the same momentum distribution of the nucleons. Due to the large effect of multiple nuclear scattering no definite conclusions can be made regarding the momentum distribution of nucleons in heavy nuclei on basis of the quasi-elastic scattering spectra in Cu and U.

The authors are grateful to K. N. Fyodorova and I. V. Popova for programming the calculations and carrying them out; thanks are also due to S. M. Bilenky, N. I. Klepikov, L. M. Soroko and N. A. Chernikov for useful discussions.

References

1) G. Chew and M. Goldberger, Phys. Rev. **77** (1950) 470
2) J. Hadley, and H. York, Phys. Rev. **80** (1950) 345
3) W. Selove, Phys. Rev. **101** (1956) 231
4) L. S. Azhgirey, I. K. Vzorov, V. P. Zrelov, M. G. Mescheryakov, B. S. Neganov and A. F. Shabudin, JETP **33** (1957) 1185
5) L. S. Azhgirey, I. K. Vzorov, V. P. Zrelov, M. G. Mescheryakov and V. I. Petrukhin, JETP **34** (1958) 1357
6) E. Henley, Phys. Rev. **85** (1952) 204
7) C. Richman and H. Wilcox, Phys. Rev. **78** (1950) 496
8) J. Cladis, W. Hess and B. Moyer, Phys. Rev. **87** (1952) 425
9) J. Wilcox and B. Moyer, Phys. Rev. **99** (1955) 875
10) J. McEwen, W. Gibson and P. Duke, Phil. Mag. **2** (1957) 231
11) A. Wattenberg, A. Odian, P. Stein, H. Wilson and R. Weinstein, Phys. Rev. **104** (1956) 1710
12) S. Belyaev and G. Budker, Doklady **107** (1956) 807
13) C. Møller, Mat. Fys. Medd. Dan. Vid. Selsk. **23**, No. 1 (1945)

14) N. Chernikov, Doklady **114** (1957) 530
15) R. Wolff, Phys. Rev. **87** (1952) 434
16) M. G. Mescheryakov, B. S. Neganov, I. K. Vzorov, V. P. Zrelov and A. P. Shabudin, Doklady **109** (1956) 499
17) B. Bransden, Proc. Phys. Soc. A **65** (1952) 738
18) W. Hess and B. Moyer, Phys. Rev. **101** (1956) 337
19) T. Coor, D. Hill, W. Hornyak, L. Smith and G. Snow, Phys. Rev. **98** (1955) 1369
20) F. Chen, C. Leavitt and A. Shapiro, Phys. Rev. **99** (1955) 857
21) N. Booth, B. Ledley, D. Walker and D. White, Proc. Phys. Soc. A **70** (1957) 209
22) Yu. M. Kazarinov and Yu. N. Simonov, JETP **31** (1956) 169
23) N. Metropolis, R. Bivins, M. Storm, A. Turkevich, J. Miller and G. Friedlander, Phys. Rev. **110** (1958) 185, 204
24) W. Hess, Revs. Mod. Phys. **30** (1958) 368
25) A. Batson, B. Culwick, J. Klepp and L. Riddiford, communicated by O. Piccioni, Proceedings 1958 Annual International Conference on High Energy Physics at CERN (1958) p. 73

1.D.2:
2.I

Nuclear Physics **13** (1959) 281—291; © *North-Holland Publishing Co., Amsterdam*
Not to be reproduced by photoprint or microfilm without written permission from the publisher

THE SHAPE OF THE NUCLEAR PHOTO-RESONANCE IN DEFORMED NUCLEI

BEN R. MOTTELSON and SVEN GÖSTA NILSSON †
NORDITA (*Nordisk Institut for Teoretisk Atomfysik*), *Copenhagen*

Received 22 April 1959

Abstract: The characteristic features of photonuclear resonance spectra of deformed nuclei are discussed on the basis of some simple estimates in which we employ nucleonic wave functions in the approximate, "asymptotic" form. The likelihood, in different regions of deformed nuclei, of a resolution of the resonance spectrum into two separate peaks is discussed. Finally, in the appendix, we exhibit a convenient operator method for deriving various nuclear matrix elements in the representation based on the "asymptotic" wave functions.

1. Introduction

In an ellipsoidal potential the frequency of particle motion is higher for motion along the symmetry axis than for motion perpendicular to that axis. Thus, one expects that the nuclear dipole photo-resonance will be split or at least broadened in deformed nuclei, and indeed such an effect has recently been observed ††. This effect has been discussed earlier by D. H. Wilkinson (ref. [5])), who calculated the actual resonance shape for a few representative nuclei, employing the detailed wave functions of ref. [6]). The present calculations are based on the more approximate "asymptotic" wave functions (see the appendix). In the latter case one can obtain simple estimates in a closed form, which may facilitate the understanding of the different physical effects that determine the resonance shape.

If we start from an axially symmetric, but non-isotropic, harmonic oscillator potential for the single-particle motion, we would expect the photo-resonance to consist of two lines, one at $\hbar\omega_z$, corresponding to excitation of particle motion along the symmetry axis, and one at $\hbar\omega_\perp$ for excitation of motion in a plane perpendicular to the symmetry axis. Since all the well-known non-spherical nuclei have a prolate shape, ω_z is smaller than $\omega_\perp$. Also, the total strength of the line at $\hbar\omega_\perp$ is twice that of the line at $\hbar\omega_z$.

These lines will be broadened by a number of effects. First, the nucleus

† On leave from the University of Lund, Sweden.

†† For a summary of the theoretical and experimental data on this effect see ref.[1]); cf. also refs. [2–4]).

may be set into rotation as a consequence of its interaction with the photon. If the ground-state spin is I_0, the rotational states with total angular momenta I_0+1, I_0 and I_0-1 may be excited. In the rare-earth nuclei and for the heavy elements the energy difference between these states will be only a few hundred keV; however, in the region of deformed nuclei around $A = 25$ these rotational energies should amount to about 2 MeV (for $I_0 = \frac{5}{2}$). In any case for $I_0 = 0$ (as in even nuclei) the E1 process can excite only states with $I = 1$.

A second source of broadening of the lines is associated with the deviations from a harmonic oscillator potential. It is easy to see that the types of deviation which have been especially considered [6]) will tend systematically to broaden the line at $\hbar\omega_\perp$ more than the line at $\hbar\omega_z$. Thus, the spin-orbit force depends, in first approximation, only on the component of the orbital angular momentum of the particle along the symmetry axis, Λ; for the transitions corresponding to $\hbar\omega_z$ this angular momentum is not changed, and the corresponding line is not split by this term. The transition with $\hbar\omega_\perp$ is associated with a change $\Delta\Lambda = \pm 1$, and there is thus a splitting of the high-frequency line due to the spin-orbit force. Also deviations from the harmonic oscillator potential that are proportional to the square of the angular momentum of the particle, $\mathbf{l}^2$, are found to broaden the high-frequency line more than the lower one. It is the main purpose of this note to consider these effects somewhat more quantitatively in order to obtain a better estimate of the systematics to be expected for the dipole resonance in deformed nuclei.

Finally, another important source of broadening should be mentioned. The final state of motion described by a single, highly excited nucleon moving with respect to the rest of the nucleus is of course very far from a stationary state of the system; the excited nucleon may either fly out of the nucleus or, more likely, make a collision with one of the other nucleons, leading eventually to the complicated many-particle states of motion characteristic of the compound nucleus. This mechanism, which tends to damp the single-particle motion, will thus also lead to a broadening of the photo-resonance. One may obtain an estimate of these effects from the magnitude of the absorptive part of the optical potential used to describe the interaction of nucleons with the nucleus. From this source we might expect a broadening of a few MeV. The absorptive potential is an increasing function of excitation energy in this region; in the energy interval between $\hbar\omega_z$ and $\hbar\omega_\perp$ one might expect a change of the order of about 30 %.

2. Photo Excitation Spectrum in the Asymptotic Limit

The sum of the transition intensities of the E1 transitions leading from a state (I, K) associated with a wave function $\chi_K D^I_{MK}$ to all members of a

rotational band based on an intrinsic state $\chi_{K'}$ is proportional to the squared matrix element of the multipole operator involving only the *intrinsic* wave functions of initial and final states:

$$T(\mathrm{E1}; IK \to K') = \tfrac{16}{9}\pi \frac{1}{\hbar}\left(\frac{\omega}{c}\right)^3 \left| \int \chi^*_{K'} M(\mathrm{E1}, K'-K)\, \chi_K \, \mathrm{d}\tau \right|^2 . \qquad (1)$$

As a basis for a description of the intrinsic states we first assume an average potential of a pure harmonic oscillator type. An anisotropy of the oscillator potential corresponding to $\omega_z \neq \omega_\perp = \omega_x = \omega_y$ removes some of the degeneracy, and the states can now be characterized by the quantum number n_z, the number of nodal planes perpendicular to the z-axis, in addition to the quantum number N, the total number of nodes of the nucleonic wave function.

Further, Λ, the component of orbital angular momentum along the nuclear symmetry axis, is a constant of the motion by virtue of the assumed rotational symmetry about the z-axis. We may characterize the state of the nucleonic spin by the quantum number $\Sigma = \pm\frac{1}{2}$, representing the component of spin along the symmetry axis. And finally Λ and Σ add up to K, the component of total angular momentum characterizing the intrinsic state. There is of course in this description a complete degeneracy among the different values of Σ and Λ (consistent with a certain value of $n_\perp = N - n_z$). The wave functions may be written in product form as

$$|N n_z \Lambda \Sigma\rangle = |z; n_z\rangle |x\, y; n_\perp \Lambda\rangle |\Sigma\rangle, \qquad (2)$$

where $|z; n_z\rangle$ denotes that the state vector associated with the quantum number n_z depends solely on the z-coordinate, etc.

We first note from eq. (1) that there occur two groups of E1 transitions in this limit: one group represents transitions with $\Delta K = 0$ and corresponds to the multipole operator z, the other group corresponds to $\Delta K = \pm 1$ and the operator $2^{-\frac{1}{2}}(x \pm iy)$. From the form of the wave function (2) it is immediately apparent that the $\Delta K = 0$ transitions obey the selection rules $\Delta n_\perp = \Delta\Lambda = \Delta\Sigma = 0$ and $\Delta n_z = \pm 1$ and involve a change of energy equal to $\hbar\omega_z$. The other types of transitions, $\Delta K = \pm 1$, are associated with the selection rules $\Delta n_z = \Delta\Sigma = 0$, $\Delta n_\perp = \pm 1$, $\Delta\Lambda = \pm 1$. The fundamental frequency of these transitions is $\hbar\omega_\perp$. This simplified situation is illustrated in fig. 1, where we have taken as an example a filled $N = 2$ shell from which nucleons are excited into the empty $N = 3$ shell. As a consequence of the fact that the transitions are associated with ΔK equal to both $+1$ and -1, the $\hbar\omega_\perp$ transition line is twice as strong as the $\hbar\omega_z$ line in this description.

Introduction of other terms in the nucleon potential of the type $-(2\mathbf{l}\cdot\mathbf{s} + \mu\mathbf{l}^2)\kappa\hbar\omega_0$ will now remove the Λ and Σ degeneracy. However, the "asymptotic quantum" numbers $(N, n_z, \Lambda, \Sigma)$ still remain useful as long as

these added terms are small compared with the splitting, $\hbar\omega_\perp - \hbar\omega_z$, caused by the deformation of the nuclear field. This condition seems to be fairly well satisfied (i.e. with an accuracy of about 10 % for the greatly deformed nuclei, and thus we may still use the wave function (2) as a first approximation.

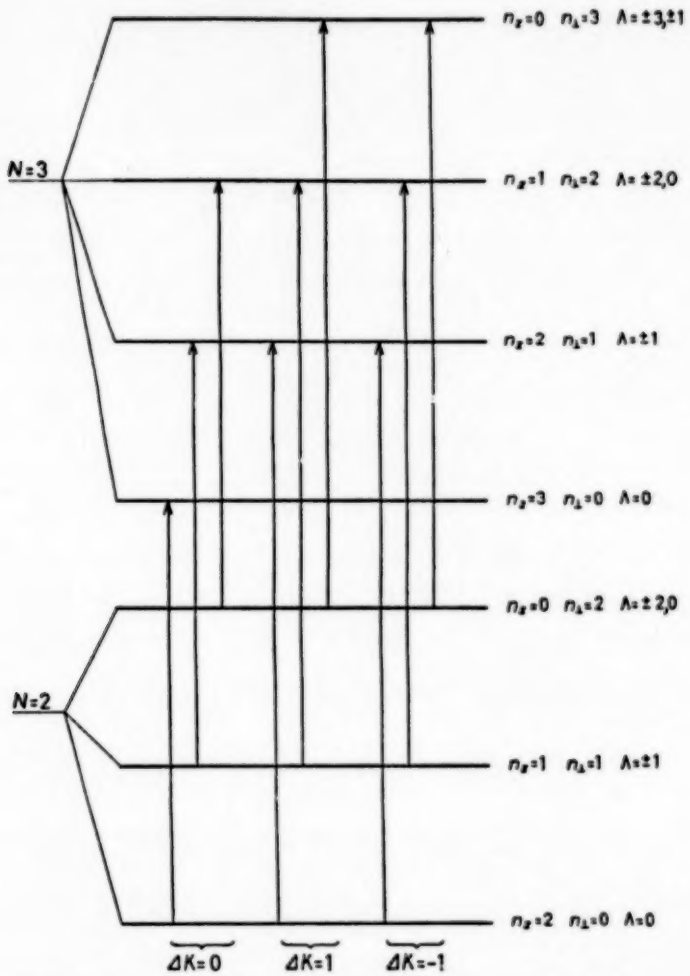

Fig. 1. The diagram illustrates possible single-particle E1 excitations from a filled harmonic oscillator shell $N = 2$ into an empty $N = 3$ shell. Part of the spherical degeneracy of the N shell is removed by a quadrupole deformation of the oscillator field having $\omega_z < \omega_\perp$. In this example, however, in contrast to the case of fig. 2, the levels are assumed degenerate in Λ and Σ.

The energy eigenvalues of each intrinsic orbital may now be written (to lowest approximation)

$$E(n_z n_\perp \Lambda\Sigma) = (n_\perp+1)\hbar\omega_\perp + (n_z+\tfrac{1}{2})\hbar\omega_z - \kappa\hbar\omega_0[2\Lambda\Sigma+\mu(2n_z n_\perp+2n_z+n_\perp+\Lambda^2)]. \quad (3)$$

2.1 TRANSITION LINES CORRESPONDING TO $\Delta K = 0$

The multipole operator corresponding to $\Delta K = 0$, being associated with the selection rules $\Delta n_\perp = \Delta\Lambda = \Delta\Sigma = 0$ and $\Delta n_z = \pm 1$, connects states

with energy differences

$$E(n_z+1, n_\perp \Lambda\Sigma) - E(n_z n_\perp \Lambda\Sigma) = \hbar\omega_z + \delta E^{\mathrm{I}} 2\mu\kappa\hbar\omega_0, \tag{4}$$

where

$$\delta E^{\mathrm{I}} = -(n_\perp+1). \tag{4a}$$

The splitting of the group is caused by the $\mathbf{l}^2$-term and corresponds to the occurrence of the quadratic terms proportional to $n_\perp n_z$ in eq. (3).

The different transitions within the group $\Delta K = 0$ and the corresponding intensities are listed below in table 1.

TABLE 1

n_z	$n_\perp$	$-\delta E^{\mathrm{I}}$	degeneracy	$2\lvert$matr. elem.$\rvert^2$	deg. $\times\, 2\lvert$matr. elem.$\rvert^2$
0	N	$N+1$	$N+1$	1	$(N+1)\cdot 1$
1	$N-1$	N	N	2	$N\cdot 2$
2	$N-2$	$N-1$	$N-1$	3	$(N-1)\cdot 3$
.	.	.	.	.	.
.	.	.	.	.	.
n_z	$N-n_z$	$N-n_z+1$	$N-n_z+1$	n_z+1	$(N-n_z+1)\cdot(n_z+1)$
.	.	.	.	.	.
.	.	.	.	.	.
$N-1$	1	2	2	N	$2\cdot N$
N	0	1	1	$N+1$	$1\cdot(N+1)$

The intensity of the transitions from a state of given n_z and characterized by $\Delta K = 0$ is thus proportional to the following expression:

$$f_z(n_z) = (N-n_z+1)(n_z+1). \tag{5}$$

We can now combine (5) with the expression (4) for the energies of the various transitions to obtain the line shape for the transitions with $\Delta K = 0$, i.e. those transitions which for $\kappa = 0$ would have the energy $\hbar\omega_z$. Several examples illustrating the effect of the added terms in broadening the line are shown in the figures. The line width may be characterized by the mean square deviation

$$\sigma^2 = \frac{\sum I(E)(E-\bar{E})^2}{\sum I(E)} = (\mu\kappa\hbar\omega_0)^2 \tfrac{1}{5} N(N+4). \tag{6}$$

2.2. TRANSITION LINES CORRESPONDING TO $\Delta K = \pm 1$

The $\Delta K = \pm 1$ transitions will be broadened by both the $\mathbf{l}^2$ and the $\mathbf{l}\cdot\mathbf{s}$ term in the nuclear potential. The energy differences connected with these transitions are then given in the asymptotic limit as

$$E(n_z, n_\perp+1, \Lambda\pm 1, \Sigma) - E(n_z n_\perp \Lambda\Sigma) = \hbar\omega_\perp + 2\mu\kappa\hbar\omega_0 \cdot \delta E^{\mathrm{II}}, \tag{7}$$

where

$$\delta E^{\mathrm{II}} = -(N+1)\mp\frac{1}{2\mu}\Sigma+2\begin{Bmatrix}s\\r\end{Bmatrix}, \quad \text{for } \Delta\Lambda = \pm 1, \tag{7a}$$

with

$$2r = n_\perp+\Lambda, \quad 2s = n_\perp-\Lambda, \tag{7b}$$

s and r thus corresponding, in eq. (7a), to $\Delta\Lambda = +1$ and $\Delta\Lambda = -1$ respectively.

The quantum numbers r and s are especially convenient for the discussion of the spectrum and matrix elements in the asymptotic limit (cf. the appendix). Considering first, for instance, the case of $\Delta K = +1$, the energy

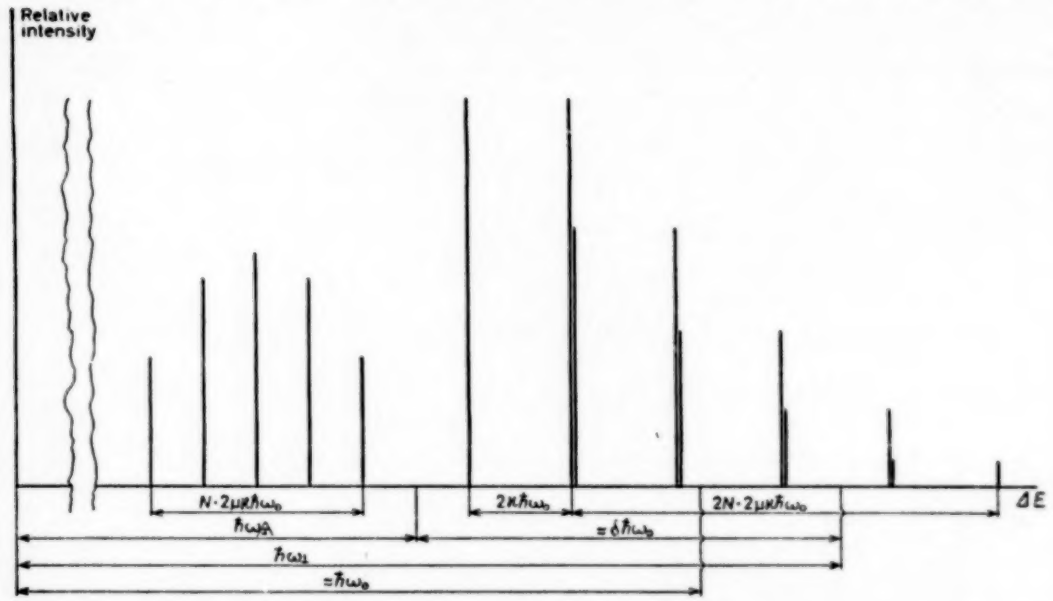

Fig. 2. The diagram exhibits the theoretical line spectrum in the giant-resonance region, calculated on the basis of the single-particle energies of a harmonic oscillator potential, where diagonal terms of $\mathbf{l}\cdot\mathbf{s}$ and $\mathbf{l}^2$ have been included. The effect of these added terms is to remove the degeneracy of the single-particle spectrum in Λ and Σ (the components of angular momentum and spin) and thereby to broaden the two fundamental peaks of energy $\hbar\omega_\parallel$ and $\hbar\omega_\perp$ (cf. fig. 1).

differences are expressible solely in terms of Σ and s (see eq. (7)). Each such energy difference is associated with a degeneracy in r, since r may be $0, 1, \ldots, N-s$, and each of these transitions is in its turn connected with an intensity $\propto(r+1)$. The total oscillator strength attributed to the radiation energy $E(s, \Sigma)$ is thus proportional to

$$\sum_{r=0}^{N-s}(r+1) = \tfrac{1}{2}(N-s+1)(N-s+2) = f_\perp(s). \tag{8}$$

We obtain the line shape by combining $f_\perp(s)$ with the expression (7) and letting s take on each of the allowed values $0 \leqq s \leqq N$. There are then two

line spectra of the type $f_\perp(s)$, transposed an energy $\kappa\hbar\omega_0$ with respect to one another, corresponding to the two values of $\Sigma = \pm\frac{1}{2}$ (see eq. (7)).

The intensity distribution corresponding to the case of $\Delta K = -1$ is identical with the $\Delta K = +1$ spectrum. One may note that for this latter spectrum Σ corresponds to $-\Sigma$ and r to s in the former case.

We may now write the total intensity distribution corresponding to $\Delta K = \pm 1$ as

$$\sum_x f_\perp(x) = \sum_{x=0}^{N} \{(N+1-x)(N+2-x)\} + \sum_{x=\frac{1}{4\mu}}^{N+\frac{1}{4\mu}} \left(N+1+\frac{1}{4\mu}-x\right)\left(N+2+\frac{1}{4\mu}-x\right). \quad (9)$$

where the integral values of x correspond to equidistant spectral lines with a spacing equal to $4\mu\kappa\hbar\omega_0$. For this line shape we have a mean square width

$$\sigma^2 = \left[\tfrac{3}{5}N(N+4)+\left(\frac{1}{2\mu}\right)^2\right](\mu\kappa\hbar\omega_0)^2. \quad (10)$$

2.3. CHARACTERISTICS OF THE TOTAL RESONANCE SPECTRUM

Comparing the two peaks associated with $\hbar\omega_\perp$ and $\hbar\omega_z$, for instance for the case of $\mu \approx 0.5$ and $N \approx 4-5$ (corresponding to the "rare earth" region and the "heavy element" region of nuclei, displaying large equilibrium deformations), one finds a ratio between the mean square widths of the order 1.7.

In figs. 3 and 4 we have smeared out the sharp lines given by this model over energy intervals of the order 0.5 MeV in the heavy-element region †. Fig. 3 illustrates the expected type of resonance spectrum at the beginning of the "rare earth" region of deformed nuclei ††, say Tb^{159}, corresponding to a very large deformation $\delta \approx 0.35$. Fig. 4 is representative of the expected resonance spectra of the heavy elements beyond $A \approx 230$ [and also of nuclei

† We have so far, in deriving the spectral distributions (5) and (9), implicitly assumed that the single-particle states are filled through the whole shell N_0. Only nucleons of the shell N_0 may then be excited and lifted up to the shell N_0+1.

We have thus neglected the fact that, owing to the spin-orbit forces, these shells may largely overlap. The result will be that some orbitals of the N_0+1 shell are filled before the N_0 shell is completed. This effect will tend to slightly broaden both resonance peaks in a similar way. It can be approximately provided for by the use of an intermediate value of N between N_0 and N_0+1 in calculating the widths.

Furthermore, in two of the regions of large nuclear deformation the neutron and proton numbers differ considerably, and actually the N_0 shell is filled for protons simultaneously with the N_0+1 shell for neutrons. Of course one may take this effect into account simply by calculating the neutron and proton spectra (with the respective effective charges) separately and finally adding them up. This correction is small, of the order $1/N$, and parallel for the two resonance peaks.

†† Cf. the new experimental results by E. G. Fuller and M. S. Weiss (ref. [4]), which may indicate a resolved double peak for Tb and Ta.

at the end of the "rare earth" region, say Ta^{181}], where the deformation is smaller, $\delta \approx 0.25$, and the width of each of the two peaks is larger,

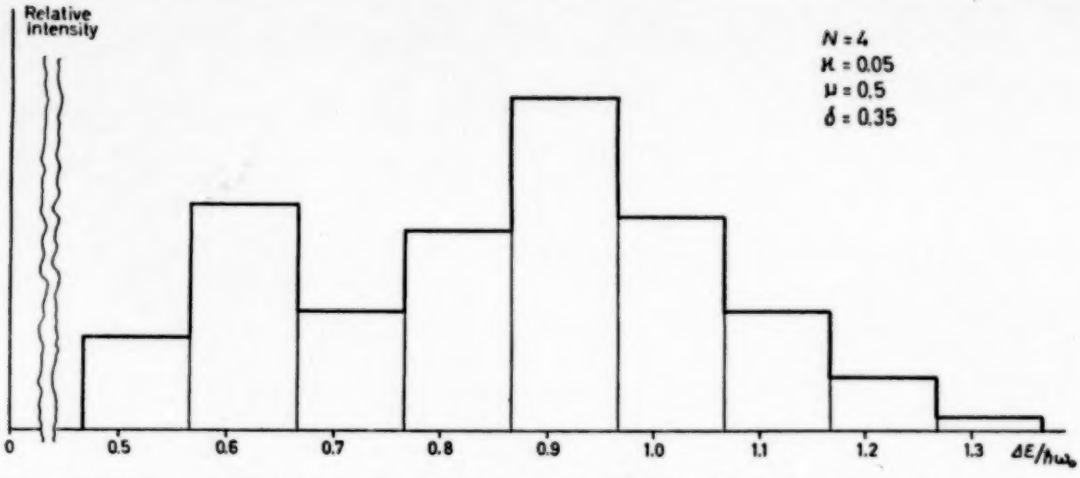

Fig. 3. Histogram plotted on the basis of the theoretical line spectrum of fig. 2 for the case of $N = 4$ and $\delta \approx 0.35$. The shell parameters of this spectrum are chosen so as to be applicable to nuclei at the beginning of the rare-earth region, say $153 \lesssim A \lesssim 170$. It appears that it might be possible to resolve experimentally the two peaks of the spectrum in this region of nuclei.

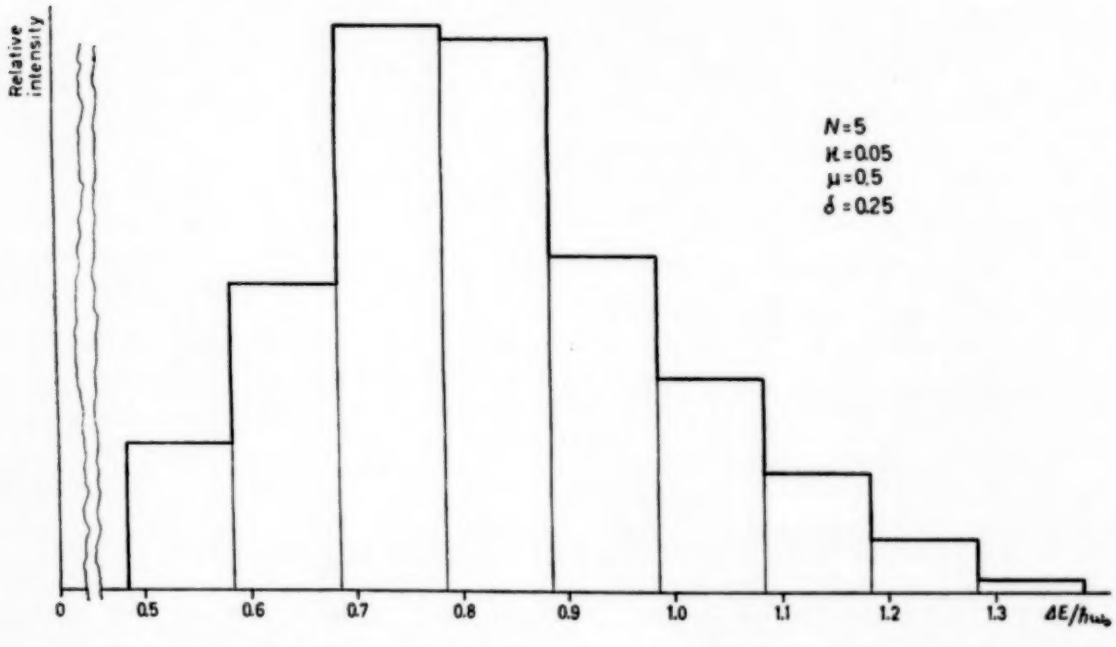

Fig. 4. The same as fig. 3 with the parameters $N = 5$ and $\delta \approx 0.25$. The theoretical spectrum is meant to show the general features of giant-resonance spectra in the regions of deformed nuclei $A \gtrsim 230$ and $170 \lesssim A \lesssim 190$.

owing to a larger effective N-value. Here the two peaks appear no longer to be resoluble, even when the broadening due to additional effects discussed in the introduction is neglected.

Appendix

CONSTRUCTION OF ASYMPTOTIC STATES †

It is well known that one can construct one-dimensional oscillator wave functions by the aid of the following creation and annihilation operators:

$$\Gamma_z^* = \frac{1}{\sqrt{2}}\left(\zeta - \frac{\partial}{\partial\zeta}\right), \tag{A.1a}$$

$$\Gamma_z = \frac{1}{\sqrt{2}}\left(\zeta + \frac{\partial}{\partial\zeta}\right), \tag{A.1b}$$

which obey the commutation relation

$$[\Gamma_z, \Gamma_z^*] = 1. \tag{A.2}$$

The dimensionless coordinate ζ is related to the coordinate z as follows:

$$\zeta = \sqrt{\frac{M\omega_z}{\hbar}}\, z.$$

A normalized state corresponding to n_z oscillator quanta can then be expressed by means of the operator Γ_z^*:

$$|n_z\rangle = \frac{1}{\sqrt{n_z!}}(\Gamma_z^*)^{n_z}|0\rangle, \tag{A.3}$$

where $|0\rangle$ is the "vacuum" state, corresponding to $n_z = 0$.

We denote by Γ_x and Γ_y etc. the corresponding operators in the x and y dimensions. They obviously fulfil relations analogous to (A.2). It is useful to consider Γ_x^*, Γ_y^*, Γ_z^*, and Γ_x, Γ_y, Γ_z, as components of the vector operators $\boldsymbol{\Gamma}^*$ and $\boldsymbol{\Gamma}$.

We now want to construct eigenstates corresponding to a three-dimensional oscillator with rotational symmetry only about the z-axis, i.e. with frequencies ω_x and ω_y equal to one another (denoted $\omega_\perp$), but different from ω_z. The energy only depends on $n_\perp (= n_x + n_y)$ and n_z. Of the $(n_\perp+1)$-fold degenerate eigenstates with given $n_\perp$ one may then form linear combinations which are eigenfunctions of the z-component of the angular momentum operator L_z.

Such states are denoted $|n_\perp \Lambda\rangle$, where Λ is the eigenvalue of L_z, and may now be constructed in analogy with (A.3) by the aid of the following operators:

$$\Gamma_+^* = \frac{1}{\sqrt{2}}(\Gamma_x^* + i\Gamma_y^*) = R^*, \tag{A.4a}$$

$$\Gamma_+ = \frac{1}{\sqrt{2}}(\Gamma_x + i\Gamma_y) = S, \tag{A.4b}$$

† *Note added in proof:* Similar operator methods have been employed by Dr. B. Bayman in constructing wave functions for the case considered here as well as for the three-dimensional isotropic case with L^2 and L_z being constants of the motion (private communication from B. Bayman). Cf. also ref. [7]).

$$\Gamma_-^* = \frac{1}{\sqrt{2}}(\Gamma_x^* - i\Gamma_y^*) = S^*, \tag{A.4c}$$

$$\Gamma_- = \frac{1}{\sqrt{2}}(\Gamma_x - i\Gamma_y) = R, \tag{A.4d}$$

which, apart from a sign, are the conventional spherical components of the vector operators $\boldsymbol{\Gamma}^*$ and $\boldsymbol{\Gamma}$.

These operators obey the commutation relation

$$[S, S^*] = [R, R^*] = 1 \tag{A.5}$$

in analogy with (A.2). All other commutators vanish identically.

The selection rules of the operators (A.4a), . . . , (A.4d) may be studied in table A.1. Thus, for instance, Γ_+^* increases the number of quanta in $n_\perp$

TABLE A1

	$\Delta n_\perp$	$\Delta\Lambda$	$\Delta r = \Delta\frac{1}{2}(n_\perp+\Lambda)$	$\Delta s = \Delta\frac{1}{2}(n_\perp-\Lambda)$
$\Gamma_+^* = R^*$	+1	+1	+1	0
$\Gamma_+ = S$	−1	+1	0	−1
$\Gamma_-^* = S^*$	+1	−1	0	+1
$\Gamma_- = R$	−1	−1	−1	0

by one unit, which is obvious, since it is linear and homogeneous in Γ_x^* and Γ_y^*. Furthermore it increases Λ by one unit, which is apparent from the fact that, apart from a sign, it is the +1 component of the *vector* operator Γ^*.

One may also directly verify the relation

$$L_z\{\Gamma_+^*|n_z\Lambda\rangle\} = (\Lambda+1)\{\Gamma_+^*|n_z\Lambda\rangle\}. \tag{A.6}$$

As is clearly indicated by the table, the quantum number associated with R and the hermitian conjugate R^* is $r = \frac{1}{2}(n_\perp+\Lambda)$, while $s = \frac{1}{2}(n_\perp-\Lambda)$ may be associated with S and S^*.

In summary, we now have a system of operators, R, R^*, S, S^*, and Γ_z, Γ_z^*, which fulfil the commutation relations (A.2) and (A.5), while all other commutators between any two of these operators vanish. The eigenvalues associated with these operator pairs are r, s and n_z respectively.

The total three-dimensional eigenfunction may now be constructed as

$$|r\rangle|s\rangle|n_z\rangle = \frac{1}{\sqrt{r!}}(R^*)^r|0\rangle\frac{1}{\sqrt{s!}}(S^*)^s|0\rangle\frac{1}{\sqrt{n_z!}}(\Gamma_z^*)^{n_z}|0\rangle. \tag{A.7}$$

In a representation in terms of the previously used quantum numbers $n_\perp$ and Λ one may rewrite the $x-y$ part of the wave function

$$|n_\perp\Lambda\rangle = \frac{1}{\sqrt{(\frac{1}{2}(n_\perp+\Lambda))!\,(\frac{1}{2}(n_\perp-\Lambda))!}}(\Gamma_-^*)^{\frac{1}{2}(n_\perp-\Lambda)}(\Gamma_+^*)^{(\frac{1}{2}n_\perp+\Lambda)}|00\rangle. \tag{A.8}$$

One may note at this point that the quantum numbers r and s provide a useful basis for the classification of the asymptotic states. We have so far

labelled the latter by $n_\perp$ and Λ, allowing $n_\perp$ to take on the values 0, 1, 2, . . ., N; for a given $n_\perp$-value, permissible values of Λ are

$$\Lambda = \pm n_\perp, \quad \pm(n_\perp-2), \quad \pm(n_\perp-4), \ldots, 0 \text{ or } 1,$$

depending on whether $n_\perp$ is even or odd. If one uses the alternative classification, one must let r take on all values 0, 1, 2, . . ., N, while for a given r the quantum number s can assume all values 0, 1, 2, . . ., $(N-r)$.

MATRIX ELEMENTS

Matrix elements of various transition operators between asymptotic states are most easily derived by expressing the operators in terms of R and S. Thus

$$\left(\frac{\hbar}{M\omega_\perp}\right)^{-\frac{1}{2}}(x+iy) = \xi+i\eta = S+R^*, \tag{A.9a}$$

$$\left(\frac{\hbar}{M\omega_\perp}\right)^{-\frac{1}{2}}(x-iy) = \xi-i\eta = S^*+R. \tag{A.9b}$$

Using the relations

$$R^*|r\rangle = \sqrt{r+1}\,|r+1\rangle \tag{A.10}$$

and

$$R|r\rangle = \sqrt{r}\,|r-1\rangle, \tag{A.11}$$

which hold, in accordance with the commutation relations (A.2) and (A.5), for all the operator pairs R, R^* and S, S^* as well as Γ_s, Γ_s^*, one immediately obtains the matrix elements

$$\langle r+1, s|\xi+i\eta|rs\rangle = \sqrt{r+1} \tag{A.12a}$$

$$\langle r, s-1|\xi+i\eta|rs\rangle = \sqrt{s}. \tag{A.12b}$$

References

1) J. S. Levinger, Nuclear Physics **8** (1958) 428
2) S. A. E. Johansson, Arkiv f. Fysik **26** (1958) 331
3) Fuller, Petree and Weiss, Phys. Rev. **112** (1958) 554
4) M. G. Fuller and M. S. Weiss, Phys. Rev. **112** (1958) 560
5) D. H. Wilkinson, Phil. Mag. **3** (1958) 567
6) S. G. Nilsson, Mat. Fys. Medd. Dan. Vid. Selsk. **29**, No. 16 (1955)
7) H. Pilkuhn, Nuclear Physics **12** (1959) 269

2.1 *Nuclear Physics* **13** (1959) 292—299; © *North-Holland Publishing Co., Amsterdam*
Not to be reproduced by photoprint or microfilm without written permission from the publisher

FAST PHOTONEUTRONS FROM TANTALUM AND GOLD

L. B. AULL, G. C. REINHARDT and W. D. WHITEHEAD
University of Virginia, Charlottesville, Virginia †

Received 9 July 1959

Abstract: The photonuclear cross sections for the production of neutrons with energies greater than the $Si^{28}(n, p)Al^{28}$ threshold have been determined for tantalum and gold from a maximum bremsstrahlung energy of 18 to 65 MeV. The integrated cross section to 65 MeV is about 800 MeV · mb for tantalum and 700 MeV · mb for gold. The fast neutron integrated cross section is compared with total neutron production cross section at several energies and is about 10 % at all energies.

1. Introduction

Evidence of a direct photonuclear effect was first obtained from measurements of photoproton emission, which indicated that the photoprotons emitted by heavy elements were more numerous and more energetic than had been predicted by the statistical mode of decay [1]). Later a study of nuclear emulsions which had been exposed to photoneutrons [2]) revealed a higher percentage of high energy neutrons than is predicted statistically. Wilkinson's shell model prediction [3]) of the direct to total photoneutron ratio was investigated recently [4]) using the $Si^{28}(n, p)Al^{28}$ reaction, with an effective threshold of approximately 5 MeV, to detect the fast neutrons. The results for heavy elements show excellent correlation between experiment and Wilkinson's theory in the incident gamma ray energy range between threshold and 30 MeV. The same group observed a break in the fast neutron yield curves for tantalum, chromium, arsenic and iodine [5]) in the region between 20 and 30 MeV, thus indicating a double peak in the fast neutron cross section for these four elements. Cortini *et al.* [6]) measured the tantalum photoneutron energy distribution for incident bremsstrahlung with peak energies of 20 and 30 MeV using nuclear emulsions. The greater percentage of fast neutrons in the 30 MeV spectrum was interpreted as a confirmation of the tantalum fast neutron yield measurement [5]).

We have determined the cross section for the Ta(γ, fast n) and Au^{196}(γ, fast n) reactions in the incident gamma ray energy range 18 to 65 MeV, using the bremsstrahlung from the University of Virginia synchrotron, by measuring the Al^{28} activity induced in pure silicon samples by the photoneutrons ejected from the irradiated tantalum and gold. The yield functions,

† This research was supported by United States Air Force Office of Scientific Research.

determined with respect to the $Cu^{63}(\gamma, n)Cu^{62}$ cross section of Berman and Brown [7]), were unfolded by means of the Leiss-Penfold matrices [8]) to give the integrated cross sections and the cross sections as functions of incident gamma ray energy.

2. Experimental Procedure

A one-inch diameter tantalum or gold sample was mounted on a lucite holder, which had been centered in the beam using X-ray plates, 1.5 meters from the internal target of the synchrotron. The gold sample was $\frac{19}{32}$ inch

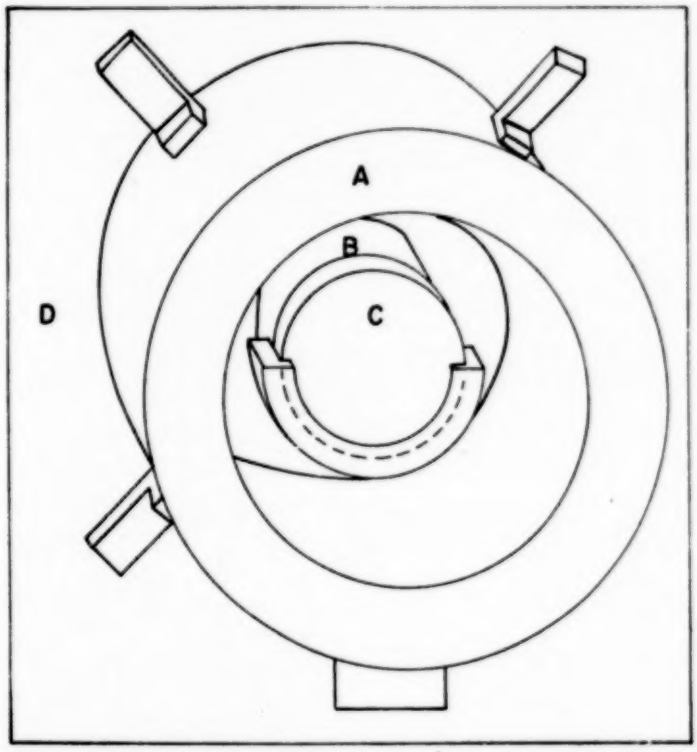

Fig. 1. Sample-detector arrangement, as seen from the synchrotron. (A) silicon filled wall of the neutron detector; (B) irradiated gold or tantalum sample; (C) one inch diameter copper monitor disk; (D) lucite mounting.

thick, the tantalum two inches. Lead and paraffin collimaters defined a beam of approximately one-inch diameter at the sample. The 0.007 inch thick copper monitor disk, was mounted coaxially with the sample, but about 0.25 inch closer to the synchrotron target. The powdered silicon, which was utilized to detect the fast photoneutrons, was packed in a hollow wall cylinder made of thin lucite, and this cylinder was mounted concentric with the irradiated sample. The silicon neutron detector, gold or tantalum sample, copper monitor disk arrangement is shown in fig. 1. In effect, a silicon cylinder (A) with a 0.25 inch wall thickness surrounded the irradiated sample (B) and the copper monitor disk (C).

To determine the fast neutron yield curve the sample, copper disk and silicon neutron detector were mounted in the lucite holder and the disk and the sample were irradiated for eight minutes at each energy. The silicon cylinder was then removed from the holder and placed concentric with an array of three thin wall Geiger counters (Victoreen 1B85, aluminium wall thickness of 30 mg/cm^2) and the 2.31 ± 0.06 minute Al^{28} β^- activity [9]), resulting from the $Si^{28}(n, p)Al^{28}$ reaction was monitored. The 9.73 ± 0.02 minute $Cu^{62}\beta^+$ activity [7]), which had been produced in the copper disk, was measured with another Geiger counter to determine the beam intensity.

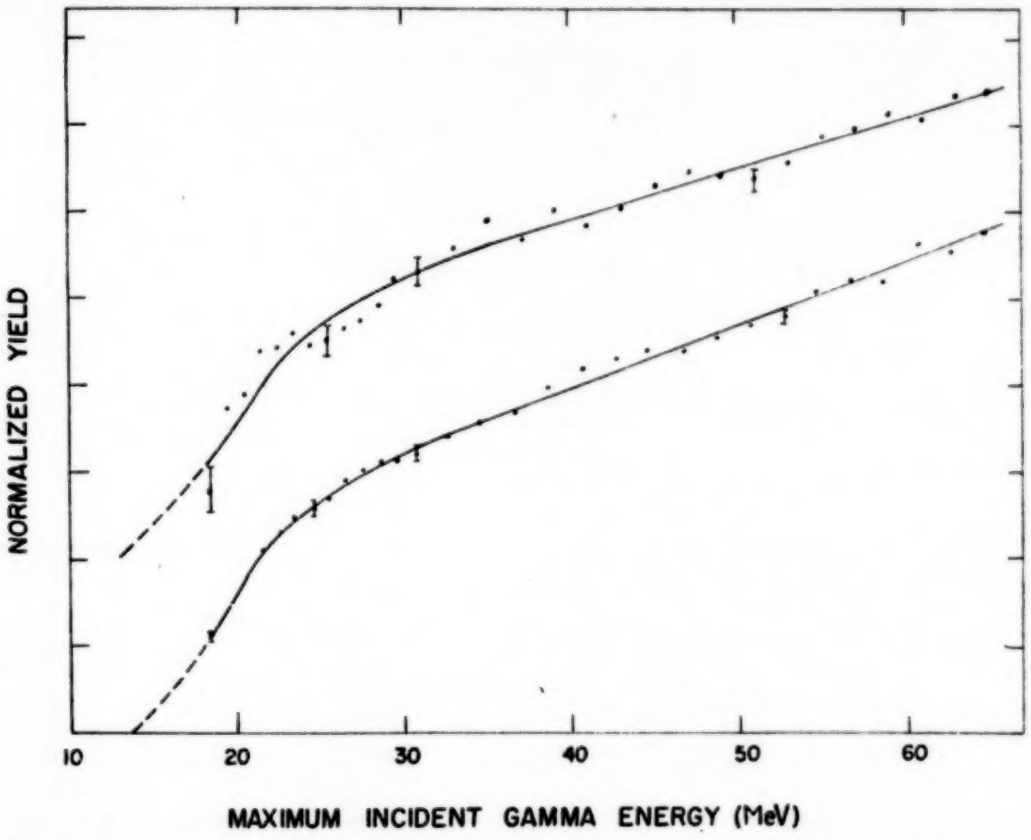

Fig. 2. Gold (upper curve) and tantalum (γ, fast n) yield curves. The ordinate is dimensionless [8]); counting errors are indicated.

To measure the neutron background, the sample was removed from the lucite holder and a similar irradiation was performed with an identical silicon cylinder and copper disk mounted in position in the holder. The yield of high energy neutrons for a particular energy setting is proportional to the difference between the "sample in" and "sample out" Al^{28} decay rates, after correction for counter background and counter efficiency and normalization to the same beam intensity. The neutron yield was then computed from this "difference decay rate", as extrapolated to the end of the irradiation, and the neutron detection efficiency, as calculated from detection

geometry, the photoneutron energy spectrum and the $Si^{28}(n, p)Al^{28}$ cross section. The high energy neutron yields for tantalum and gold are shown in fig. 2. Counting statistics are indicated at several points on each curve; data were taken at two MeV intervals in the region 34 to 64 MeV and at one MeV intervals between 18 and 34 MeV. The maximum energy of the bremsstrahlung was determined by means of an integrating flux meter [10]), and the energy scale of the machine was established with reference to the $C^{12}(\gamma, n)C^{11}$ threshold of 18.73 ± 0.03 MeV [11]). The estimated uncertainty in the maximum photon energy obtained from the integrator is ± 0.25 MeV.

The efficiency of the Geiger counter array which was used to monitor the Al^{28} activity was determined experimentally by comparing the measured counting rate produced in the cylindrical neutron detector, as a result of irradiation with a standard RaBe source, with the calculated decay rate as computed from geometry, known source strength and the $Si^{28}(n, p)Al^{29}$ cross section [9, 12]). The end window counter used as the Cu^{62} monitor, was compared with a previously calibrated scintillation counter [13]) to determine the counting efficiency.

During the eight minute irradiation a small amount of Cu^{61} (3.3 hour half-life) was produced in the copper disk in addition to the Cu^{62}. To correct for this activity the copper count, as measured above, was reduced by 0.7 ± 0.3 %. The only activity detectable in the silicon sample after irradiation was the 2.31 minute half-life of Al^{28}. Since natural silicon consists of 92.27 % Si^{28}, 4.68 % Si^{29} and 3.05 % Si^{30}, it is possible that the Al^{28} activity could originate either from $Si^{28}(n, p)Al^{28}$ or from the $Si^{29}(\gamma, n)Al^{28}$. The sample out runs at each energy determined the effect of direct gamma irradiation of the silicon. To check for $Si^{29}(\gamma, n)Al^{28}$ activity resulting from gamma rays scattered from the sample, a carbon cylinder was mounted in place of the silicon detector and several 30-minute irradiations were made with the sample in position. No activity was detected in the carbon thus indicating that no gamma rays of energy greater than 18.73 MeV passed through the detector. Carbon was used for the test because it is free of other radioactive products; however, the threshold for the $C^{12}(\gamma, n)C^{11}$ reaction is greater than the 12.3 MeV threshold for $Si^{29}(\gamma, n)Al^{28}$. The maximum energy of a compton scattered gamma from the sample into the detector is 4.3 MeV at $E_{max} = 60$ MeV.

3. Results and Discussion

The Leiss-Penfold method [8]) was used to extract the integrated cross sections directly from the yield curves. For this purpose an integral matrix, incorporating the energy dependent factors, gamma absorption by the sample and photon energy, was constructed from the Leiss-Penfold matrix.

This integral matrix was multiplied by the measured yield points to obtain the integrated cross section points directly. The technique of moving averages [14]) was then employed to smooth the integrated cross section. By this technique successive overlapping sections of the data are fitted to a polynomial using the method of least squares. At each integrated cross section point the three next higher points and the three next lower points together with the point of interest, were fitted to a cubic to obtain the smoothed value.

Figs. 3 and 4 show the smoothed integrated cross sections for both tantalum and gold. The statistics represent the counting errors in each case. The smooth

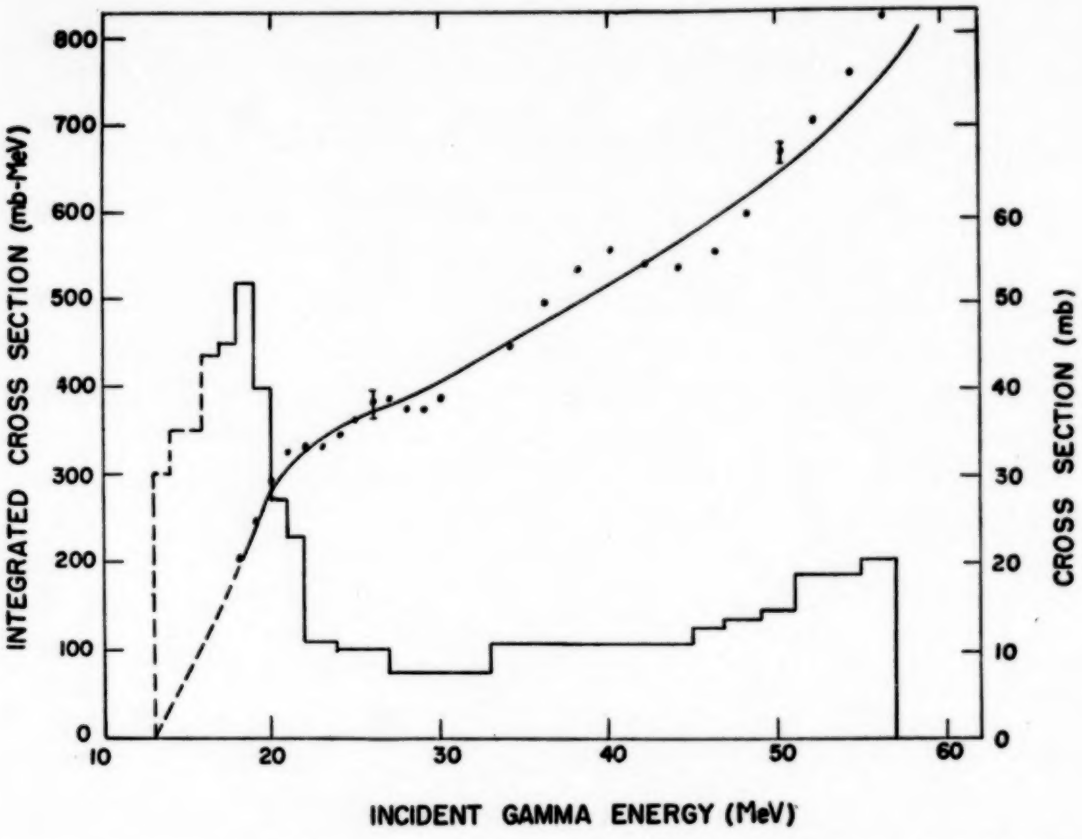

Fig. 3. Tantalum (γ, fast n) smoothed integrated cross section and cross section. The points and the smooth curve represent the smoothed integrated fast neutron cross section (see text) as defined by

$$\int_0^E \sigma_{(\gamma,\ \text{fast n})}\, dE$$

where $\sigma_{(\gamma,\ \text{fast n})}$ is the cross section for photoproduction of neutrons with energies above the $Si^{28}(n, p)Al^{28}$ threshold and E is the incident gamma ray energy. The errors indicated were obtained by propagating the counting uncertainties in the yield data through the integral cross section matrix. The histogram represents the first differences of the integrated cross section curve.

curves in each figure were fitted to the points by eye, and the first differences of these smooth curves are plotted as the cross section histograms.

In addition to the counting statistics there are several systematic sources of uncertainty in the experiment. The efficiency of the copper counter is uncertain by ± 5 % due to uncertainty in the calibrated scintillation counter which was used as a standard, and the efficiency of the silicon counter by about ± 15 % due to counting statistics in the measurement of the RaBe spectrum [15]). Possible errors in the Al^{28} (9) and Cu^{62} (7) half-lives yield error components of 1 % and 0.5 % respectively for the normalized points. If these errors are combined with 3 % to 10 % errors due to counting statistics, the integrated cross section is probably known to about 20 %.

The rise in the fast photoneutron cross sections for both tantalum and

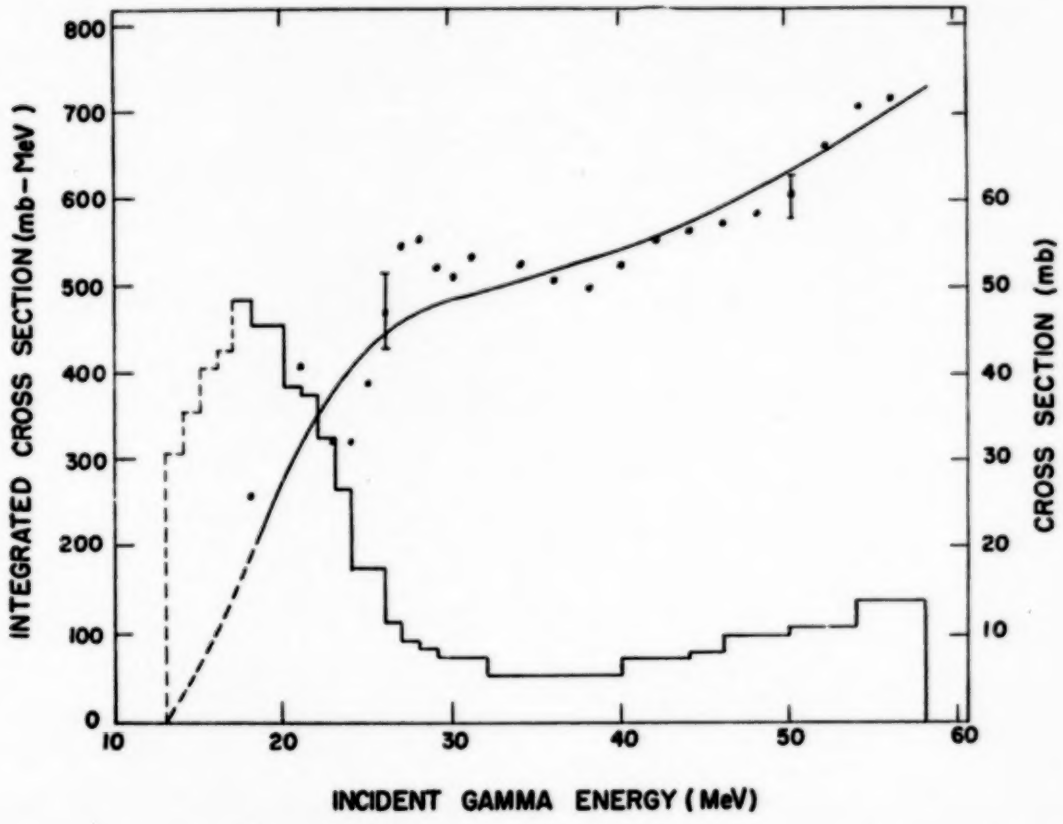

Fig. 4. Gold (γ, fast n) smoothed integrated cross section and cross section, as described under fig. 3.

gold in the region above 40 MeV may not be significant. The neutron detection efficiency of the silicon detector is proportional to the product of the photoneutron energy spectrum and the Si^{28}(n, p)Al^{28} cross section, integrated over the neutron energy. Only photoneutron energy spectrums for 20 and 30 MeV bremsstrahlung [6, 16]) were available for tantalum and gold; the 30 MeV spectrum was used for all computations at energies greater than 30 MeV. If it turns out that the actual neutron spectrum changes as the bremsstrahlung maximum energy is increased from 30 to 60 MeV so as to make the

silicon detector more efficient at the higher energies, then the rising tail, indicated on the cross section curve, may not be real. To eliminate this uncertainty in the experiment, measurements of the tantalum and gold photoneutron energy distributions have been initiated at this laboratory.

The ratios of the fast neutron integrated cross sections to the total neutron integrated cross sections as measured in other laboratories are shown in the table below:

TABLE 1

Ratio of fast neutron integrated cross section to total neutron integrated cross section

	24 MeV	30 MeV	60 MeV
Tantalum	10.3±2.4 % [a])	7.3±1.7 % [b])	10.6±2.2 [b])
Gold	10.9±2.7 % [a])		17.4±4.3 [c])

[a]) Compared to (γ, n) cross section of Fuller and Weiss [17]);
[b]) Compared to (γ, xn) of Terwilliger and Jones [18]);
[c]) Compared to (γ, n) of Edwards and McMillan (data taken at 70 MeV) [19]).

The fraction of neutrons in the fast group corresponds very closely to the fraction of "resonance direct" neutrons predicted by Wilkinson [3]) for heavy elements.

The double peaks suspected in the tantalum fast neutron cross section between threshold and 30 MeV were not observed. Examination of the tantalum yield curve (fig. 2) does show a dip at about 26 MeV but the counting statistics are too poor to discount statistical variation. The integrated cross section curves for tantalum and gold are quite similar, thus indicating that the deformation of the nucleus has little effect upon the gross features of the high energy photoneutron cross section.

We would like to thank R. F. Askew, R. W. Fast, P. A. Flournoy and R. S. Tickle for help in various phases of the experiment.

References

1) Curtis, Hornbostel, Lee and Salant, Phys. Rev. **77** (1950) 290;
B. C. Diven and G. M. Almy, Phys. Rev. **80** (1950) 407;
M. E. Toms and W. E. Stephens, Phys. Rev. **92** (1953) 362
2) G. A. Price, Phys. Rev. **93** (1954) 1279
3) D. H. Wilkinson, Physica **22** (1956) 1039
4) F. Ferrero, A. O. Hanson *et al.*, Nuovo Cimento **4** (1956) 418;
F. Ferrero, L. Gonella, R. Malvano *et al.*, Nuovo Cimento **5** (1957) 242
5) F. Ferrero, F. Malvano and C. Tribuno, Nuovo Cimento **6** (1957) 385L
6) G. Cortini, C. Milone *et al.*, Nuovo Cimento **9** (1958) 85
7) A. I. Berman and K. L. Brown, Phys. Rev. **96** (1954) 83
8) A. S. Penfold and J. E. Leiss, Analysis of Photo Cross Sections, (University of Illinois, 1958)

9) A. V. Cohen and P. H. White, Nuclear Physics **1** (1956) 73
10) J. E. Leiss, Private Communication
11) B. M. Spicer and A. S. Penfold, Phys. Rev. **100** (1955) 1375
12) J. B. Marion, R. M. Brugger and R. A. Chapman, Phys. Rev. **101** (1956) 247
13) L. B. Aull and W. D. Whitehead, Phys. Rev. **110** (1958) 1113
14) M. G. Kendall, The Advanced Theory of Statistics, Vol. II (Charles Griffin and Co., London (1951)) p. 372
15) D. C Hill, A. E. C. Report, AECD-1945 (1947) (unpublished)
16) S. Cavallaro, V. Emma, C. Milone and A. Rubbino, Nuovo Cimento **9** (1958) 736
17) E. G. Fuller and M. S. Weiss, Phys. Rev. **112** (1958) 560
18) L. W. Jones and K. M. Terwilliger, Phys. Rev. **91** (1953) 699
19) L. S. Edwards and F. A. MacMillan, Phys. Rev. **87** (1952) 377

8.A *Nuclear Physics* **13** (1959) 300—301; © *North-Holland Publishing Co., Amsterdam*
Not to be reproduced by photoprint or microfilm without written permission from the publisher

PROTONIC DECAY OF A Σ^+ HYPERON WITH AN ASSOCIATED ELECTRON PAIR

LADISLAV ROB and ZDENĚK KORBEL
Faculty of Technical and Nuclear Physics, Charles University, Prague

Received 5 July 1959

During the work on the stack of nuclear emulsions irradiated with K^- mesons from Berkeley accelerator we found a protonic decay of a Σ^+ hyperon with an associated electron pair. The Σ^+ hyperon was emitted from a star produced by K^- meson capture at rest; one π^- meson and a recoil was observed simultaneously. The hyperon after travelling 890 μ decayed in flight into a proton and an electron pair. Some details of the event are given in the table 1. The proton energy, (29.4 ± 0.5) MeV, was estimated from the range.

TABLE 1

Particle	Angle to the direction of flight of the Σ^+ hyperon	Energy (MeV)	Method of energy determination
Proton	35°	29.4	Range
Σ^+ Hyperon	0°	1.1 3.1	Dynamics Ionization
π^0 Meson	129°	83.0	Dynamics
Electron pair	8° †	90.0 105.0	Opening angle Dynamics

† To the direction of flight of π^0 meson.

If we interpret the event as a decay of a Σ^+ hyperon in flight according to the scheme

$$\Sigma^+ \rightarrow p + \pi^0$$

and assume that the mass of the Σ^+ hyperon is 1189 MeV, we can calculate the momentum of the primary particle from the dynamics of the decay. According to our calculations the momentum of the decaying Σ^+ hyperon is $pc = 50$ MeV. This value is in agreement with the experimentally determined value $pc = (85 \pm 50)$MeV. It is therefore possible to interpret the event as a Σ^+ hyperon decay in flight.

Further it was calculated that the π^0 meson was emitted at the angle of 129° to the direction of flight of the Σ^+ hyperon. Its energy was 83 MeV.

The opening angle of the electron pair was 1.2°, and it was emitted at an angle of 8° to the direction of flight of the π^0 meson.

Fig. 1.

The most probable explanation of this pair is that it arises from the internal conversion [1, 2]) of one of the two photons in the normal decay of the π^0 meson.

A similar event was observed by Ekspong and Nilsson [3]) and by Davis *et al.*[4]).

The authors would like to thank Professor M. Danysz for his efforts in procuring the emulsion stack, and the scanners for their work.

References

1) R. H. Dalitz, Proc. Phys. Soc. A **64** (1951) 667
2) N. M. Kroll and W. Wada, Phys. Rev. **98** (1955) 1355
3) A. G. Ekspong and S. Nilsson, Phys. Rev. Letters **1** (1958) 36
4) D. H. Davis, M. A. Shaukat and F. R. Stannard, Nuovo Cimento **11** (1959) 468

1.E.2 *Nuclear Physics* **13** (1959) 302—309; © *North-Holland Publishing Co., Amsterdam*
Not to be reproduced by photoprint or microfilm without written permission from the publisher

ÉTUDE DE QUELQUES ISOTOPES TRÈS DÉFICIENTS EN NEUTRONS DU PROMÉTHÉUM ET DU SAMARIUM

I. GRATOT, M. LE PAPE et J. OLKOWSKY
Section des Réactions Nucléaires à Moyenne Énergie
et
G. RANC
Section des Réactions Nucléaires à Basse Énergie
Centre d'Études Nucléaires de Saclay, Gif s/Yvette (Seine et Oise)

Reçu le 11 juin 1959

Abstract: The not well known ^{141}Pm, ^{142}Pm, ^{142}Sm, ^{143}Sm isotopes were obtained from several reactions. The mass of ^{141}Pm has been measured with the isotope separator. The masses of ^{142}Sm and ^{143}Sm were determined by excitation functions (α, xn). The half-lives were re-determined. Gamma spectra yield the ratios of K-electron capture to positon emission.

1. Obtention de ces isotopes

Lorsque le présent travail a été entrepris, les connaissances sur les isotopes ^{141}Pm, ^{142}Pm, ^{142}Sm, ^{143}Sm étaient les suivantes [1, 2]):

isotope	classe	période	activité	origine
^{141}Pm	B	20 min	β^+ 2.6 MeV (spect.)	formé par ^{142}Nd(p, 2n), $E_p \geqq 20$ MeV [3])
^{142}Pm	C	$\approx$30 s	β^+ 3.78 MeV; E.C.	
^{142}Sm	D	72 min	β^+; E.C	parent du ^{142}Pm 30 s
^{143}Sm	B	9 min 8.3 min 8 min	β^+ 2.3 MeV (abs.)	Sm(γ, n) ^{144}Sm(n, 2n)

Deux sortes de cibles ont été utilisées:

a) ^{141}Pr (qui est un monoisotope) sous forme d'oxyde très pur (Johnson Matthey).

b) ^{142}Nd, également sous forme d'oxyde, séparé à Oak Ridge, la composition de cette cible étant la suivante:

A	142	143	144	145	146	148	150
%	93.93	2.46	2.59	0.29	0.72	—	—

Nous avons utilisé les faisceaux d'alpha et de protons du cyclotron de Saclay, les énergies maximums étant respectivement de 44 et 11 MeV.

Nous avons également obtenu ^{142}Sm dans la spallation de ^{144}Sm par le faisceau de protons du synchrocyclotron d'Orsay ($\approx$ 150 MeV).

2. Séparations chimiques. Détermination des nombres atomiques

C'est seulement pour le mécanisme de la spallation que nous avons procédé à une séparation chromatographique [4]) des éléments formés.

Dans les réactions produites avec le cyclotron de Saclay, seuls les radioéléments provenant des bombardements de l'oxygène par alpha ou protons (c'est-à-dire ^{17}F, ^{18}F, ^{13}N) ont été éliminés par séparation chimique.

Dans les réactions (p, n), il n'y a pas d'ambiguïté concernant le nombre atomique. Avec les alpha d'énergie 44 MeV, il peut se produire des réactions (α, xn) et (α, pn), mais avec les cibles utilisées dans ce travail, cette dernière réaction aboutit à ^{143}Nd stable et à ^{143}Pm dont les propriétés nucléaires sont très différentes de celles des isotopes étudiés ici. Nous avons d'ailleurs reformé ^{143}Pm par la réaction ^{143}Nd séparé (p, n) pour nous en assurer.

3. Détermination des nombres de masse

3.1. ^{141}Pm ($\approx$ 22 min)

Fisher [3]) a pu former cet isotope par la réaction ^{142}Nd(p, 2n), l'énergie des protons utilisés étant supérieure à 20 MeV. En bombardant ^{141}Pr par des alpha de 36 MeV, aucune activité de 20 minutes n'était visible[3]). Nous avons renouvelé cette expérience avec des α de 44 MeV et constaté que l'isotope de 22 minutes se forme en grande quantité.

Nous avons procédé à la séparation massique des produits formés au séparateur d'isotopes de Saclay. Une source d'ions, permettant l'introduction rapide des produits radioactifs durant le fonctionnement de la machine a été construite à cet effet. La séparation d'isotopes proprement dite a duré dix minutes et le marquage des masses a été obtenu avec les masses des isotopes stables du lanthane et du cérium.

Seule la portion du collecteur étalonné à la masse 141 présente une activité γ notable (X_K et 511 keV) décroissant avec une période d'environ 22 minutes.

3.2. ^{142}Sm et ^{143}Sm

En irradiant ^{142}Nd par des alpha de 44 MeV, nous observons, avec notre spectromètre γ et des compteurs Geiger, des activités X_K, 511 keV, e ou β de 8.6 et de 73 minutes. En bombardant plusieurs sachets empilés et en interposant des écrans appropriés pour réduire l'énergie du faisceau, on constate que, seule, l'activité de 8.6 minutes subsiste lorsque l'énergie est $\leqq$ 38 MeV.

Or, les résultats expérimentaux de plusieurs auteurs et les nôtres ont montré qu'il était possible de faire les réactions suivantes dans la région des terres rares:

α : 44 MeV

(α, xn), $x = 4, 3, 2, 1$ ($x = 4$ et 3 étant les plus importants);

(α, pn), très peu probable.

α : 38 MeV

(α, xn), $x = 3, 2, 1$;

(α, pn)

($x = 3$, 2 et (α, pn) étant les plus probables).

Avec ^{142}Nd comme cible, la réaction $(\alpha, 2n)$ aboutit à ^{144}Sm qui est stable, la réaction (α, n) à ^{145}Sm bien connu et de période longue et la réaction (α, pn) à ^{144}Pm de période longue.

En conclusion, les résultats expérimentaux montrent clairement que l'activité de 8.6 minutes provient de la réaction ^{142}Nd$(\alpha, 3n)^{143}$Sm et que l'activité de 73 minutes provient de la réaction ^{142}Nd$(\alpha, 4n)^{142}$Sm.

4. Études des propriétés radioactives de ces isotopes

Les spectres γ ont été obtenus avec un spectromètre à cristal de INa, les décroissances β et e mesurées avec les compteurs Geiger du type cloche à paroi mince (< 2 mg). Les corrections d'efficacité, du pic d'échappement, etc, ont été effectuées.

4.1. ^{141}Pm

La figure 1 présente la décroissance de l'activité mesurée au compteur Geiger et celle de la raie X mesurée au spectromètre γ.

Fisher [3]) établit que pour cet isotope $\log ft = 5.3$ et que la transition est permise. D'après la théorie [5]), pour $Z = 60$ (nombre atomique du ^{141}Nd produit) et pour un β^+ de 2.8 MeV, on trouve un rapport de la capture-K à l'émission β^+ de ≈ 0.65.

Or, nous trouvons expérimentalement:

X_K	195 keV	511 keV
100	20	165

Le taux de fluorescence étant de 0.91 dans le cas présent [6]), on a donc $(K/\beta^+)_{exp.} \approx 0.67$. Ceci est en excellent accord avec la valeur théorique.

4.2. ^{142}Pm($\approx$ 40 s)

Cet isotope a été formé par irradiation de ^{142}Nd par des protons de 11 MeV.

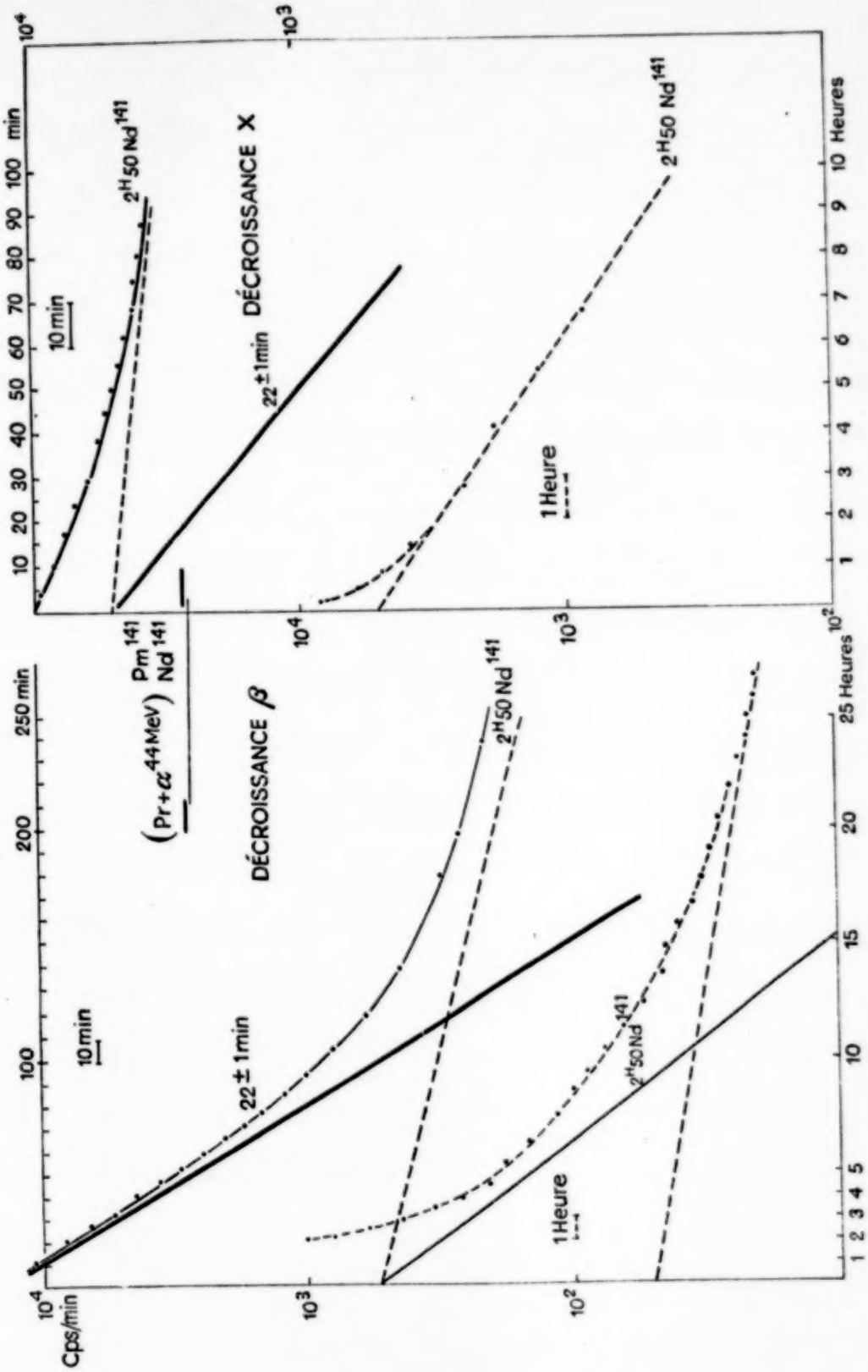

Fig. 1. Décroissance β et décroissance X de ^{141}Pm.

La durée des irradiations a été de 1 minute. Il s'écoulait environ 2 minutes entre l'arrêt de l'irradiation et le début des mesures. Aucune séparation chimique n'étant possible à cause de la période, on obtient donc simultané-

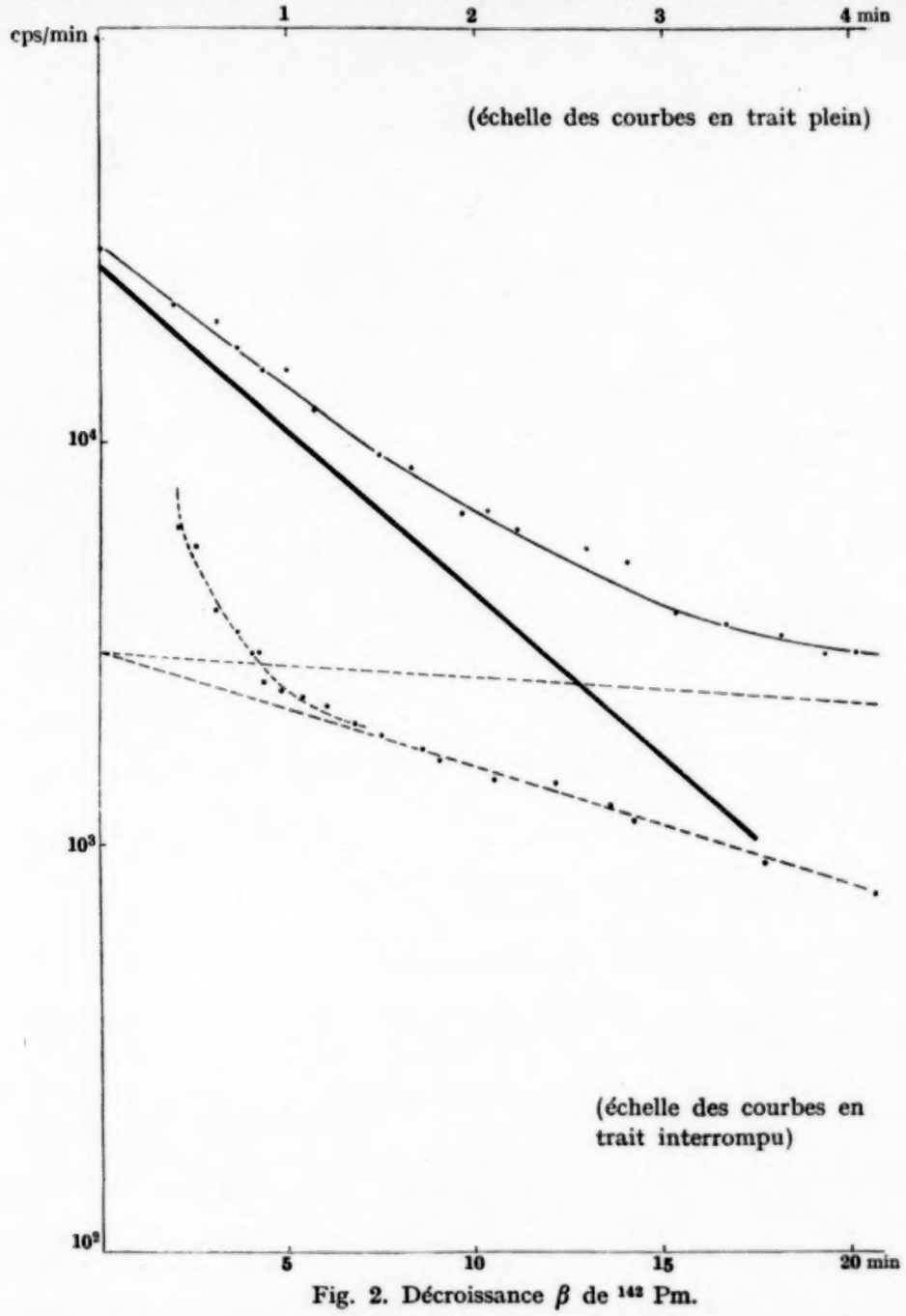

Fig. 2. Décroissance β de ^{142} Pm.

ment le ^{142}Pm et le ^{17}F qui présente une période de 1 minute environ, une activité β^+ et n'émet pas de γ.

Pour connaître le rapport X_K/β^+ de cet isotope, nous avons procédé de la manière suivante: une source a été mesurée directement au spectromètre γ pour obtenir la décroissance X_K.

Pour obtenir l'activité β^+ de ^{142}Pm, nous utilisons le fait que ces β^+ ont une énergie de 3.78 MeV, alors que ceux de ^{17}F ont une énergie de 1.7 MeV. Nous absorbons les β^+ de ^{17}F dans l'aluminium (fig. 2) et nous retrouvons

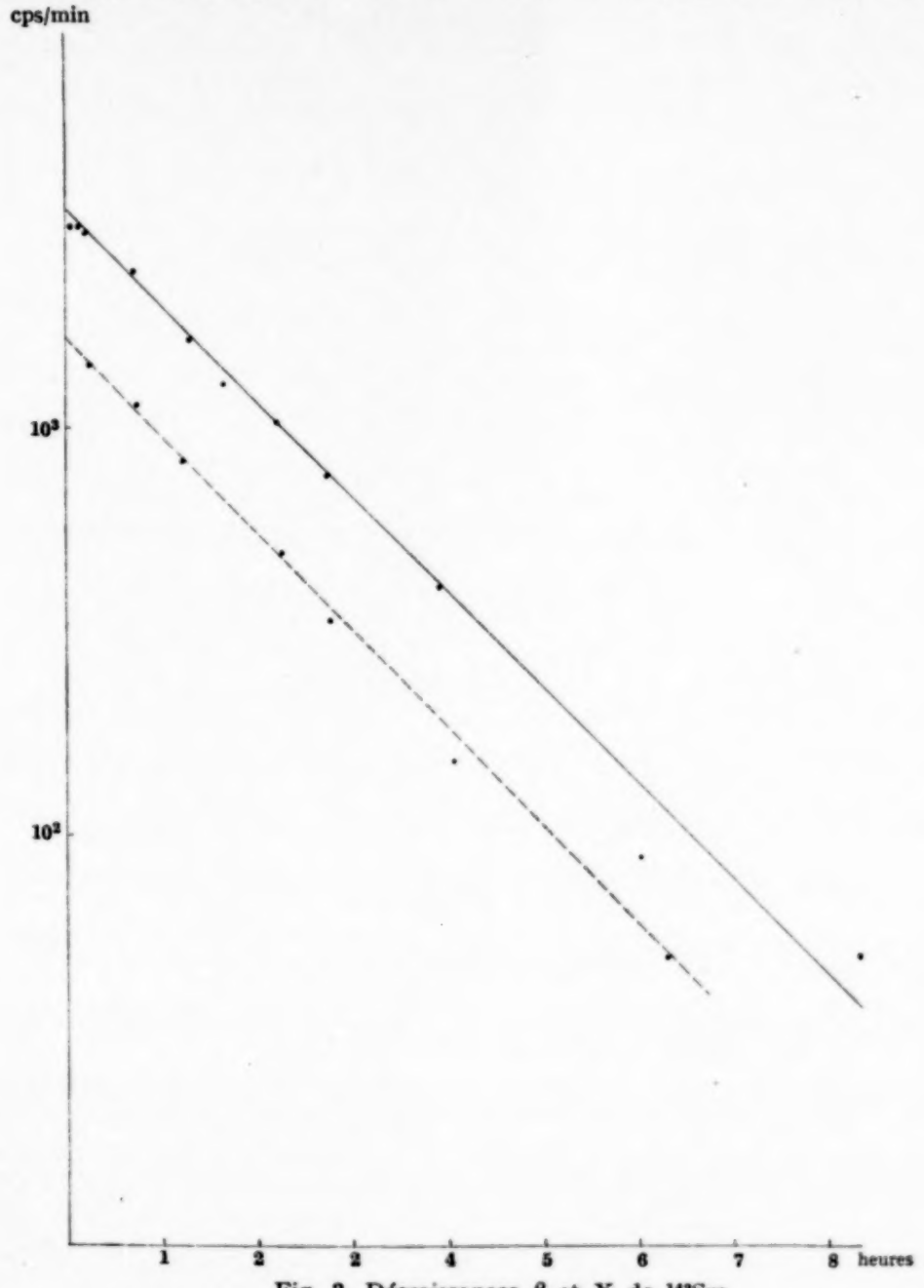

Fig. 3. Décroissances β et X de ^{142}Sm.
——— Décroissance de la raie X ----- Décroissance de la raie à 511 keV

l'activité due à ^{142}Pm en utilisant les courbes d'efficacité de l'installation [7]) et de correction d'absorption que nous avons établies [8]). Nous avons utilisé le facteur $d_{\frac{1}{2}} = 540$ mg/cm² pour $\beta = 3.78$ MeV. Nous comparons ensuite, sous le même détecteur, les deux sources (avec les activités résiduelles ^{13}N, ^{18}F).

Le résultat de cette comparaison est le suivant:

$$X_K/\beta^+ \approx 0.05.$$

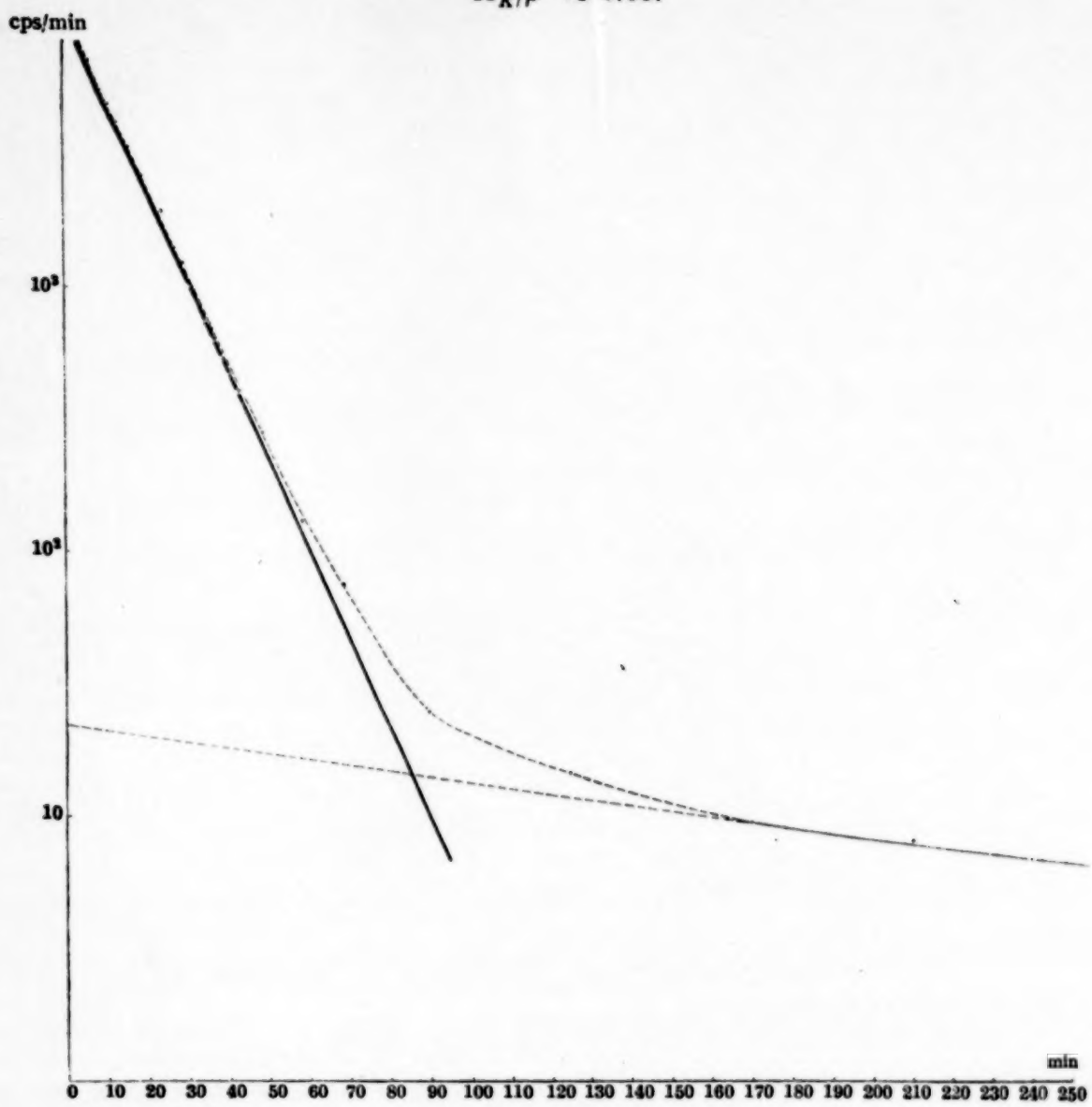

Fig. 4. Décroissance β de ^{143}Sm.

4.3. ^{142}Sm ($\approx$ 73 min)

Dans la réaction ^{142}Nd(α, 4n), après la décroissance du ^{143}Sm de 8.6 minutes, la raie 511 keV décroît avec une période de 73 minutes et la raie X_K avec une période plus longue, car il y a un mélange de produits formés.

Dans la spallation de ^{144}Sm par protons de 150 MeV environ, après séparation chromatographique des éléments, le samarium présente des raies X_K et de 511 keV décroissant avec la période 73 min (fig. 3) et nous permettant de donner le rapport

$$K/\beta^+ = 1.4 \text{ pour } ^{142}\text{Sm} + ^{142}\text{Pm de filiation.}$$

Nous observons plusieurs raies γ entre 150 et 350 keV, mais elles sont très faibles. La comparaison des rapports K/β^+ pour ^{142}Pm seul et pour ^{142}Sm+^{142}Pm nous permet de conclure que ^{142}Sm seul ne présente pas d'émission β^+.

4.4. ^{143}Sm (8.6 min)

La figure 4 présente la décroissance β sous le compteur Geiger. Nous ne trouvons pas d'autres γ, ce qui confirme les résultats connus [1]).

Le tableau ci-dessous résume les propriétés que nous avons pu établir:

	T	K/β^+	spectre γ		
^{141}Pm	22 ±1 min	0.67 en bon accord avec la valeur théorique	X_K 100	195 keV 20	511 keV 165
^{142}Pm	40 ±5 s	≈ 0.05	—		
^{142}Sm	73 ±2 min	pas de β^+	plusieurs raies γ entre 150 et 350 keV très faibles		
^{143}Sm	8.6±0.1 min	≈ 1.7	pas de γ		

Nous remercions les équipes du cyclotron et du séparateur de Saclay ainsi que celle du synchro-cyclotron d'Orsay.

Bibliographie

1) D. Strominger, J. M. Hollander et G. T. Seaborg, Revs. Mod. Phys. **30** (1958) 585
2) J. M. Hollander, I. Perlman et G. T. Seaborg, Revs. Mod. Phys., **25** (1953) 469
3) V. K. Fisher, Thèse, UCRL 1629
4) I. Gratot, Rapport C.E.A. No 913 (1958)
5) E. Feenberg et G. Trigg, Revs. Mod. Phys. **22** (1950) 399
6) C. D. Broyles, D. A. Thomas et S. K. Haynes, Phys. Rev. **89** (1953) 715
7) J. Beydon, R. Chaminade, M. Crut, H. Faraggi, J. Olkowsky et A. Papineau, Nuclear Physics **2** (1956/57) 593
8) J. Olkowsky, M. Le Pape, I. Gratot et L. Cohen, Nuclear Physics **12** (1959) 527

2.C *Nuclear Physics* **13** (1959) 310—316; © *North-Holland Publishing Co., Amsterdam*
Not to be reproduced by photoprint or microfilm without written permission from the publisher

RESONANCES FOR PROTON CAPTURE IN MAGNESIUM

S. L. ANDERSEN, T. HOLTEBEKK, O. LÖNSJÖ and R. TANGEN
Institute of Physics, University of Oslo, Blindern

Received 11 July 1959

Abstract: The yield of beta-rays and gamma-rays from magnesium targets of natural isotopic composition has been measured in the proton energy range of 490 keV to 1390 keV, with special emphasis on the region 490 keV to 670 keV. Thirteen new resonances are reported. For some resonances the absolute yield of beta-rays per incoming proton is given. Resonance energies and upper limits for the half-widths are given for a number of resonances.

1. Introduction

In all the self-conjugate odd nuclei the level density is expected to be much higher than in adjacent nuclei at the same excitation energy. A typical example of this is the Al^{26} nucleus where new levels have been reported regularly [1–7]). About 40 levels between 6.6 MeV and 7.6 MeV excitation energy are now known. From 6.79 to 6.89 MeV 9 levels are found. Information on the level density in this energy region is most conveniently obtained from the reaction $Mg^{25}(p, \gamma)Al^{26}$. However, the high level density and the rather low reaction yield require good proton energy resolution, high counting efficiency and careful selection and preparation of targets.

2. Target Technique

Metallic magnesium exposed to air is rapidly oxidized. The target technique previously described [8]) whereby the target material is evaporated in the target chamber, was therefore used. Even then targets do not give really good resolution after more than one day in the vacuum chamber, probably because of oxidation or some other reaction with the residual gas (gettering).

The small spacing between the resonances, of the order of a few keV, makes it necessary to use quite thin targets in many regions. But targets as thin as one keV never seem to be quite uniform, and are not well suited for accurate measurements.

3. Experimental Procedure

The targets were bombarded with protons from the Blindern Van de Graaff generators. For the resonances between 450 keV and 750 keV the

H_2^+ beam was used, whereas the H^+ beam was used from 750 keV to 1400 keV. The energy scale used is the one based on Bumiller's [9]) 990.8 keV value for the strong Al^{27} resonance. The resolution of the electrostatic proton energy analyzer and the effect of using the H_2^+ beam have been discussed previously [8, 10]). In the region below 670 keV both gamma radiation and beta activity were measured, whereas beta activity only was measured on most of the resonances above 670 keV.

The gamma radiation was measured with a 1.5" NaI (Tl) crystal, with discriminator setting at 2.5 MeV. In a few cases the discriminator setting was varied, or the gamma spectrum was observed on a 120 channel pulse height analyzer to make sure that the assignments were correct.

The beta activity was measured with a Geiger Müller counter of the type Philips 18 505 placed in a lead shielding. The target system used most of the time was that previously described [8]). An instrument similar to that described by Snowdon [11]) was used to measure the bombarding current. The procedure for counting was as follows:

After bombarding the target for a few half-lives, the beam was cut out by a shutter and the target cylinder turned until the bombarded spot came in the position nearest to the counter. Counting was performed for three half-lives, whereupon the counter was automatically switched over from one scaler to another and the number of counts recorded for another three half-lives period. The number of counts on the last scaler was used as background correction to eliminate any long-lived activity built up in the target. This, of course, also had the effect that the observed activity was reduced from the 90 % radiated in the first three half-lives to 80 % of the total activity. Searching at the same time for resonances in the yield of Al^{25} with a half-life of 7.6 sec and of Al^{26} with a half-life of 6.6 sec, a time constant was used for the *RC* circuit corresponding to a half-life of 7 sec. The error introduced by this method is negligible.

4. Experimental Results

The work falls in three separate groups:

a) For a number of the low lying levels attempts were made to measure half-widths, particularly since rather large widths were reported previously for some of the levels [12]). Only in the case of the strong resonance at 823 keV in Mg^{24} did the measured interquartile range exceed that expected from the proton energy spread. The results are given in table 1.

b) The proton energy range from 490 keV to 670 keV was very carefully studied in order to resolve all resonances. A variety of target thicknesses were used to bring out the best result. Representative examples of the curves obtained are shown in fig. 1 and fig. 2 and the results are given in

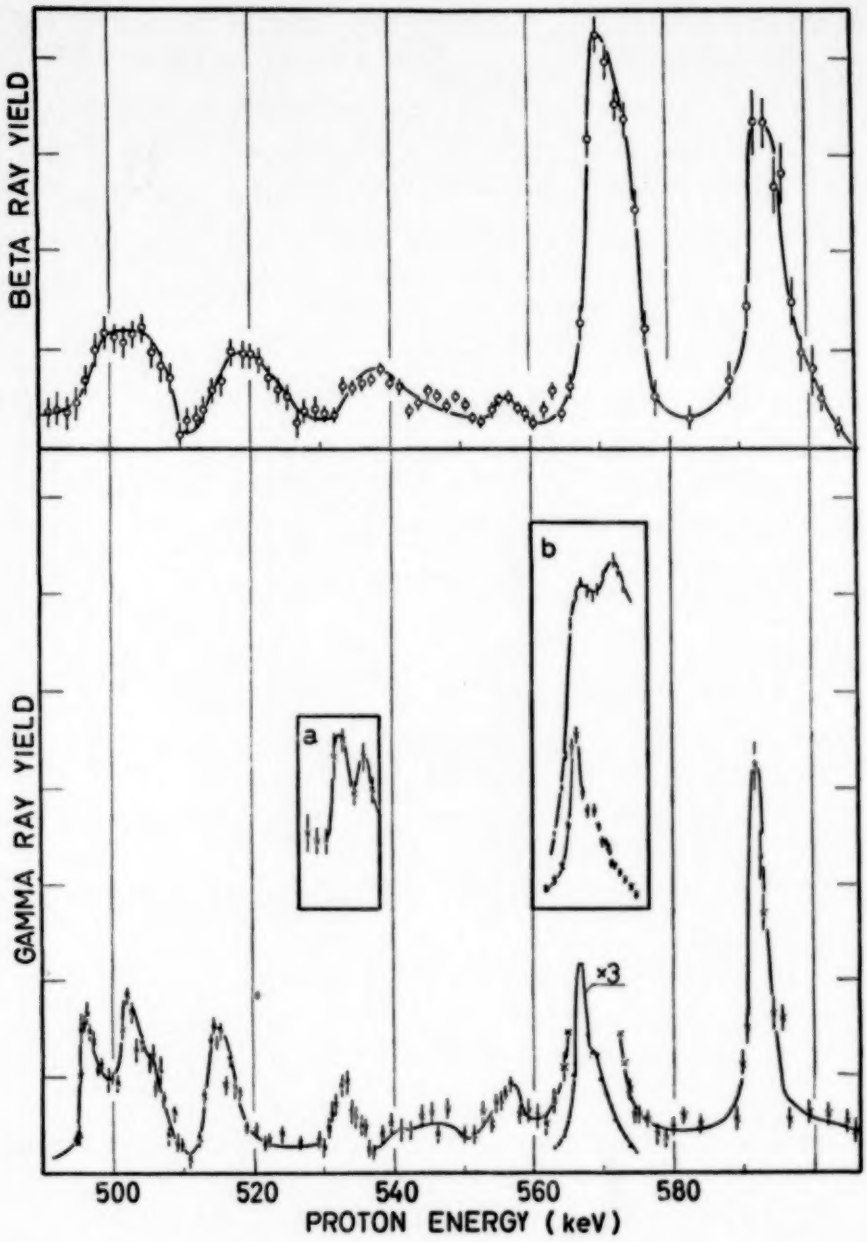

Fig. 1. The yield of gamma rays for protons with energies from 490 keV to 600 keV. The results summarized here have been obtained on a large number of targets of varying thicknesses, generally somewhat thicker for the beta ray curve. Insert a shows the 530 keV doublet resolved with a rather thin target, and insert b shows the 565 keV doublet measured both with a very thin and a semi-thick target.

table 2. Three resonances, at 500 keV, 530 keV and 570 keV were resolved in doublets. There are still regions, however, where the yield seems to be above zero, and it is quite likely that more resonances can be found.

c) The yield of beta rays was measured from 820 keV to 1390 keV and some new resonances were found. The yield curve is shown in fig. 3 and the results are summarized in table 3. The distance between the observation

TABLE 1

Resonance energies and half-widths of the stronger resonances below 490 keV and from 670 keV to 840 keV

Resonance energy	Half-width in keV	Target isotope	Resonance energy	Half-width in keV	Target isotope
222 †	<1.0	24	723.2±0.5	<2	25
312 †	<2.0	25	777.7±0.5	<2	25
338.3±0.12	<0.3	26	808.8±0.5	<0.5	26
390.2±0.6	<1.0	25	811.0±0.8	<2	25
418.8±0.14	<0.4	24	823.1±0.5	1.3±0.4	24
453.4±0.14	<0.4	26	838.7±0.5	<0.5	26
682.6±0.5	<2	25			

† Measured with the 500 keV low resolution Van de Graaff.

TABLE 2.

Resonances in the proton energy range from 490 keV to 670 keV shown in fig. 1 and fig. 2

Resonance energy in keV	Half-width in keV	Target isotope	Absolute yield	Relative yield of gamma rays	Relative yield of beta rays
495.2±1.0	<1	25	$(8.1\pm1.4)\times10^{-13}$	22	26
501.1±1.0	<2	25		25	26
513.3±1.0	<2	25	$(7.8\pm1.2)\times10^{-13}$	19	23
532.0±1.0	<2	25	$(4.6\pm0.7)\times10^{-13}$	9	13
535.0±1.0	<2	25		6	6
556.0±2.0	<3	25		5	7
565.4±0.5	<0.5	25	$(31\ \pm5\ )\times10^{-13}$	100	100
570.0±1.5	<3	25		15	10
590.7±0.5	<0.5	25	$(22.1\pm1.8)\times10^{-13}$	70	71
647.5±0.8	<1	26		35	0
654.0±1.5	<2	25	$(4.6\pm0.8)\times10^{-13}$	20	13
660.5±0.5	<0.8	26		170	0

This region has been carefully investigated to find as many of the resonances as possible. The column marked "absolute yield" gives, for the best resolved resonances, the number of beta-emitting nuclei produced per incoming proton, integrated over the whole resonance (thick target yield). For all resonances the yields, relative to the resonance at 565 keV, are given for beta rays and for gamma rays above the discriminator setting of 2.5 MeV.

points is such that at least one point for each resonance is believed to represent the thick target yield. The heights of the peaks, therefore, are proportional to the integrated cross sections for each resonance. The measurements in this region were done at an early stage of the work [11]), and the resolution is lower than in the measurements under a) and b). It is quite likely that more resonances can be found.

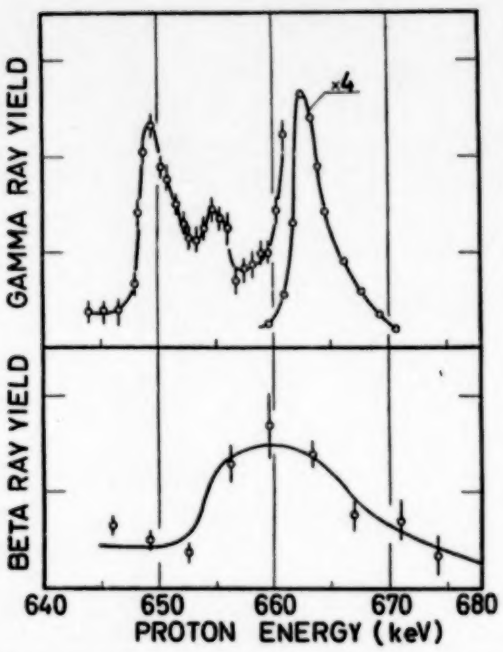

Fig. 2. The yield of gamma rays and beta rays. The gamma curve shows three resonances, at 647.5 keV, 654.0 keV and 660.5 keV, while only the one at 654.0 keV is visible in the beta curve.

TABLE 3

Resonances for proton capture in Mg^{24} and Mg^{25} in the energy range 820 keV to 1390 keV. Values marked with an asterisk are not previously reported

Resonance energy	Target isotope	Resonance energy	Target isotope
823.1±0.5	24	1104.7±1.3	25
870 ±3 †	25	1136.1±1.0	25
882.4±0.7	25	1148 ±3	25
890 ±1.5†	25	1163 ±2 †	25
902 ±4 †	25?	1184 ±3 †	24, 25?
928.6±0.6	25	1195.2±0.7	25
955 ±4	25	1200 ±1.0	24
969 ±2 †	25	1236.9±0.8	25
1026 ±1 †	25	1283.4±0.6	25
1042.6±0.6	25	1303.9±0.5	25
1070 ±3 †	25	1352 ±3 †	25?
1084 ±2	25	1373.5±2.5	25

5. Discussion

By gamma-ray spectroscopy it will be possible to ascribe the resonances to the right isotopes, but for the weaker resonances it might be difficult to get enough observations for a reliable spectrum. Whereas Al^{25} always and Al^{26} usually give beta emission, this is never the case with Al^{27}. Observation

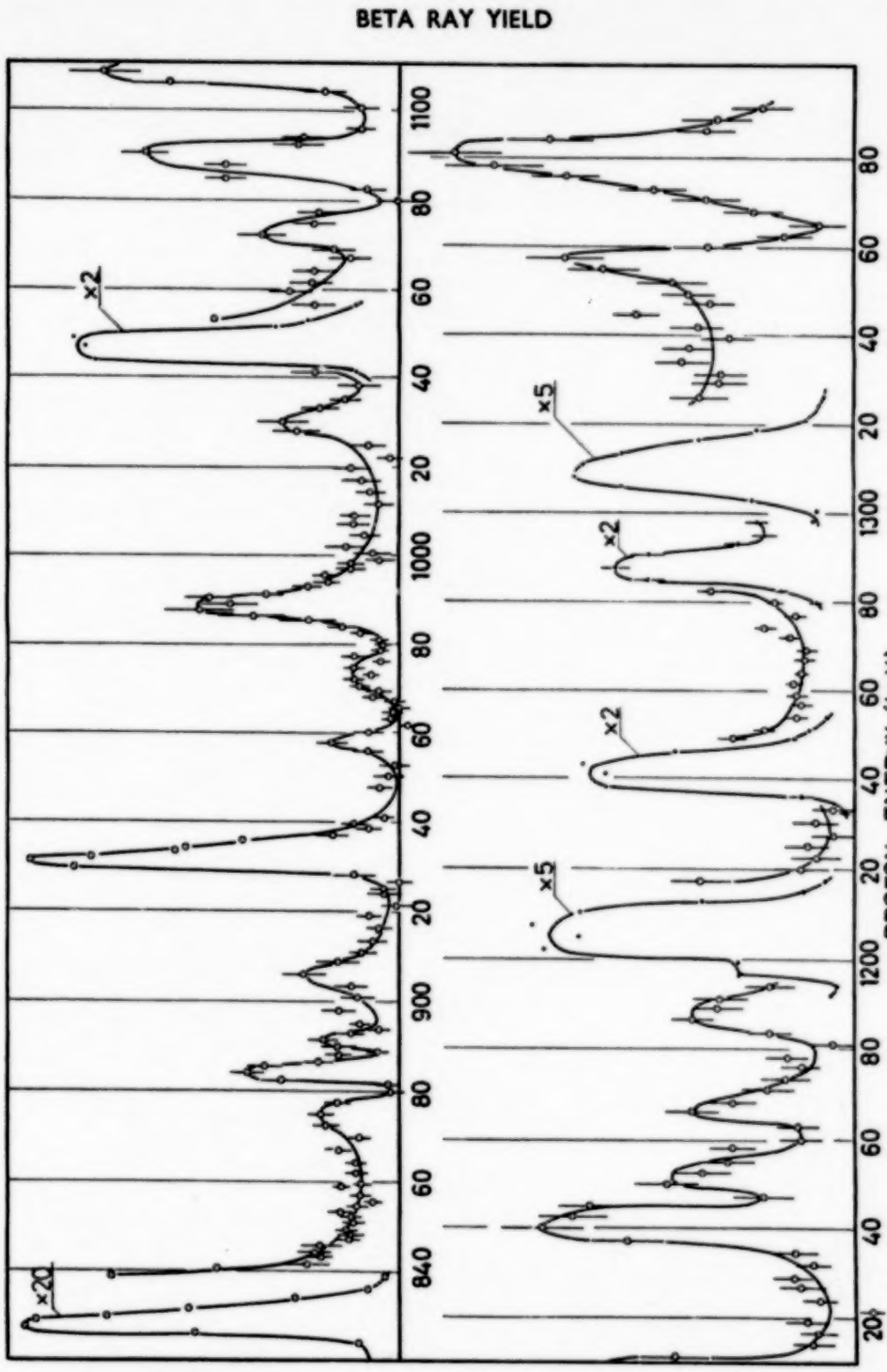

Fig. 3. The yield of beta rays from magnesium targets of thickness 6—8 keV, bombarded with protons of energy from 820 keV to 1390 keV. In some regions, as around 860 keV, 1010 keV, 1270 keV and 1330 keV there are indications of more resonances, which we were not able to resolve.

of positons, therefore, excludes Mg^{26} from being involved. Furthermore the Mg^{24} reaction has a Q value of 2.3 MeV only, whereas the Mg^{25} reaction has a Q value of 6.3 MeV. It is easy, therefore, to use a discriminator level setting excluding all, or the larger part, of the gamma rays from Al^{25}. As Al^{26} only partly goes to the short-lived excited level, whereas all the Al^{25} produced, immediately goes to the ground state, the beta to gamma ratio for the Mg^{24} reaction will always be considerably higher than for the Mg^{25} reaction. This fact is also helpful when trying to identify a resonance.

As seen from fig. 1 it has been possible to resolve 3 previously known resonances in doublets. The pair at 495 keV and 501 keV is already reported resolved by Kuperus *et al.* [7]). The apparent discrepancy between the values obtained by Kuperus and by us for the relative yields of these two resonances may be due to the fact that Kuperus has discriminated against radiation below 4 MeV and we below 2.5 MeV. The resonances at 565.4 keV and 570 keV have been carefully checked. From the yield curve only, it could not be excluded that the apparent double peak might be due to irregularities of targets, but the adjacent 590 keV resonance showed no such double peak, and it was concluded that there is a small resonance at 570 keV. The relatively high gamma yield compared with the beta yield makes it possible to interpret it as a Mg^{25} resonance.

The resonance at 647.5 keV is not previously reported, although it has a considerable strength. The resonance is identified as due to Mg^{26} by the high-energy gamma rays following this reaction.

The authors wish to thank cand. real. L. A. Berteig, cand. real. J. Kne and cand. real. B. Styve, who, as graduate students, contributed to various parts of this work.

The work was supported by The Royal Norwegian Council for Scientific and Industrial Research.

References

1) R. Tangen, Kgl. Norske Vid. selsk. Skrifter (1946) no. 1
2) Cooper, Taylor, Harris and Grove, Phys. Rev. **80** (1950) 131
3) Taylor, Russell and Cooper, Phys. Rev. **93** (1954) 1056
4) S. E. Hunt and D. A. Hancock, Phys. Rev. **97** (1955) 567
5) Barjon, Lambert et Schmouker, Journ. Phys. Radium **19** (1958) 47
6) S. Hinds and R. Middleton, Proc. Phys. Soc. **73** (1959) 501
7) Kuperus, Smulders and Endt, Physica
8) Andersen, Bö, Holtebekk, Lönsjö and Tangen, Nuclear Physics **9** (1958/59) 509
9) Bumiller, Staub and Weaver, Helv. Phys. Acta **29** (1956) 83
10) Andersen, Gjötterud, Holtebekk and Lönsjö, Nuclear Physics **7** (1958) 384
11) S. C. Snowdon, Phys. Rev. **78** (1950) 299
12) Hunt, Jones, Churchill and Hancock, Proc. Phys. Soc. A **67** (1954) 443
13) J. Kne, Thesis, University of Oslo (1957)

2.B *Nuclear Physics* **13** (1959) 317—332; © *North-Holland Publishing Co., Amsterdam*
Not to be reproduced by photoprint or microfilm without written permission from the publisher

STUDY OF THE DIRECT (α, NUCLEON) REACTION, INCLUDING POLARIZATION

ERNEST M. HENLEY †

Institute for Theoretical Physics, University of Copenhagen

and

CERN, *Geneva*

Received 29 June 1959

Abstract: A theoretical study of the differential cross-section and nucleon polarization of the direct (α, N) reaction at medium to high energies is carried out. An expression for the transition matrix element is derived from the distorted wave description, but only the distortion of the α-particle by the nucleus is taken into account in an illustrative calculation. It is argued that experimental studies of the polarization are useful for gaining insight into the reaction mechanism. This is explicitly demonstrated by including the spin-dependence and first order size effects of the interaction responsible for a knock-out process. The reaction examined has several advantages over the similar deuteron stripping process, one of which is the considerably higher degree of the nucleon polarization.

1. Introduction

The deuteron stripping reaction has been extensively studied, and recently, particular attention has been paid to the polarization of the resulting nucleon [1]) and of the daughter nucleus [2]). Part of this interest derives from the use of the stripping reaction to obtain spins of nuclear levels, and part of it rests on the simple interpretation of the reaction first given by Butler [3]). Polarization studies allow one to gain some insight into the validity of various theoretical approximations and add to our understanding of the reaction mechanism.

By contrast to the (d, N) reaction ††, little effort has yet been expended in theoretical [4]) or experimental studies [5]) of the medium energy (α, N) reaction. If this reaction occurs in the surface of the nucleus †††, it can proceed by either a stripping or a knock-out process, or both. In the first instance the nucleon is emitted by the incident α-particle and in the second it stems from the target nucleus. Although both processes are also present in the (d, N) reaction, the low binding energy of the deuteron favours the stripping mode.

† U.S. National Science Foundation Senior Postdoctoral Fellow, on leave of absence from the University of Washington, Seattle, Washington.

†† The symbol N stands for either nucleon, whereas n and p designate neutron and proton respectively.

††† The terms surface reaction and direct reaction are used interchangeably in this paper.

It is clear that if the deuteron or α-particle penetrate into the nucleus, where they lose their internal structure, the differentiation between stripping and knock-out loses all meaning. Formally this comes about in part by the anti-symmetrization of the initial state wave-function between all nucleons, which is here neglected.

A study of polarization in the (α, N) reaction offers several advantages, both experimental and theoretical, over the (d, N) process. Experimentally, the maximum polarization of the nucleon is 100 % in an (α, N) reaction, whereas the unit spin of the deuteron limits it to $\frac{1}{3}$ of this value in the (d, N) reaction [1, 6]). Theoretically, the distortion of the incoming spinless α-particle is easier to take into account than that of its counterpart in the deuteron stripping process.

The (α, N) differential cross-section is not expected to be very sensitive to the mode of interaction discussed above and we shall show that this expectation is valid. The diffraction patterns obtained [5]) from the medium energy (20—40 MeV) α-particle bombardment of light nuclei does, however, lend credence to the interpretation of the process as a direct reaction, be it stripping or knock-out. Part of the usefulness of an experimental and theoretical investigation of the polarization produced in an (α, p) or (α, n) transition would be to clarify the reaction mechanism. For example, as in the (d, p) reaction, no polarization is expected if the Born approximation holds; this is true even if the radial integral involved in the matrix element is cut off at the nuclear radius, as is usually done [3]). Furthermore, the polarization may yield information as to whether the reaction proceeds primarily by means of stripping or knock-out †; the interactions responsible for the two types of processes are different, and we shall see to what extent the polarization is influenced by the interaction structure. In any result sensitive to this structure and to the deviation from Born approximation, it is obviously important to have an accurate theoretical description of the process. As an example, the polarization of the proton in a (d, p) reaction has the opposite sign, depending on whether the distortion of the incoming deuteron or outgoing proton is dominant [1, 2]). In this sense, the work described below is only a first, but reasonable step. It considers only the most important deviations from a Born approximation description in order to retain a manageable mathematical treatment. Thus, the description is restricted to medium energy (say, larger than 20 MeV) incoming α-particles. Experimentally, this seems to be the region of most interest for direct processes, and theoretically it has the advantage of negligible Coulomb distortion effects, except in the forward direction, when light target nuclei are employed. In

† When the nucleon binding energy in the target and in the α-particle are approximately the same, both processes may be of equal importance, and it may not be sensible to differentiate between them phenomenologically.

any case, it is generally only for such targets that reactions to different final states can be distinguished experimentally.

In addition to the above restrictions, the important physical approximations made in the treatment below, can be summarized as follows:

1) A distorted wave approximation treatment [7]) on the elastic scattering solution is employed. This type of treatment has been successful in studies of inelastic scattering, (d, p) reactions, and other direct processes [8]).

2) The distortion (scattering) of the proton (or neutron) by the final nucleus is omitted in the calculation, but not in the formulation. Of the two particles, the proton certainly has the larger mean free path in nuclear matter, and the polarization must arise principally due to the distortion of the incoming alpha-particle. In the (d, p) reaction, it has similarly been shown that the deuteron distortion is more important, and that its neglect leads to a polarization of the wrong sign [1, 2]). Here too, the distortion of the outgoing proton wave leads to a polarization of opposite sign to that caused by the α-particle.

3) The effect of the structure of the interaction mechanism is studied principally by including the result of the spin dependence of the α—N interaction on (a) the angular distribution and (b) the polarization of the nucleon produced in a knock-out process. By this means it should be possible to establish the ability of the polarization to differentiate between various reaction modes. Thus, the spin-dependence of the p—H^3 interaction [9]), which enters in the (α, p) stripping process is quite different from that for p—α, which is present in the knock-out process. If the structure (in this case, the spin-dependence) is neglected, similar angular distributions and polarizations are expected for the two modes.

In addition to the above physical limitations, several mathematical approximations are made. Some of these are best discussed in the text. The most important one, perhaps, is the use of the WKB high energy approximation, suggested by L. I. Schiff [10]), which is valid for $R_0/\lambda\!\!\!^{-} \gg 1$, where R_0 is the nuclear radius and $\lambda\!\!\!^{-}$ is the reduced wave length of the incoming particle. Since an alpha-particle has a small wave length ($\lambda\!\!\!^{-} \approx \frac{1}{2} \times 10^{-13}$ cm for a 20 MeV particle), owing to its relatively large mass, this approximation can readily be justified.

2. Theoretical Development

2.1. FORMULATION

In a direct (α, N) reaction, the neutron may be stripped from the alpha-particle or it may be emitted from the nucleus. The formulation of the reaction matrix element is similar in the two cases, but differs in the specific interactions involved. If the alpha-particle knocks a nucleon out of the

nucleus, the internal structure of the α-particle plays no role and the Hamiltonian can be written as

$$H = T_\alpha + H_A + \sum_{i=1}^{A} V_{\alpha N_i}, \tag{1}$$

where T_α is the kinetic energy of the α-particle, H_A is the Hamiltonian of the struck nucleus, and $V_{\alpha N_i}$ represents the interaction of the α-particle with the nucleon N_i. The transition matrix element is then [11])

$$R_{fi} = \langle \Psi_f^- | \sum_i V_{\alpha N_i} | \phi_i \rangle, \tag{2}$$

where ϕ_i is the ground state wave function of the target nucleus multiplied by a plane wave for the α-particle, and Ψ_f^- is the incoming wave final state scattering solution

$$\Psi_f^- = \phi_f + \frac{1}{E - H - i\varepsilon} U \phi_f. \tag{3}$$

In Eq. (3) ϕ_f is the final nuclear wave function multiplied by a plane wave for the nucleon, and U stands for the interaction of the outgoing nucleon with all other particles. One can split [1,12]) $\sum_i V_{\alpha N_i}$ phenomenologically into a central average (complex) potential V, and an interaction with one or more single surface nucleons, V_N. The interaction V is the so called optical potential. It gives rise to an elastically scattered wave, which is the solution of the integral equation

$$\psi_i^+ = \phi_i + \frac{1}{E - T_\alpha - H_A + i\varepsilon} V_\alpha \psi_i^+ \tag{4}$$

and should account for the measured elastic scattering cross-section of α-particles.

The same split for the nucleon interaction U gives $U = V_N + V_{\alpha N}$, and the elastical scattering solution

$$\psi_f^- = \phi_f + \frac{1}{E - T_N - H_{A+3} - i\varepsilon} V_N^\dagger \psi_f^-, \tag{5}$$

where H_{A+3} is the Hamiltonian of which the final nuclear bound state is an eigenfunction and $V_N^\dagger$ is the Hermitian adjoint (complex conjugate) of the complex potential V_N. By means of standard manipulations [11]), the transition matrix element then becomes

$$\begin{aligned} R_{fi} &= \langle \psi_f^- | V_{\alpha N} | \Psi_i^+ \rangle + \langle \phi_f | V_N | \psi_i^+ \rangle \\ &\approx \langle \psi_f^- | V_{\alpha N} | \psi_i^+ \rangle. \end{aligned} \tag{6}$$

The matrix element $\langle \phi_f | V_N | \psi_i^+ \rangle$ is zero because V_N does not connect the initial and final states. The matrix R_{fi}, eq. (6), is often called the distorted wave approximation [7]); the interaction $V_{\alpha N}$, which is responsible for the

process, connects the outgoing wave initial state elastic scattering solution to the ingoing final scattering state.

If the nucleon is stripped from the alpha-particle, then the formulation is the same as for the deuteron stripping process (the internal structure of the α-particle now plays a decisive role) and one obtains † with the usual approximations and procedures [1, 12])

$$R_{fi} = \langle \psi_f^- | V_{\mathrm{NH^3}} | \psi_i^+ \rangle. \tag{7}$$

It is clear that one cannot replace $V_{\alpha N}$ and $V_{\mathrm{NH^3}}$ by zero-range central potentials if one wishes to distinguish which of the two possible mechanisms, represented by eqs. (6) and (7) is dominant in a particular situation. An exact formulation of the problem requires the presence of both transition matrices and inclusion of the interaction structure. Indeed, it will be shown that inclusion of the latter, greatly modifies the expected polarization. Furthermore, if ψ_f^- and ψ_i^+ are both replaced by their respective plane wave states, ϕ_f and ϕ_i, then the polarization of the emitted nucleon is zero [3]) ††. This result follows even if $V_{\mathrm{NH^3}}$ and $V_{\alpha N}$ are spin dependent.

In the following development, as a means of illustration, and in order to gain some insight into the sensitivity of both the angular distribution and polarization measurements to the structure of the interaction, we shall explicitly consider a knock-out process, eq. (6). Furthermore, in this preliminary treatment, we shall (a) neglect the distortion of the final nucleon (e.g. $\psi_f^- \approx \phi_f$) (b) find ψ_i^+ by means of a WKB type treatment [10]), (c) assume a short range spin-dependent interaction $V_{\alpha N}$, (d) consider the nucleus to be described by the shell model and the alpha-particle to be captured into an angular momentum zero state relative to the rest of the nucleus. It should be noted that *none* of these approximations are essential to the problem, and that they are made solely for the sake of simplicity. The results should be correct, at least semi-quantitatively, and will be confirmed in a later more rigorous calculation.

2.2. ELASTIC SCATTERING SOLUTION

The elastic scattering of the α-particle by the nuclear optical potential is found below by means of a WKB type of approximation suggested by L. I. Schiff [10]). The solution to eq. (4) is then ($\hbar = c = 1$ here and throughout)

$$\psi_i^+ = u(\mathbf{r}_1 \ldots \mathbf{r}_{A-1}) e^{i\left[\mathbf{k}_0 \cdot \boldsymbol{\rho} - \frac{1}{v}\int_0^\infty V_\alpha(\boldsymbol{\rho} - \hat{\mathbf{k}}_0 s)\,ds\right]} \tag{8}$$

and is valid for high incident momenta and at small angles where the elastic scattering cross-section is largest. In eq. (8) $u(\mathbf{r}_1 \ldots \mathbf{r}_{A-1})$ is the internal nuclear wave function, $\mathbf{k}_0$ is the relative momentum in the centre of

† So-called "heavy-particle stripping" is neglected in eq. (7). See ref.[18]).

†† The polarization is zero even when the only radial integral that must be performed with a δ-function interaction is cut off at the edge of the nucleus.

mass system, a hat over a symbol (e.g. $\hat{\mathbf{k}}_0$) indicates a unit vector, and $\boldsymbol{\varrho}$ is the relative position of the α-particle with respect to the nucleus. The optical potential V_α should be adjusted[13]) to fit the elastic scattering of α-particles, but this requires a computational programme, which we wish to avoid in this paper. For purposes of illustration, ψ_1^+ is calculated for a square well of radius b and depth $-(U_0+iW_0)$, and for a finite harmonic oscillator

$$\begin{aligned} V_\alpha &= -\tfrac{1}{2}(K_0+iK_1)(b^2-\rho^2) \quad \text{for} \quad \rho < b \\ &= 0 \qquad\qquad\qquad\qquad\quad \text{for} \quad \rho > b. \end{aligned}$$

Substitution into eq. (8) gives for the square well

$$\psi_1^+ = u(\mathbf{r}_1 \ldots \mathbf{r}_{A-1}) e^{i\left[\mathbf{k}_0 \cdot \boldsymbol{\rho} + \frac{1}{v}(U_0+iW_0)(B-A)\right]} \tag{9}$$

and for the harmonic oscillator potential

$$\begin{aligned} \psi_1^+ = {} & u(\mathbf{r}_1 \ldots \mathbf{r}_{A-1}) e^{i\mathbf{k}_0 \cdot \boldsymbol{\rho}} \\ & \times e^{-\frac{i}{2v}(K_0+iK_1)[(\rho^2-b^2)(B-A)+\frac{1}{3}(B^3-A^3)-\rho\cos\Phi(B^2-A^2)]}. \end{aligned} \tag{10}$$

In eqs. (9) and (10), Φ is the angle between $\hat{\boldsymbol{\varrho}}$ and $\hat{\mathbf{k}}_0$, and B and A are given by

$$\begin{aligned} &A = 0, \quad B = \rho\cos\Phi + (b^2-\rho^2\sin^2\Phi)^{\frac{1}{2}} \quad \text{for} \quad 0 \leqq \rho \leqq b, \\ &A = \rho\cos\Phi - (b^2-\rho^2\sin^2\Phi)^{\frac{1}{2}} \quad \text{for} \quad b \leqq \rho \leqq \frac{b}{\sin\Phi} \\ &B = \rho\cos\Phi + (b^2-\rho^2\sin^2\Phi)^{\frac{1}{2}} \qquad \cos\Phi > 0, \\ &A = 0, B = 0 \quad \text{for} \quad b \leqq \rho \leqq \frac{b}{\sin\Phi}, \quad \cos\Phi < 0 \\ &\qquad\qquad \text{and for} \quad \frac{b}{\sin\Phi} \leqq \rho \leqq \infty. \end{aligned} \tag{11}$$

The main feature to note in eqs. (9) and (10) is that $|\psi_1^+|$ is very rapidly damped whenever B and A, eq. (11), are not zero. This result is illustrated in table 1 and follows from the short mean free path of α-particles inside nuclear matter. The optical potential must therefore have a large imaginary part to fit the elastic scattering data [13]). Table 1 also illustrates the main difference between a square well and a more smoothly varying potential, namely that the angular and radial variations of $|\psi_1^+|$ are more gradual for the latter. Here we shall stress and make use of the dominant feature, given above. We assume that $\psi_1^{(+)}$ is

$$\begin{aligned} \psi_1^{(+)} &= e^{i\mathbf{k}_0 \cdot \boldsymbol{\rho}} u(\mathbf{r}_1 \ldots \mathbf{r}_{A-1}) \text{ for } \begin{cases} \rho \geqq b/\sin\Phi \\ b \leqq \rho \leqq b/\sin\Phi, \quad \cos\Phi \leqq 0 \end{cases} \\ &= 0 \quad \text{for } \begin{cases} b \leqq \rho \leqq b/\sin\Phi, \ \cos\Phi > 0 \\ 0 \leqq \rho \leqq b, \end{cases} \end{aligned} \tag{12}$$

which corresponds to a model with a sharp absorption edge or infinite W_0.

TABLE 1

Penetration depth of α-particles

Φ	ξ	η square well	η harmonic oscillator
0	∞	0	0
45°	$(2)^{\frac{1}{2}}b$	$\frac{1}{8}\left(\frac{2W_0b}{v}\right)^{-2} = 0.0022$	$\left[8\frac{K_1b^3}{v}\frac{(2)^{+\frac{1}{2}}}{3}\right]^{-\frac{1}{2}} = 0.107$
90°	b	$\frac{1}{2}\left(\frac{2W_0b}{v}\right)^{-2} = 0.0089$	$\left[\frac{4(2)^{\frac{1}{2}}}{3}\frac{K_1b^3}{v}\right]^{-\frac{1}{2}} = 0.171$
135°	b	$\left[\frac{2W_0b}{v}\times(2)^{\frac{1}{2}}\right]^{-1} = 0.094$	$\left[(2)^{\frac{1}{2}}\frac{K_1b^3}{v}\right]^{-\frac{1}{2}} = 0.306$
180°	b	$\left(\frac{2W_0b}{v}\right)^{-1} = 0.133$	$\left(\frac{K_1b^3}{v}\right)^{-\frac{1}{2}} = 0.365$
at centre		$e^{\frac{-2W_0b}{v}} = e^{-7.5}$	$e^{-\frac{1}{2}\frac{K_1b^3}{v}} = e^{-5}$

ξ is the smallest distance for which there is no absorption, and η is the fractional distance, $(\xi-\rho)/\rho$ in which $|\psi_1^+|^2$ has fallen to 1/e. The numerical values have been evaluated for 30 MeV α-particles and for a square well of range $b = 5.5\times10^{-13}$ cm (eg. ≈ Be^9) and imaginary depth $W_0 = 15$ MeV, as suggested by Igo [13]). For the harmonic oscillator, the strength $\frac{1}{2}K_1b^2$ was set equal to W_0.

2.3. EVALUATION OF TRANSITION MATRIX ELEMENT

In order to demonstrate the effect of the interaction structure, we restrict ourselves to the emission of a nucleon from a definite single particle state of orbital angular momentum l and total angular momentum j. The latter is also taken to be the ground state spin of the nucleus and anti-symmetrization is neglected. The α-particle is assumed to be captured into a relative S-state of orbital angular momentum, giving rise to a final nuclear state of zero spin. None of these assumptions are essential but they all considerably simplify the algebra involved.

If we label by $\mathbf{R}$ the centre of mass co-ordinate of the $(A-1)$ nucleons in the target nucleus not directly involved in the reaction, by $\mathbf{r}_N$ the co-ordinate of the ejected nucleon and by $\mathbf{R}_\alpha$ that of the centre of mass of the α-particle, then ϕ_f is

$$\phi_f = u(\mathbf{r}_1 \ldots \mathbf{r}_{A-2})v_\alpha(\mathbf{R}_\alpha-\mathbf{R})\chi_{\frac{1}{2}}^m \times \exp i\left[\mathbf{k}_N\cdot\mathbf{r}_N+\mathbf{K}\frac{M_\alpha\mathbf{R}_\alpha+M_{A-1}\mathbf{R}}{M_\alpha+M_{A-1}}\right]. \quad (13)$$

Here v_α is the final state wave function of the captured α-particle, and $\chi_{\frac{1}{2}}^m$ that of the nucleon spin. In the centre of mass system, the momentum $\mathbf{k}_N$ of the nucleon (mass M) and the momentum of the recoil nucleus (mass

$M_{A-1}+M_\alpha$) are equal in magnitude and oppositely directed. The initial state wave function ψ_1^+, in this system is

$$\psi_1^+ = v_N(\mathbf{r}_N-\mathbf{R})u(\mathbf{r}_1 \ldots \mathbf{r}_{A-2}) \exp\left\{if\left[\mathbf{k}_0 \cdot \left(\mathbf{R}_\alpha - \frac{M\mathbf{r}_N+M_{A-1}\mathbf{R}}{M+M_{A-1}}\right)\right]\right\} \quad (14)$$

with the function f defined by eq. (12). For the interaction $V_{\alpha N}$ that given by Sack, Biedenharn and Breit † [14]) is applicable in the energy region of interest:

$$V_{\alpha N}(\mathbf{r}_N-\mathbf{R}_\alpha) = -\mathscr{A}\left(1+\frac{2\beta}{a^2}\boldsymbol{\sigma}\cdot\mathbf{L}\right)e^{-\frac{|\mathbf{r}_N-\mathbf{R}_\alpha|^2}{a^2}} \quad (15)$$

The constants $\mathscr{A}$, β and a are adjusted to fit the low energy proton-alpha scattering phase shifts and are [14]) $\mathscr{A} = 47$ MeV, $\beta = 7.4(\hbar/Mc)^2$ and $a = 2.3\times 10^{-13}$ cm. The spin-orbit interaction is given by the term proportional to $\boldsymbol{\sigma}\cdot\mathbf{L}$.

If use is made of the orthogonal relative co-ordinate $\mathbf{x} = \mathbf{r}_N-\mathbf{R}_\alpha$ and centre of mass co-ordinate $\mathbf{X} = (M\mathbf{r}_N+M_\alpha\mathbf{R}_\alpha)/(M+M_\alpha)$ the transition matrix element, eq. (6), becomes

$$\begin{aligned} R_{mn} &= \langle\phi_f^m|V_{\alpha N}|\psi_1^{n+}\rangle \\ &= -\mathscr{A}\int d^3R\,d^3X\,d^3x\, v_\alpha^*(\mathbf{X}-\mathbf{R}-\tfrac{1}{5}\mathbf{x})e^{-i\mathbf{k}_N\cdot(\mathbf{X}+\frac{4}{5}\mathbf{x})}\chi_{\frac{1}{2}}^{m*} \\ &\times \exp\left[-i\mathbf{K}\cdot(\mathbf{X}-\tfrac{1}{5}\mathbf{x})\frac{M_\alpha}{M_\alpha+M_{A-1}} - i\mathbf{K}\cdot\mathbf{R}\frac{M_{A-1}}{M_\alpha+M_{A-1}}\right]\left[1+\frac{2\beta}{a^2}\boldsymbol{\sigma}\cdot\mathbf{L}(x)\right] \\ &\times e^{-\frac{x^2}{a^2}} v_N^n(\mathbf{X}+\tfrac{4}{5}\mathbf{x}-R) \qquad (16) \\ &\times \exp if\left[\mathbf{k}_0\cdot\left(\frac{M_{A-1}}{M_A}\mathbf{X}-\tfrac{1}{5}\mathbf{x}\frac{M_\alpha+M_A}{M_A}-\frac{M_{A-1}}{M_A}\mathbf{R}\right)\right], \end{aligned}$$

where m and n are the magnetic quantum numbers of the final and initial states, respectively. Because of the small mean free path of α-particles in nuclear matter, the only values of $\mathbf{R} = \mathbf{X}-\frac{1}{5}\mathbf{x}$ wich contribute to the matrix element are those which lie outside the nucleus. It is thus reasonable to assume that the range of interaction between the α-particle and nucleon is sufficiently small that an expansion in powers of $\mathbf{x}/(\mathbf{X}-\mathbf{R})$ can be carried out. (An approximation that is often made is to actually take the range to be zero [1, 12]).) Four our particular example, in which the α-particle is captured into an S-state of orbital motion, it is simplest to expand $v_\alpha(\mathbf{X}-\mathbf{R}-\frac{1}{5}\mathbf{x})$ in powers of $\mathbf{x}/|\mathbf{X}-\mathbf{R}| \equiv x/r$. In the region near the edge of the nucleus where the integrand of eq. (16) differs appreciably from zero, the wave function of the α-particle can be represented to sufficient accuracy by

† The interaction, developed in ref.[14]) is for the p—α system, but should be equally valid for the He^5 case.

$$\lim_{x \ll r \simeq b} v_\alpha(\mathbf{r}-\tfrac{1}{5}\mathbf{x}) = \mathcal{N}_\alpha \frac{e^{-\alpha|\mathbf{r}-\frac{1}{5}\mathbf{x}|}}{|\mathbf{r}-\frac{1}{5}\mathbf{x}|}$$

$$\approx \mathcal{N}_\alpha \frac{e^{-\alpha r}}{r} e^{\frac{1}{5}\alpha r \frac{\mathbf{r}\cdot\mathbf{x}}{r^2}} \left(1+\tfrac{1}{5}\frac{\mathbf{r}\cdot\mathbf{x}}{r^2}\right) \tag{17}$$

$$\approx v_\alpha(r) e^{\frac{1}{5}\alpha r\left(1+\frac{1}{\alpha r}\right)\frac{\mathbf{r}\cdot\mathbf{x}}{r^2}},$$

where $\mathcal{N}_\alpha$ is a normalization constant and α is related to the binding energy B_α of the α-particle by $\alpha = (2M_\alpha B_\alpha)^{\frac{1}{2}}$. Note that the exponential in eq. (17) has not been expanded; we have assumed that $x \ll r$, but not $\alpha x \ll 1$. The $\mathbf{x}$ and $\mathbf{R}$ integrations of eq. (16) can now be developed as follows. By carrying out the momentum-conservation integral and a partial integration over the variable x, one obtains

$$R_{mn} = -\mathcal{A}\int d^3r d^3x v_\alpha^*(r) \exp\left[-i\mathbf{k}_N\cdot\mathbf{r}\frac{M_{A-1}}{M_\alpha+M_{A-1}}\right]\chi_{\frac{1}{2}}^{m*}$$
$$\times\left[1+\frac{2\beta}{a^2}\boldsymbol{\sigma}\cdot\mathbf{x}\times\mathbf{s}\right]e^{-\frac{x^2}{a^2}} \tag{18}$$
$$\times \exp\left[if(\mathbf{k}_0\cdot\mathbf{r}\frac{M_{A-1}}{M_A}-\mathbf{k}_0\cdot\mathbf{x})\right]v_N^n(\mathbf{r})e^{-i\mathbf{q}'\cdot\mathbf{x}}$$

with

$$\mathbf{s} = \tfrac{4}{5}\frac{M_A+M_\alpha}{M_{A-1}+M_\alpha}\mathbf{k}_N+\tfrac{1}{5}i\alpha\hat{\mathbf{r}}\left(1+\frac{1}{\alpha r}\right)$$

$$\mathbf{q}' = \mathbf{k}_N\frac{M_\alpha}{M_\alpha+M_{A-1}}+i\alpha\hat{\mathbf{r}}\left(1+\frac{1}{\alpha r}\right).$$

The integration over the variable x can then be performed, if use is made of the fact that, to lowest order in x, the limitation on the range of integration imposed by ψ_1^+, eq. (12), is only on the variable r. One obtains [15]) †

$$R_{mn} = -\mathcal{A}(\pi a^2)^{\frac{3}{2}}\int_{\mathcal{R}} d^3r v_\alpha^*(\mathbf{r})\chi_{\frac{1}{2}}^{m*}e^{-\frac{1}{4}q^2a^2}v_N^n(\mathbf{r})e^{i\mathbf{Q}\cdot\mathbf{r}}$$
$$\times\left[1+i\beta\boldsymbol{\sigma}\cdot(\Gamma\mathbf{k}_0\times\mathbf{k}_N+i\Delta\alpha\mathbf{k}_0\times\hat{\mathbf{r}}+i\Lambda\alpha\mathbf{k}_N\times\hat{\mathbf{r}})\right] \tag{19}$$

with

$$v_N^n = \sum_{\mu,\nu}(l\tfrac{1}{2}\mu\nu|jn)v_l(r)Y_l^\mu(\theta,\phi)\chi_{\frac{1}{2}}^\nu,$$

$$\mathbf{q} = \mathbf{q}'+\mathbf{k}_0 = \mathbf{k}_0+\frac{M_\alpha}{M_\alpha+M_{A-1}}\mathbf{k}_N+i\alpha\hat{\mathbf{r}},$$

$$\Gamma = -\tfrac{4}{5}\frac{M_A+M_\alpha}{M_{A-1}+M_\alpha},\quad \Delta = -\tfrac{1}{5},\quad \Lambda = \tfrac{1}{5}\frac{M_\alpha}{M_\alpha+M_{A-1}}\left(-1+\frac{M_A+M_\alpha}{M}\right),$$

$$\mathbf{Q} = \mathbf{k}_0\frac{M_{A-1}}{M_A}-\mathbf{k}_N\frac{M_{A-1}}{M_{A-1}+M_\alpha}.$$

† In eq. (19) all terms $(1+1/\alpha r)$ have been approximated by unity, since the correction is of the order of $(\alpha b)^{-1}$ and is small in the region $\mathcal{R}$.

In eq. (19) $\mathscr{R}$ represents the region of integration delineated by $\psi_1^+(\mathbf{r}) \neq 0$, as given by eq. (12), $(l\frac{1}{2}\mu\nu|jn)$ is a Clebsch-Gordan coefficient, and $\mathbf{Q}$ is the momentum transfer.

To carry out the remaining integrations in eq. (19), note that the dominant contributions of the radial integral arise from the region $r \approx b = R_0$, where R_0 is the nuclear radius. This follows from the fact that $\psi_1^+ \approx 0$ for $r < R_0$ and that $v_l(r)$ rapidly falls to zero when $r > R_0$. For this reason the angular integration is carried out at $r = R_0$, and the radial integration is performed with $v_l(r)$ given by

$$v_l(r) = \mathscr{N}_l \gamma h_l^{(1)}(i\gamma r) \xrightarrow[r\to\infty]{} -\frac{i^{-l}\mathscr{N}_l e^{-\gamma r}}{r}. \tag{20}$$

For our purpose it is sufficient to use the asymptotic expression for $v_l(r)$, since our concern is with light nuclei ($l \lesssim 2$) and radial distances $r > R_0$ †. Consistent with the restriction to medium or high energy α-particles, $k_0 R_0 \gg 1$, and a short range α–N interaction, $a/R_0 \ll 1$, the radial integration in eq. (19) can then readily be performed by neglecting terms of order $k_0 \alpha a^2/QR_0 \approx \alpha a^2/R_0$ relative to 1. In this respect, it is significant that the momentum transfer $\mathbf{Q}$ is never zero and is in fact always larger than $\approx \frac{1}{2}k_0$. This occurs because the reaction energy is usually small. One thus obtains

$$R_{mn} = \sum_{\mu\nu} (l\tfrac{1}{2}\mu\nu|jn) T \int_{\hat{\mathbf{k}}_0 \cdot \hat{\mathbf{R}} < 0} d\Omega f_\mu(\theta, \phi)[\delta_{m\nu} + i\beta\boldsymbol{\sigma}_{m\nu} \cdot (\Gamma\mathbf{k}_0 \times \mathbf{k}_N + i\alpha\Lambda\mathbf{k}_0 \times \hat{\mathbf{R}}_0 + i\alpha\Lambda\mathbf{k}_N \times \hat{\mathbf{R}}_0)]$$

where

$$T = \mathscr{A}(\pi a^2)^{\frac{3}{4}} \mathscr{N}_\alpha \mathscr{N}_l i^{-l} \exp\left\{-\left[\left|\mathbf{k}_0 + \mathbf{k}_N \frac{M_\alpha}{M_\alpha + M_{A-1}}\right|^2 - \alpha^2\right]\tfrac{1}{4}a^2\right\}$$

and

$$f_\mu = Y_l^\mu(\theta, \phi) \frac{e^{-(\alpha+\gamma-iQ\cos\theta)R_0}}{\alpha + \gamma - iQ\cos\theta}. \tag{21}$$

Seemingly, the restriction $\hat{\mathbf{k}}_0 \cdot \hat{\mathbf{R}}_0 < 0$ is most easily considered by choosing $\hat{\mathbf{k}}_0$ as the axis of quantization and integration, but this is not actually the case, and $\mathbf{Q}$ was chosen as this axis. The angles (θ, ϕ) are the angles of integration and $\boldsymbol{\sigma}_{m\nu}$ is the matrix element of $\boldsymbol{\sigma}$ between states of spin $\frac{1}{2}$ and magnetic quantum numbers m and ν. If the scattering plane is chosen to be the x–z plane, the azimuthal integration of f_μ results in

$$F_\mu \equiv \int_{\hat{\mathbf{k}}_0 \cdot \hat{\mathbf{R}}_0 < 0} f_\mu d\Omega = 2\pi \int \sin\theta \, d\theta \, g(\theta) \frac{e^{-(\alpha+\gamma-iQ\cos\theta)R_0}}{\alpha + \gamma - iQ\cos\theta} \tag{22a}$$

† The approximation made to carry out the angular integration is similar to that used by R. Huby in ref.[6]). However, the further approximation made there, namely $l > k_0 R_0$, is hardly justifiable when the transition is being studied in light nuclei.

where $g(\theta)$ is defined for $\cos\Theta' \equiv \hat{\mathbf{k}}_9 \cdot \hat{\mathbf{Q}} = 1$ by

$$\begin{aligned} g(\theta) &= \delta_{\mu,0} Y_l^{\mu}(\theta, 0) \quad \text{for} \quad \theta > 90^\circ \\ &= 0 \qquad\qquad\quad \text{for} \quad \theta < 90^\circ, \end{aligned} \tag{22b}$$

and for $\cos\Theta' < 1$ by †

$$\begin{aligned} g(\theta) &= \delta_{\mu,0} Y_l^{\mu}(\theta, 0) && \text{for} \quad \tfrac{1}{2}\pi + \Theta' \leqq \theta \leqq \pi \\ &= \left(\delta_{\mu,0} - \frac{1}{\mu\pi} \sin \mu\phi_1\right) Y_l^{\mu}(\theta, 0) && \text{for} \quad \tfrac{1}{2}\pi - \Theta' \leqq \theta \leqq \tfrac{1}{2}\pi + \Theta' \\ &= 0 && \text{for} \quad \theta < \tfrac{1}{2}\pi - \Theta'. \end{aligned} \tag{22c}$$

The angle ϕ_1 is defined by

$$\phi_1 = \cos^{-1}[-\cot\Theta' \cot\theta], \quad 0 \leqq \phi_1 \leqq \pi. \tag{22d}$$

The remaining angular integration of F_{μ}, which is required for the first two terms in the bracket of eq. (19) was performed numerically. The last two terms in this bracket are of order α/k_0 of the first spin dependent term, proportional to Γ. Their θ-integration was therefore only carried out to leading order in an expansion of α/Q by means of an integration by parts. The result is especially simple for $\Theta' \gtrsim (k_0 R_0)^{-1}$, in which case one readily obtains

$$\begin{aligned} G_{\mu} &= i\alpha \int_{\hat{\mathbf{k}}_0 \cdot \hat{\mathbf{R}}_0 < 0} \mathrm{d}\Omega f_{\mu}(\theta) \boldsymbol{\sigma}_{m\nu} \cdot (\Delta \mathbf{k}_0 \times \hat{\mathbf{R}}_0 + \Delta \mathbf{k}_{\mathrm{N}} \times \hat{\mathbf{R}}_0) \\ &\approx 2\pi\alpha\delta_{\mu,0} Y_l^{\mu}(\pi, 0) \frac{\boldsymbol{\sigma}_{m\nu} \cdot \mathbf{k}_0 \times \mathbf{k}_{\mathrm{N}}}{Q} (\Delta + \Lambda) \frac{\mathrm{e}^{-(\alpha+\gamma+iQ)R_0}}{QR_0(\alpha+\gamma+iQ)}. \end{aligned} \tag{23}$$

For $\Theta' \lesssim (k_0 R_0)^{-1}$, the approximation made is not valid, but G_{μ} can also be readily evaluated to order α/Q. However, because a) the effect of G_{μ} on the cross-section is small at all angles, b) the polarization is small at angles $\lesssim (k_0 R_0)^{-1}$, and c) Coulomb effects are important in this region, we approximate G_{μ} by eq. (23) at all angles. The reaction matrix element is thus, finally,

$$R_{mn} = \sum_{\mu\nu} (l\tfrac{1}{2}\mu\nu|jn) T[F_{\mu}\delta_{m\nu} + i\beta\boldsymbol{\sigma}_{m\nu} \cdot \mathbf{n}(\Gamma F_{\mu} + G_{\mu})] \tag{24}$$

where $\mathbf{n} = \mathbf{k}_0 \times \mathbf{k}_{\mathrm{N}}$.

2.4. DIFFERENTIAL CROSS-SECTION AND POLARIZATION

With the use of Racah algebra [16]) it is now straightforward to compute the angular distribution, for which one obtains

$$\begin{aligned} \frac{\mathrm{d}\sigma}{\mathrm{d}\Omega} &= \frac{2\pi}{(2\pi)^3} \frac{{k_{\mathrm{N}}}^2}{v v_0} \sum_{mn} |R_{mn}|^2 \\ &= \frac{1}{4\pi^2} \frac{{k_{\mathrm{N}}}^2}{v v_0} |T|^2 \frac{2j+1}{2l+1} |M|^2, \end{aligned} \tag{25}$$

† The function $\cos\Theta'$ is always larger than zero in an (α, N) reaction, except for the unusual circumstance that $k_{\mathrm{N}} \geqq k_0$, in which case the momentum transfer can be zero.

where $|M|^2$ is the sum of $|M_{\rm pt}|^2$ for a central point interaction and a correction term

$$|M|^2 = |M_{\rm pt}|^2 + \sum_{\mu} \beta^2 \mathbf{n}^2 [\Gamma^2 |F_\mu|^2 + 2\Gamma \,\mathrm{Re}\,(F_0^* G_0) + |G_0|^2] + (-1)^{j+l+\frac{1}{2}} 4[3(2l+1)]^{\frac{1}{2}} (l1 1 -1|l0) \begin{Bmatrix} l & l & 1 \\ \frac{1}{2} & \frac{1}{2} & j \end{Bmatrix} |\mathbf{n}| \beta \,\mathrm{Re}\,(F_{-1}^* G_0) \tag{26a}$$

with

$$|M_{\rm pt}|^2 = \sum_{\mu} |F_\mu|^2. \tag{26b}$$

In eq. (26), v_0 and v are the initial and final relative velocities, respectively, and the Racah co-efficient $\{\ \}$ is defined as in refs. [16]) and [17]).

The polarization of the outgoing nucleon can also readily be evaluated:

$$\mathbf{P} = \frac{\sum_{nmm'} |R^+_{nm'} \boldsymbol{\sigma}_{m'm} R_{mn}|}{\sum_{mn} |R_{mn}|^2} = 2\hat{\mathbf{n}} \Big\{ \beta |\mathbf{n}| \,\mathrm{Im}\,(F_0 G_0^*) + \sum_{\mu>0} (-1)^{j+l+\frac{1}{2}} 2[3(2l+1)]^{\frac{1}{2}} (l1\mu -1|l\mu -1) \begin{Bmatrix} l & l & 1 \\ \frac{1}{2} & \frac{1}{2} & j \end{Bmatrix} \tag{27a}$$

$$\times [P_{\rm pt} + \beta^2 \mathbf{n}^2 \Gamma \,\mathrm{Im}\,(\Gamma F^*_{\mu-1} F_\mu + \delta_{\mu,1} G_0^* F_1)] \Big\},$$

where the relevant quantity for a point-interaction is the term proportional to $P_{\rm pt}$, which is given by

$$P_{\rm pt} = \mathrm{Im}\,(F^*_{\mu-1} F_\mu). \tag{27b}$$

In evaluating eqs. (26) and (27), use has been made of the symmetry $F_{-\mu} = (-1)^\mu F_\mu$.

2.5. NUMERICAL EVALUATION FOR P-STATE

For reactions of the type a) $Be^9(\alpha, n)C^{12}$ and b) $C^{13}(\alpha, n)O^{16}$, the binding energy of the last neutron is considerably less than that of any nucleon in the α-particle. It is therefore likely that the reaction proceeds predominantly by the mechanism used for the illustrative example, namely by a knock-out process. Furthermore, the maximum polarization which is 100 % can occur if the nucleon is initially in a $P_{\frac{1}{2}}$ state of angular momentum.

For purposes of illustration, the angular distribution and polarization have been calculated for a nucleon knocked-out of a $P_{\frac{1}{2}}$ and $P_{\frac{3}{2}}$ state under conditions which simulate (but do not exactly correspond to examples a) and b) given above. The relevant kinematical quantities employed were $k_0 = 2.38 \times 10^{13}$ cm^{-1} (this corresponds to an α-particle energy of 30 MeV in the centre of mass system), $k_N/k_0 = 0.56$, $(\alpha+\gamma)\, R_0 = 7.3$. These values are intermediate between those for † $C^{13}(\alpha, n)O^{16}$ and $Be^9(\alpha, n)C^{12}$. Recoil effects were neglected in evaluating Γ, Δ and Λ, for which one then obtains

† For C^{13} one obtains $(\alpha+\gamma)R_0 \approx 9.0$ and for Be^9 one finds $(\alpha+\gamma)R_0 \approx 6.6$ if $R_0 \approx (1.4A^{\frac{1}{3}} + 2.2) \times 10^{-13}$ cm as suggested in ref.[19]).

($M_A \to \infty$) $\Gamma = -0.8$, $\Delta = -\frac{1}{5}$, $\Lambda = \frac{4}{5}$. In this limit $|T|^2$ is constant and this was assumed in plotting fig. 1.

The angular distribution for an initial $j = \frac{1}{2}^-$ nuclear state is shown in fig. 1 for a) a central point interaction, b) the spin-dependent interaction given in the text, and c) the Born-approximation with a central point interaction. The latter obtains when the angular integration in eq. (21) is carried out over the whole angular range of 0 to π. The cross-sections plotted in fig. 1 have all been multiplied by the same, but arbitrary constant. For an initial $j = \frac{3}{2}^-$ state, the structure dependent corrections are even smaller than for the $j = \frac{1}{2}^-$ case, and have therefore not been included in the figure.

In figs. 2 and 3 the polarizations predicted for a) a point interaction and b) the spin-dependent interaction are compared for an initial nucleon in a $j = \frac{1}{2}^-$ and $j = \frac{3}{2}^-$ state.

3. Discussion

A comparison of the various curves of figs. 1, 2 and 3 confirms the results anticipated in the introduction.

a) Fig. 1 demonstrates that the angular distribution of the process is considerably modified by inclusion of the nuclear distorting effects on the

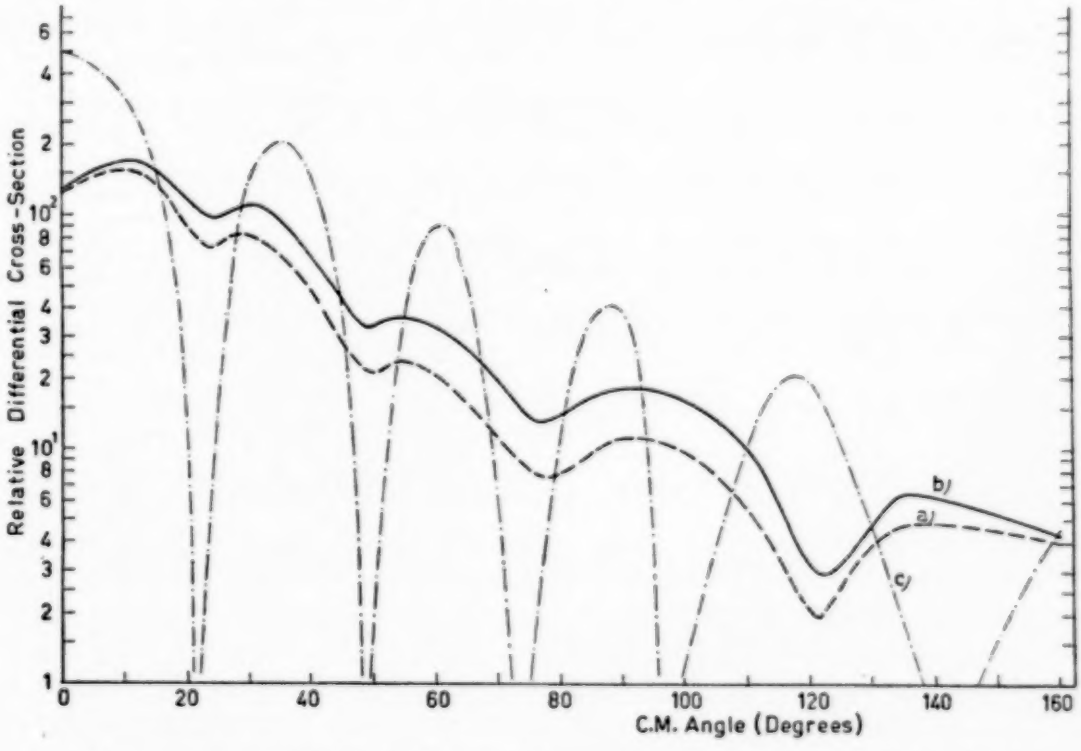

a) ———— point interaction b) ———— spin dependent interaction
c) —·—·— Born approximation.

Fig. 1. Correctly normalized relative angular distributions for a knock-out (α, N) transition from a $j = \frac{1}{2}^-$ state. In curve a) a δ-function interaction is assumed, in b) the spin dependent interaction described in the text is used, and in c) the Born approximation result is shown.

incident α-particle. Thus, the sharp diffraction pattern of the Born approximation is markedly smoothed out, in agreement with the angular distributions measured by Hunting and Wall [5]), for the reactions $Al^{27}(\alpha, p)Si^{30}$ and $P^{31}(\alpha, p)S^{34}$. In fact, the experimental differential cross-sections bear a striking resemblance to that predicted here, even though the curves cannot be compared directly. On the other hand, the measurements of Rickey and Sherr [5]) with 30 and 40 MeV α-particles incident on C^{12} show deeper minima than those anticipated from figs. 1b and 1c. However, this discrepancy may

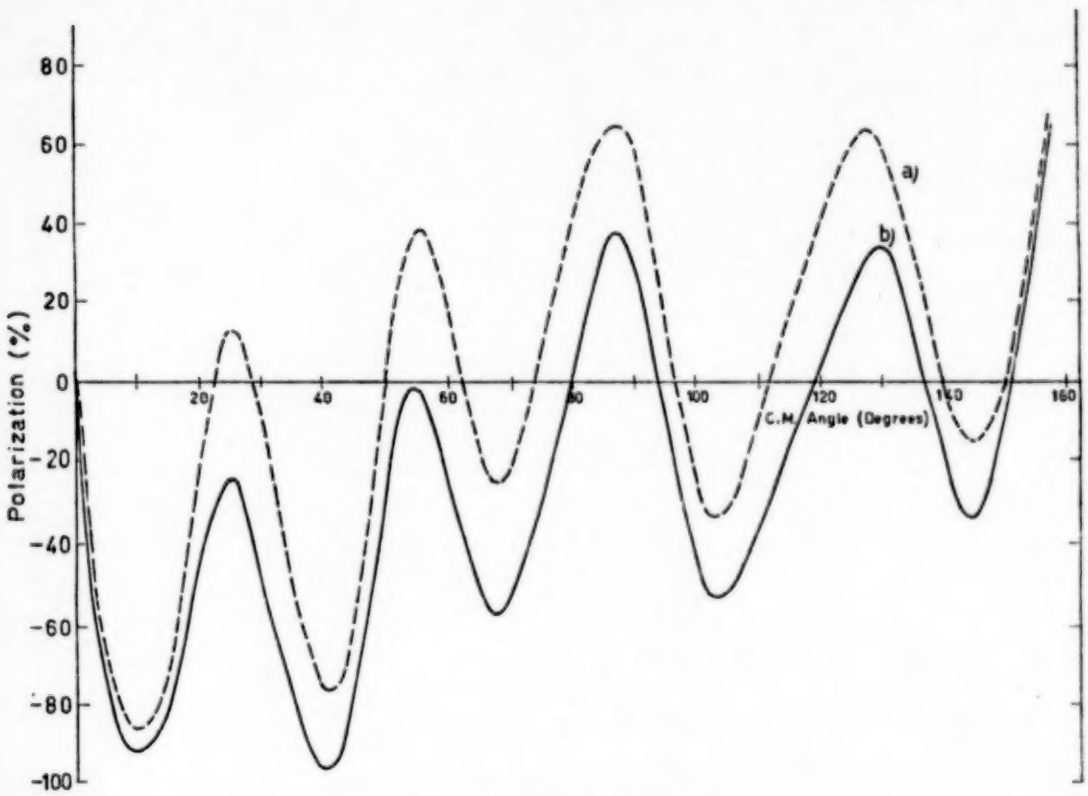

a) $P_{pt}(j = \frac{1}{2}^-)$ b) $P(j = \frac{1}{2}^-)$.

Fig. 2. Polarization of nucleon emitted from a $j = \frac{1}{2}^-$ state in an (α, N) reaction for cases a) and b) of fig. 1.

be partially or totally attributable to the higher nucleon binding energy in C^{12} than in the illustrative example used in fig. 1. An increase of $(\alpha+\gamma)/Q$ can be shown to cause a sharper diffraction pattern.

b) The mode and structure of the interaction of an (α, N) reaction does not significantly alter the angular distribution. This was specifically shown when the spin dependence (and first order size effects) of the interaction responsible for a knock-out process was included. The differential cross-section for the stripping process should closely resemble that of a central point interaction, since the spin dependence of the H^3—N interaction [9]) is smaller than that of a nucleon and an alpha-particle.

c) As stated in the introduction, one advantage of the (α,N) reaction is

that the maximum polarization of the ejected nucleon is 100 %. Fig. 2 reveals that this limit is almost reached at some angles. The polarization should thus be easily detectable, for example by a scattering from He^4. Furthermore, the (α, N) process may serve as a source of highly polarized medium energy nucleons.

d) Figs. 2 and 3 demonstrate the effect of the interaction structure on the polarization of the nucleon produced by a knock-out process. The inclusion of first order size effects are negligible for the example used to plot

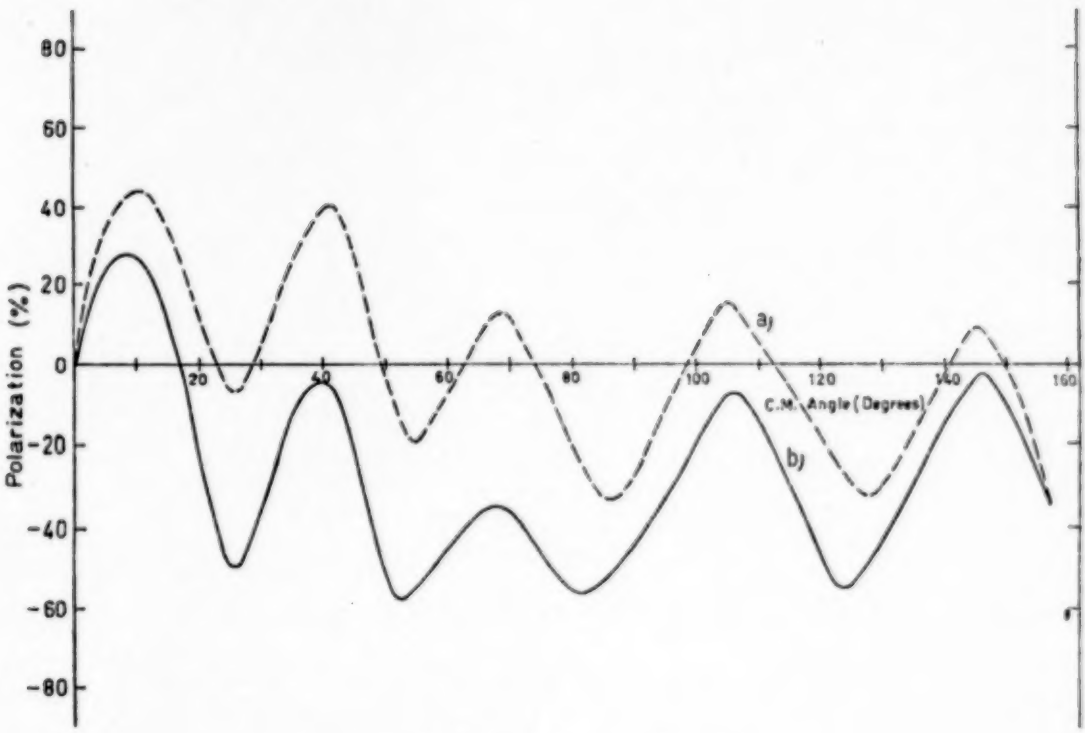

a) $P_{pt}(j = \frac{3}{2}^-)$ b) $P(j = \frac{3}{2}^-)$

Fig. 3. Polarization of nucleon ejected from a $j = \frac{3}{2}^-$ state in an (α, N) reaction for cases a) and b) of fig. 1.

this figure. The main result of a non-zero range interaction is to slightly increase the differential cross-section at large angles. It is clear from the two figures that the inclusion of the spin dependence of the interaction greatly modifies the polarization. Although the general shape of the angular dependence remains the same, the magnitude and sign of the polarization are affected. The change is especially pronounced for a nucleon in a $j = \frac{3}{2}^-$ state. Since the spin-dependence of the stripping interaction is smaller [9]), and certainly different, one might be able to use experimental measurements to differentiate between the two modes by which the direct reaction can proceed. However, such a differentiation, when meaningful, may require a more refined calculation than was carried out herein.

In conclusion, it is clear that further study of the polarization in an (α, N)

reaction will materially aid our understanding of the reaction mechanism, as well as that of nuclear structure. For the latter, the zero spin of the α-particle and the large polarization anticipated should make this reaction more useful than the deuteron stripping process.

The author is grateful to Professor S. Berko for his interest and stimulating communications and to Professor L. C. Biedenharn for several discussions.

He would also like to thank Professors N. Bohr and A. Bohr for the hospitality extended to him at the Institute for Theoretical Physics and to Professors C. J. Bakker and M. Fierz for the hospitality he found at CERN. Lastly, he thanks Mr. W. Klein of the Theoretical Division at CERN for computational help.

References

1) See for example H. A. Weidenmüller, Z. Physik **150** (1958) 389; This paper also contains extensive references to earlier work
2) L. F. Chase, Jr. and G. Igo (in press)
3) S. T. Butler, Nuclear Stripping Reactions (John Wiley and Sons, New York, 1957)
4) S. T. Butler, Phys. Rev. **106** (1957) 272;
G. F. Pieser and N. P. Heydenburg, Phys. Rev. **111** (1958) 264
5) See, however, C. E. Hunting and N. S. Wall, Phys. Rev. **108** (1957) 901;
M. E. Rickey and R. Sherr, Bull. Amer. Phys.Soc. **2** (1957) 29; and private communication;
J. G. Likely and F. P. Brady, Phys. Rev. **104** (1956) 118;
Burcham, McCauley, Bredin, Gibson, Prowse and Rotblat, Nuclear Physics **5** (1958) 141
6) H. C. Newns, Proc. Phys. Soc. A **66** (1953) 477
7) N. F. Mott and H. S. W. Massey, The Theory of Atomic Collisions, (Oxford University Press, 2nd. Ed., 1949) p. 144
8) See for example, C. A. Levinson and M. K. Banerjee, Ann. of Physics **2** (1957) 471
9) J. M. Blatt and V. F. Weisskopf, Theoretical Nuclear Physics (John Wiley and Sons, New York, 1952) p. 208
10) L. I. Schiff, Phys. Rev. **103** (1956) 443
11) M. Gell-Mann and M. L. Goldberger, Phys. Rev. **91** (1953) 398
12) N. C. Francis and K. M. Watson, Phys. Rev. **93** (1954) 313;
R. G. Thomas, Phys. Rev. **100** (1955) 25
13) W. B. Cheston and A. E. Glassgold, Phys. Rev. **106** (1957) 1215;
G. Igo, Phys. Rev. Letters **1** (1958) 167;
See also G. Igo (in press) for further references
14) Sack, Biedenharn and Breit, Phys. Rev. **93** (1954) 321
15) G. N. Watson, Theory of Bessel Functions, (Cambridge Univ. Press, 1952) p. 394
16) A. R. Edmonds, Angular Momentum in Quantum Mechanics (Princeton University Press, Princeton, 1957)
17) A. de Shalit, Phys. Rev. **91** (1953) 1479
18) G. E. Owen and L. Madansky, Phys. Rev. **105** (1957) 1766
19) Kerlee, Blair and Farwell, Phys. Rev. **107** (1957) 1343

NORTH-HOLLAND BOOKS

ANALYTICAL and CANONICAL FORMALISM in PHYSICS

by ANDRÉ MERCIER

Head of the Department of Theoretical Physics University of Berne

6×9″ VIII + 222 pp. Guilders 20.00 (40s.)

CONTENTS

i. Lagrangian Formalism
ii. Lagrangian Density
iii. Canonical Formalism
iv. Canonical Form of Electrodynamics
v. Hamiltonian Densities
vi. Transformations
vii. Canonical Formalism with Vanishing Jacobian Determinant

Those who are not highly specialized in these matters but do want to get a fairly broad knowledge of the subject are not aware of the fact that the greater parts of this formalism, including many specific conclusions of physical concern, do not involve in the least quantum theory, i.e. "quantization" of the fields. To show this and to provide the reader with a fairly complete presentation of the *classical* (i.e. not yet quantized) theory of fields is one of the main aims of the book.

This formalism is presented with great generality. Some special topics have also been included when they are found to be of importance in connection with the problems raised; however, they are not elaborated with the same generality, but just formulated as far as is found necessary for the understanding of these connections; for instance we can name: tensorial formalism and spinorial formalism.

A special chapter has been devoted to transformations of several kinds including canonical transformations, reversibility and the like as well as their interrelations, so that the ground is prepared for an understanding of the CPT-Theorems.

A short chapter on Dirac's dynamics with vanishing Jacobian closes the book.

The work builds upon the well-known *Principles of Analytical Dynamics* by the same author (in French), where particular weight is laid upon the homogeneous formalism, but it can easily be read with profit without knowledge of the latter by any advanced students in physics, astronomy or mathematics as well as by research workers who want to get a thorough practice in the use of these methods.

Many examples and as many as 124 problems illustrate the formalism exposed.

Sole Agency for U.S.A.: Interscience Publishers Inc. - New York

NORTH-HOLLAND PUBLISHING COMPANY - AMSTERDAM

NORTH-HOLLAND BOOKS

ASYMPTOTIC METHODS in ANALYSIS

by **N. G. DE BRUIJN** *Professor of Mathematics at the University of Amsterdam*

Asymptotics is that part of analysis which considers problems of the type dealt with in this book

Contents

Ch. I. Introduction
Ch. II. Implicit Functions
Ch. III. Summation
Ch. IV. The Laplace Method for Integrals
Ch. V. The Saddle Point Method
Ch. VI. Applications of the Saddle Point Method
Ch. VII. Indirect Asymptotics
Ch. VIII. Iterated Functions
Ch. IX. Differential Equations

6×9″ XII+200 pages Guilders 20.00 (40s.)